THE MINERALOGICAL MAGAZINE

AND

JOURNAL OF

THE MINERALOGICAL SOCIETY

No. 220 March, 1953 Vol. XXX

The surface structure of crystals.

(With Plates I–IX.)

By A. F. Seager, B.Sc., Ph.D., A.K.C., F.G.S.

Department of Geology, Birkbeck College, University of London.

[Read March 8, 1951.]

Introduction.

C. W. BUNN and H. Emmett[1] have observed the spreading of multi-molecular layers on growing crystals of artificial compounds, and have suggested that deposition takes place on the high-index surfaces at the edges of the layers. Their work led the author to examine crystals of several mineral species for evidence of the mechanism of growth, and this account is the result of a preliminary survey of the growth structures found.

So many growth structures could be seen with the naked eye or with a hand-lens that it was decided to use low magnifications in order that comparatively large areas of the crystal faces could be examined and photographed at one time. A metallurgical microscope with a prism reflector and 1-inch objective was used for the observations and most of the photography. This work is qualitative rather than quantitative, but it is intended to carry out a quantitative examination of the same specimens later.

The approach differs from that of Bunn and Emmett in two respects: the use of low magnifications and the observation of the crystals after rather than during growth. The structures to be described project above the general level of the crystal face, like etch hillocks. Growth by layer-spreading seems to offer the only satisfactory explanation of the origin of these structures and is further substantiated by their close similarity to the spreading layers which have been seen on growing crystals (e.g. Bunn and Emmett, loc. cit., 1949, figs. 4–7).

[1] C. W. Bunn and H. Emmett, Discuss. Faraday Soc., 1949, no. 5, p. 119. [M.A. 11–377.]

Structures on crystal faces.

The origin of the structures can be understood more easily if the mec of layer-initiation and spreading is considered first. Several hypothetica cases are considered, in which layers are initiated on different parts c a face at either a constant or a variable rate and spread with either constant or a variable velocity. Combinations of these variables gi rise to several possible structures and types of habit. Since a number c these structures has been found it suggests that some, at least, of th hypothetical cases are valid.

A general account of crystal habit in terms of layer-spreading.

Two conditions are postulated:

1. The initiation of new layers, either monomolecular or multimol cular, is a comparatively infrequent event, the previous layer havin spread completely, or nearly completely, across the crystal fac before the new layer is formed.
2. The initiation of new layers takes place so rapidly that many c the earlier-formed layers are still spreading across the crystal fac when the new layers are formed.

These two conditions must both be considered with each of the follow ing cases:

A. The layers are initiated within the edges of the crystal face.
B. The layers are initiated at the edges of the face.
C. The layers are initiated at the corners of the face.

The combinations of the conditions 1A, 1B, and 1C would all lead t the development of normal, plane-faced crystals. The combination 2 would lead to the growth of crystals with vicinal pyramids, the combina tion 2B would lead to the growth of hopper crystals, and 2C to skeleta or dendritic habits.

This concept of the development of hopper, skeletal, and dendriti crystals by very rapid layer formation agrees with the fact that suc abnormal habits are usually developed only at very high supersatura tions, when presumably layer-initiation is most rapid.

A general consideration of layer-spreading.

If it is assumed that layers may be generated at a constant, increas ing, or decreasing rate, and spread at a constant, increasing, or decreas ing velocity, nine combinations will arise, the surface profiles of whic

re given in table I. 'Increasing' and 'decreasing' in the column headed Velocity of layer-spreading' refer to the change in velocity of the edge of the layer as it spreads. 'Complex' is used for surfaces which have both concave and convex curvatures.

TABLE I. Possible combinations of rates of initiation and growth of layers and resultant surface profiles.

Case.	Rate of layer-initiation.	Velocity of layer-spreading.	Surface profiles.
1	Constant	Constant	Plane
2	Constant	Increasing	Concave
3	Constant	Decreasing	Convex
4	Increasing	Constant	Concave
5	Increasing	Increasing	Concave
6	Increasing	Decreasing	Concave or complex
7	Decreasing	Constant	Convex
8	Decreasing	Increasing	Convex or complex
9	Decreasing	Decreasing	Convex

Cases 1, 4, and 7 seem most likely to occur. Plane, concave, and convex surfaces have been found. Cases 6 and 8 seem least probable and no examples of them have been found.

The vicinal pyramid formed by rapid layer-initiation may be regarded as a large number of superimposed molecular layers growing outwards from a common origin and having a distance between adjacent layer-edges of a small number of atoms. Such a vicinal pyramid would have smooth surfaces with profiles as given in table I. Most vicinal pyramids have surfaces which are striated parallel to the layer-edges and appear to consist of multimolecular layers of approximately equal thickness. Alternating periods of rapid and slow layer-initiation, or periods of rapid initiation with pauses between them, would account for the striated vicinal pyramids. According to this interpretation each period of rapid initiation would produce one multimolecular layer, composed of a number of closely-spaced molecular layers. Each multimolecular layer would have plane, concave, convex, or complex profiles on its edges, depending upon its particular conditions of growth (see table I). The multimolecular layers would grow by deposition on the molecular steps.

THE HABIT OF GROWTH FORMS.

It has been observed that layers initiated within the edges of a crystal face may be polygonal, circular, or elliptical in plan, or bounded by intersecting arcuate lines, while occasionally they are ragged and irregular. Apart from the circular and irregular forms, the layers show the same degree of symmetry as the face on which they grew.

When layer-initiation is rapid a vicinal pyramid will be built up. In its usual crystallographic sense the word *pyramid* denotes a form in which all the faces are crystallographically equivalent. This is only true of *vicinal pyramids* in special cases, since, in the general case, they are bounded by a number of different forms, as in an etch pit. Steep vicinal pyramids closely resemble etch hillocks, so the term *vicinal hillock* will be used for all vicinal pyramids which are polygonal, or nearly polygonal in plan.

Since vicinal hillocks have been named by analogy with etch hillocks it is desirable to use a different name for the less common circular and elliptical growth forms, for which the term *vicinal boss* is suggested. *Growth forms* will be used to embrace all vicinal hillocks and vicinal bosses.

Topaz (plates I and II).

The prism {110}.

One specimen, believed to come from Cornwall, has several topaz phenocrysts, some doubly-terminated, in a fine-grained rock groundmass. The (110) face of the largest crystal has five well-developed vicinal hillocks. One vicinal hillock has been photographed twice, with different lighting, to show the curvature on the sides towards (100) and (010) (figs. 1 and 2)[1]; figs. 3–6 show the other four vicinal hillocks.

All these figures emphasize the fact that the layers travel slowly from the point of origin towards the (010) edge, faster towards the (001) and (00$\bar{1}$), and fastest towards the (100) edge. Thus strong striations are built up by the steep sides of the vicinal hillocks which face (010) (fig. 4). The latter are (hk0) surfaces with $h < k$, and the opposite side of the vicinal hillock is bounded by (hk0) surfaces with $h > k$. The other two sides of the vicinal hillock are bounded by pyramidal surfaces. The striations are not due to an oscillatory combination, if that is understood to mean an alternation of two planes. Figs. 2 and 4 show clearly that the surface profiles are concave.

The surfaces forming the striations all lie between the planes (110) and (120), except for the highest and steepest parts in figs. 3 and 6 which reflect light simultaneously with (120). Since the interfacial angle (110):(120) is 18° 44′ it represents an unexpectedly steep slope for a vicinal form. On the side of the vicinal hillock facing (100) the slope is

[1] The use of face or form symbols in this paper to describe *directions* on a crystal face does not necessarily imply that those faces or forms are present on the crystal

ess steep, although somewhat variable (figs. 1, 4, and 6). Figs. 1, 2, and 4 show examples of concave surface profiles.

The salient edge between adjacent faces of the vicinal hillock may be straight or sinuous (figs. 4 and 3). The latter case indicates changes in the relative growth velocities of the layers on adjacent sides of the salient edge.

It is interesting that nearly all these vicinal hillocks have a minute particle of impurity at or immediately adjacent to the apex of the hillock. It is not possible to assert definitely that these impurities have caused initiation of growth as there are many other particles on the face which have no visible effect.

Some of these particles have held up growth layers, causing *growth shadows*. A 'cliff' due to this cause can be seen on the steep side of the vicinal hillock in figs. 1 and 2. A similar but longer cliff appears in fig. 6, while in fig. 3 the steep edge has been held back in two successive steps by impurities.

On the sides of the hillocks bounded by pyramidal surfaces the edges of the layers make an angle of approximately 2° with the edge (110) (001). Thus the pyramidal surfaces have an index of the type {*hkl*} and not {*hhl*}.

Fine curved lines can be seen on the flatter surfaces of some vicinal hillocks (figs. 1 and 2). Similar curved lines have also been observed macroscopically, bounding the layers on {110} of a topaz crystal from Nigeria. In the figures mentioned the central, steep vicinal hillock rests on an earlier-formed hillock, like a nearly square plinth. Layers have spread from another initiation point near the edge of the plinth. They remained quadrilateral until they reached the steep side of the larger hillock, when the layer-edges became curved. The re-entrant angles formed when the two sets of layers met offered preferential positions of attachment. The additional deposition at these positions, combined with the continued spreading of the layers from the second initiation point, would account for the curvature of the layer-edges.

Crystals of topaz from the Thomas Range, Utah, usually have many intergrown vicinal hillocks similar in habit to those described from Cornwall. One vicinal hillock is shown in fig. 7.

The prism zone [001].

The common forms on the brown crystals from Ouro Preto, Minas Geraes, Brazil, are {110}, {120}, and {111}. The striated prism zone has a complex structure. Although alternating elements of {110} and {120} are present it is not only an oscillatory combination, as the adjacent

planes are often connected by concave surfaces, also many of the fine and some of the coarser striations are not parallel. Many of the narrower striations are composed of surfaces lying between {110} and {120}. Vicinal hillocks on (110) have the steep side facing (120), while those on (120) have the steep side facing (110). Fig. 8 shows a vicinal hillock on (120) elongated in the direction of the *c*-axis, parallel to which it forms striations. In fig. 8 the upper part of the steepest side is bounded by (110) (the white band), and concave pyramidal surfaces can be seen.

Fig. 9 shows a D-shaped vicinal hillock on (110) of a crystal believed to come from Nigeria. The steep side faces (120).

The elongation of such a structure would account for the curved layers in fig. 10, seen on (110) of a magenta-coloured crystal from Ouro Preto. The gently arcuate layers spread across the face until they were stopped at a striation, which was thereby increased in height. The inclined surfaces forming the striations, which are dark in the figure, lie between (110) and (120).

The magenta crystal has D-shaped vicinal hillocks on (120) (fig. 11). They are similar to the one in fig. 9, but face in the opposite direction with the steep side towards (110). The outer layers are D-shaped although the inner ones are quadrilateral, and show a transition from quadrilateral to arcuate layers.

Some of the brown crystals from Ouro Preto have D-shaped vicinal hillocks in which the arcuate part has a slightly concave profile. Several of these structures have a small particle of impurity at the apex.

Beryl (plates II and III).

On a blue crystal from Brazil, showing hexagonal prism and basal pinakoid, the layers on $\{10\bar{1}0\}$ appear to have spread rapidly in the direction of the *c*-axis and slowly normal to it, thereby forming elongated vicinal hillocks with steep prismatic and more gently inclined pyramidal surfaces. Each end of the vicinal hillock may have one or two pyramidal surfaces. Occasionally the pyramidal ends are irregular; the parallel layers with sinuous edges of fig. 12 are asymmetric extensions of a vicinal hillock, beside which is a normal hillock.

Most of the aquamarine crystals examined from Spitzkopje, South-West Africa, show the forms $\{10\bar{1}0\}$, $\{11\bar{2}0\}$, $\{10\bar{1}1\}$, $\{11\bar{2}1\}$, and $\{0001\}$. The crystals are usually prismatic in habit, but two are tabular on $\{0001\}$. On the prism $\{10\bar{1}0\}$, the numerous vicinal hillocks present are similar to those in fig. 12, but both the prismatic and pyramidal surfaces have convex profiles.

On the prism $\{11\bar{2}0\}$ the layers form vicinal bosses which are elliptical nearly circular in plan, and each boss has an etch pit at its centre. . 13 shows the initiation points of four vicinal bosses and part of other bosses. In fig. 14 the prismatic surfaces are concave and the amidal surfaces conical and slightly concave.

The bipyramid $\{11\bar{2}1\}$ has numerous vicinal hillocks, one of which is wn in fig. 15. The layers are nearly in the form of a parallelogram, hough there is a slight curvature of the edges. The two upper faces seen, and one of the lower, which is in deep shadow. The two upper faces are convex, and presumably have high indices. They lie in zones ssing through $\{11\bar{2}1\}$ and $\{10\bar{1}1\}$. The two lower surfaces lie in zones ssing through $\{11\bar{2}1\}$ and $\{10\bar{1}0\}$. The two upper faces thus belong to e form, or set of forms, and the two lower faces to another. There is a lden change in the slope of the vicinal hillock.

On the bipyramid $\{10\bar{1}1\}$ only one vicinal hillock has been found. It is comparatively thin layer which is almost an equilateral triangle in n. One side is parallel to the intersection with $\{10\bar{1}0\}$, and the other o to the intersection with $\{11\bar{2}1\}$, therefore at least two pyramidal ms are involved as growth surfaces.

The basal pinakoid (fig. 16) shows series of hexagonal layers which ve spread from numerous centres. The layer-edges are straight and rallel to the intersections with $\{10\bar{1}0\}$, and are bounded by a form zone with $\{10\bar{1}0\}$ and $\{0001\}$ which makes a small angle with the ter.

Baryte (plates III and IV).

The basal pinakoid.—The vicinal hillocks commonly have the shape a parallelogram in plan, the edges of which are parallel to the intersections of $\{001\}$ and $\{110\}$. The edges of the layers are thus bounded $\{hhl\}$ surfaces. Vicinal hillocks are well developed on the yellow ystals from Frizington, Cumberland, which have been described by iss J. M. Sweet.[1] They are elongated on the *b*-axis (figs. 17 and 18). he crystals often consist of several slightly mis-alined individuals, the dges or steps between which appear to have exerted a considerable fluence on growth. In fig. 17 a series of layers can be seen, bounded on ie side by a step. It appears that, as soon as the growing layers passed ie end of the step, some of them 'doubled back' along the other side. he sinuous nature of the salient edge of the vicinal hillock shows that

[1] J. M. Sweet, Min. Mag., 1930, vol. 22, p. 268.

the layers on adjacent sides have spread with changing relative velocities the group of layers on one side then on the other travelling faster alternately. This suggests a structure-sensitive control of growth. In fig. 1 several series of layers can be seen to have started from the ends of steps. The central parallelogram seems to have had two initiation points resulting in two obtuse corners on one side. The curvature of the layer edges between the two corners is reminiscent of the more smoothly curved layers on the topaz from Cornwall and Nigeria described above and may be due to the same cause.

On crystals from the Silverband mine, Westmorland, which are elongated on the *a*-axis, {011}, {001}, and {102} are the best developed forms. The vicinal hillocks commonly have the same form as those described from Frizington, but are not so finely striated. Sometimes the vicinal hillocks are six-sided, with an additional pair of sides in the zone [010]. On some crystals the {*hhl*} and {*h*0*l*} surfaces are convex.

A crystal from Nutfield, Surrey, shows vicinal hillocks on {001}, most of which have a minute crystal of chalcopyrite and of calcite in the centre.

The prism {110}.—Crystals from the north of England often have fine striations on {110}, parallel or normal to the *c*-axis, or in both directions. In many cases rectangular vicinal hillocks can be seen, their direction of elongation determining that of the major striations. Fig. 19 shows a vicinal hillock elongated parallel to the *c*-axis, initiated at, or very near, the edge of the face. Fig. 20, from the same specimen, shows the major striations in the other direction. The layers are bounded by pyramidal surfaces {*hhl*}, and by prismatic surfaces {*hk*0}, with $h > k$ on one side and $h < k$ on the other. As the layers spread outwards they sometimes break up into a large number of minute rectangular steps, as in fig. 20, giving rise to the curved lines sometimes seen on {110}.

The brachydome {011}.—Some crystals of baryte from the Silverband mine have numerous circular layers, as in fig. 21. They are similar to the structures on ammonium sulphate described by J. Ames, T. L. Cottrell, and Avis M. D. Sampson.[1] In fig. 21 the upper surfaces of the layers are plane, but in most cases the vicinal bosses consist of rounded hummocks. The latter are presumably formed when layer-initiation continues to the end of growth.

The macrodome {102}.—Triangular vicinal hillocks are present on some crystals from the Silverband mine.

[1] J. Ames, T. L. Cottrell, and A. M. D. Sampson, Trans. Faraday Soc., 1950, vol. 46, p. 940, and fig. 5.

Fluorite (plates IV–VI).

Reference will be made to four specimens in describing the structures on fluorite. The first, from Weardale, County Durham, is a mauve 4-cm. cube, twinned on the spinel law, on which only {100} is present. The second is a pale mauve specimen consisting of twinned 4–8-mm. cubes, with a hexakisoctahedron, from the Sedling mine, Weardale. The third is a mauve specimen consisting of twinned and untwinned cubes up to 2 cm., in combination with an {*hk*0} and an {*khl*} form. The locality is uncertain, but the specimen has the appearance of fluorite from Weardale, and will be referred to as the 'mauve fluorite'. The fourth specimen consists of two green twinned 2-cm. cubes from County Durham, and will be called the 'green fluorite'.

Fig. 22 shows part of the (100) face of the 4-cm. cube, on which a vicinal hillock has been initiated by the twin crystal. The plan view is approximately square, but the edges are slightly curved, as is common in fluorite. The salient edge of the vicinal hillock is shown in figs. 23–26, in which the angle between adjacent layer-edges is approximately 126°. Thus the edge of each layer makes an angle of 18° with the nearest cube edge. Sir Henry Miers[1] records vicinal {*hk*0} forms on fluorite, but they would not account for the curved edges of the layers. The (001) face of the 4-cm. cube has a re-entrant corner of the twin crystal projecting through it. All three edges of the re-entrant corner initiate a vicinal hillock at the point where they touch the cube face. Two of these vicinal hillocks, which are octagonal, not square, are shown in figs. 27 and 28. The alternate interior angles of the octagons are approximately 127° and 143°. Farther from the point of origin the layers do not form a continuous smooth curve between adjacent salient edges of the vicinal hillock, but break up into a number of triangular layers which form projecting tongues (as in fig. 29, of the green fluorite) or form layers with zigzag edges composed of many such tongues (fig. 30, green fluorite). In the aggregate these tongues give a gentle curvature to the outline of the vicinal hillock in plan view. The edges of the tongues in fig. 29 make an angle of approximately 18° with their nearest cube edges. In the specimen from the Sedling mine the layer-edges on both sides of the salient edge of the vicinal hillock are parallel to the intersection of the cube and hexakisoctahedron, and the layer-edges make an angle of approximately 18° with their nearest cube edge. The surface on the edge of the cube layers on the three specimens described and on the mauve fluorite thus appears to be a hexakisoctahedron.

[1] H. A. Miers, Mineralogy. 2nd edit., 1929, p. 358.

The {*hk*0} faces of the mauve fluorite are interrupted by numerous projections. Some are shown in fig. 31, which is a view normal to (100) so that (*hk*0) appears dark. As the microscope was focused on the projections, the layers on the cube face are slightly out of focus. The projections have surfaces parallel to (100) with a zigzag edge (angle 143°). It is clearly an extension of the layer-system of the cube projecting from (*hk*0). The two lower faces of the projection belong to an {*hkl*} form, for they reflect light simultaneously with such a form which is developed on the corners of the crystal. One of the {*hkl*} faces of another projection is shown in fig. 32, looking approximately normal to (*hk*0). The latter, slightly rounded and mottled, appears on the right, and the edges of the layers seen above it are on a cube face, which is viewed obliquely. On the left is the projection, looking like a spiral staircase, the 'treads' being the cube planes (similar to those seen from above in fig. 31) and the 'rises' belonging to an {*hkl*} form.

In fig. 23 three sets of edges can be seen, which all belong to the same {*hkl*} form. Since growth would be likely to occur on any of them with equal facility, the layers may travel normal to the length of the step or laterally along it. The latter is well illustrated by some thin layers in fig. 25, which also shows that the forward movement of a layer may begin at the salient edge of the vicinal hillock. A projection appears at the corner of the layer, and gives rise to layers which have travelled along and not across the steps. In fig. 22 a 'transgression' can be seen. The vicinal hillock exhibits a sudden change of slope, and the boundary between the steep and shallow parts is transgressive, the layers of the steeper part cutting obliquely across those beneath. Thus the upper layers must have been travelling faster than those beneath. The steeper part has a convex surface. Convex surfaces are also seen on the green fluorite (fig. 33), in which the ellipses are due to layers parallel to the cube face growing out of the sloping side of the vicinal hillock. (Very smooth concave surfaces have been observed on a specimen from the Stotsfieldburn mine, Weardale.)

The effect of fractures on growth.—Within the 4-cm. cube are many veil-like fractures several centimetres in length, containing liquid and gaseous inclusions. It is evident that some of the fractures were present at the surface during growth, for they have affected the layer-pattern. Where two of them cross smooth areas of the faces (100) and (010) a line of triangular, tongue-like layers appears. In some places the fractures appear to have held up the layers temporarily, producing minute steps the smallness of which testifies to the relative ease with which the layers

ere able to bridge the gaps. Fig. 22 shows the only example of a marked obstruction which was found. A shallow triangular depression may be seen near the upper left-hand corner of (100). It is bounded by a fracture on one side of which many layers collected before the obstruction was overridden. By the time growth ceased the steep front of the arrested layers was two millimetres beyond this fracture.

Growth shadows. Most of the re-entrant corners which appear within the boundary of a cube face on the mauve fluorite have formed growth shadows. Layers initiated at one end of the re-entrant corner have not spread all round the obstructing corner but continue almost undeviated after passing it, thus building up a 'cliff', as seen in fig. 34. The end of the re-entrant corner is on the left and the layers in the upper part of the figure were spreading from left to right, and formed a cliff after passing the corner. No layers were initiated by this edge of the re-entrant corner.

Pyrite (plates VI and VII).

The cube.—Variation in the shape of the layers is well illustrated by pyrite, in which four-, six-, and eight-sided layers have been found on {100}. The crystal shown in fig. 35 is bounded by {100}, {111}, and an {*hkl*} form. The layers approximate to squares, but are somewhat irregular. The layer-edges are parallel to the intersections of {100} and {111}. Another crystal with the same forms has octagonal layers (fig. 36). The layer-edges are bounded by a diploid and pentagonal dodecahedron. Neither of these crystals shows the striations characteristic of pyrite.

In some crystals of pyrite it can be seen that the oscillatory combination of adjacent pairs of faces of {210}, which may or may not be truncated by {100}, is produced by vicinal hillocks. Each ridge of the striations is one vicinal hillock, which is hexagonal in plan and very much elongated. The long sides have pentagonal dodecahedral surfaces and each end of the hillock is bounded by two surfaces which are probably diploidal. The latter are sometimes clearly defined, but more often have an irregular character. Fig. 37 shows the hexagonal vicinal hillocks on a slightly striated cubo-octahedron from Elba, and fig. 38 shows them on a very deeply striated cube the locality of which is unknown.

The octahedron.—Most of the octahedron faces examined have equilateral triangular vicinal hillocks. Figs. 39 and 40 show one face of a crystal from Elba. On (111) the edges of the vicinal hillock have a clockwise rotation of some 15° from the edges of the face, which is bounded by

{321}. On $(1\bar{1}1)$ the rotation is anti-clockwise. Supplementary twinning brings about the coincidence of (111) and $(1\bar{1}1)$, and produces a 're-entrant angle' in the vicinal hillock, as shown in fig. 40, in which the black line is the twin-boundary. The surfaces of the vicinal hillocks appear to be diploidal, with a higher index than {321}.

Another habit is shown in fig. 41. The crystal is predominantly octahedral, with small {100}, {210}, and $\{hkk\}$ faces, the last forming the sharply defined edges of the vicinal hillock.

The orientation of the vicinal hillocks which are bounded by diploid on {111} is not constant, but shows different amounts of rotation on different specimens, even when allowance is made for the forms bounding {111}.

Apatite (plate VIII).

Interesting growth forms were found on the first-order prism and bipyramid of asparagus-stone from Durango, Mexico. The centre of a vicinal hillock on the prism is shown in fig. 42. Fig. 43 shows another part of the same hillock. The vicinal hillock is bounded laterally by prismatic surfaces, which form striations parallel to the *c*-axis, and at the ends by $\{hk\bar{l}m\}$ or $\{h.h.\bar{2h}.m\}$ surfaces. Several fractures, some of which have veil-like inclusions, cross the confused area at the centre of the vicinal hillock. The remarkable regularity of the layer-spacing in both the prismatic and pyramidal zones in fig. 43 suggests the operation of a rhythmic process controlling the initiation of layers. One of the vicinal bosses on the pyramid is shown in fig. 44.

A crystal from Cornwall shows a vicinal hillock on $(10\bar{1}0)$ with layer edges bounded by prismatic and $\{h0\bar{h}l\}$ surfaces (fig. 45). Layers are initiated at, or very near, the edge of the face. Hillocks of this habit have also been found on vanadinite crystals from the Apache mine, Arizona.

Quartz (plates VIII and IX).

Figs. 46 and 47 (smoky quartz found near Andermatt, Switzerland) show that the very characteristic striations normal to the *c*-axis on the prism faces of quartz crystals are caused by elongated vicinal hillocks. The long edges of the layers are bounded by rhombohedral surfaces and the short edges are bounded by trigonal trapezohedron or trigonal pyramid surfaces, on which growth is much more rapid than on the rhombohedral surfaces.[1] In fig. 47 growth shadows can be seen, caused

[1] Since this paper was read G. van Praagh and B. T. M. Willis have corroborated this explanation of the origin of the horizontal striations on quartz. (Nature, 1952, vol. 169, p. 623).

particles of impurity on the surface. Figs. 48 and 49, of a crystal from e same locality, show the usual triangular vicinal hillocks of the unit ombohedron. The straight layer-edges have rhombohedral surfaces, d give rise to striations parallel to the edge of the prism. One of the ost interesting features is the apparent ease with which the layers mpletely surround particles of impurity on the surface of the crystal. ese particles may be seen in all stages of encirclement in fig. 49. In . 50, a rhombohedron face of a crystal from the iron mines of Cumber- id, the remarkable regularity of spacing of the layer-edges seems to dicate a rhythmic process of layer-initiation.

Magnetite (plate IX).

The crystals have the combination {111} and {110}. The {111} faces are illiant, while the {110} faces are dull and laminated, being formed by e edges of layers which have spread across the octahedron faces. The uilateral triangular layers on {111} are bounded by an {*hhl*} form near 11} in orientation (fig. 51).

Celestine (plate IX).

Fig. 52 shows a vicinal boss on (011). It occurs on a crystal from ate, Gloucestershire, on the surface of a ghost crystal which has been -exposed by fracture along a parting. Other crystals from this district ve rectangular vicinal hillocks on {001} and {102}, both having one t of edges parallel to their common intersection and another set at right gles to it.

Tourmaline (plate IX).

Vicinal hillocks have been found on the basal plane of two crystals om Arassuahy, Brazil. One example is shown in fig. 53. On the other ystal the layers have the shape so characteristic of basal sections of urmaline, an 'equilateral triangle' in which the sides are rounded.

Growth forms on other minerals.

Vicinal bosses have been found on stilbite, and vicinal hillocks n galena, haematite, wulfenite, chessylite, diopside, chabazite, and rmotome.

Discussion of observations.

One of the most interesting points is the very widespread occurrence growth forms on crystals. The frequent appearance of curved surfaces n growth forms seems to support the assumptions underlying table I, at they are due to changes in the rate of initiation or spreading of the yers, or to both factors combined.

Frequency and origin of multimolecular layers.

Multimolecular layers have been seen during growth on many crysta of soluble substances, and the layers recorded here show such similari to them that they probably also grew as multimolecular layers. If t their development seems to be more common than is generally to b expected on theoretical grounds.

According to the dislocation theory of crystal growth multimolecu layers may be generated at low supersaturations by a single screw di location having a large Burgers vector, or by a closely spaced group dislocations. At high supersaturations multimolecular layers may initiated by the same mechanism, or they may arise from the aggregat or bunching of monomolecular layers formed by two-dimensional nucl tion or by dislocations.

In most of the growth forms illustrated in this paper a large number layers can be seen to have a common origin. (In some cases the origi has moved during growth, but the subsequent layers are again conce tric with the new origin, as in fig. 1.) This seems to suggest that grow may have been caused by dislocations, unless there is any reason wh successive layers formed by two-dimensional nucleation should be cor centric. Several further observations seem to suggest the action dislocations, although they do not prove it.

In a number of vicinal hillocks on topaz, particles of impurity wer seen at the points of origin of the layers. In baryte, layers were seen t emanate from points on the surface at which structural deformation ended (fig. 18). Both phenomena suggest the presence of structura discontinuities, and hence the possibility of dislocations, in Frank' sense,[1] existing at the initiation points. Since etching is likely to start a points of structural discontinuity, the etch pits at the centres of th elliptical layers on beryl (fig. 13) may have the same significance, bu it should be noted that there are many other etch pits from which n layers emanate.

The velocity of layer-spreading.

In the dislocation theory the rate of advance of monomolecular layer has been calculated. It has been shown that the rate is dependent on th degree of supersaturation, and increases with it. Although no detaile predictions have been made for multimolecular layers, it is suggeste that their velocity of spreading will likewise be governed by super saturation.

[1] F. C. Frank, Discuss. Faraday Soc., 1949, no. 5, p. 48.

Some of the observations presented in this paper suggest that the degree of supersaturation does not entirely determine the velocity of layer-spreading on a given face of a particular crystal. Consider the salient edge between two adjacent faces of a vicinal hillock. If the two faces are crystallographically equivalent the salient edge should be straight, because the layers on both sides of the edge should have the same growth velocity, and any change in the supersaturation should affect them identically. (Differences of supersaturation should be negligible over such small distances.) But, in fact, appreciable departures from rectilinearity occur, and the salient edge has a sinuous form, often with quite sharp curvatures. Such is the case for baryte in fig. 17. Highly sinuous salient edges between crystallographically equivalent forms have also been observed on {100} of fluorite and {001} of wulfenite. The layers on adjacent sides of a salient edge are clearly spreading with changing relative velocities. Measurement shows that in the lower part of fig. 17 the layers on the right of the salient edge were spreading just over five times as fast as the corresponding layers on the left. Immediately below this area the layers on the left were spreading with approximately eight times the velocity of those on the right. These are large factors; much larger than are likely to be caused by possible slight variations in supersaturation.

The origin of these sudden, large changes of relative velocity must be sought in the structure of the face rather than in the state of the solution. There is no evidence of lineage structure or rows of dislocations parallel to the edges of the layers which might have retarded them. If, however, the edges of these multimolecular layers are vicinal in character, as suggested by Bunn and Emmett, and the index of the surface changes during growth, a change in the growth velocity would also be expected. Vicinal forms are known to be very susceptible to changes of index during growth, through causes not yet understood. A difference of the index on adjacent sides of the salient edge would account for the phenomena observed.

Another phenomenon which does not seem to be explicable in terms of the dislocation theory is the transgression of higher layers over lower ones on fluorite in fig. 22. The upper layers of the vicinal hillock were evidently spreading faster than those beneath, and it is possible that the latter had even ceased to grow. This transgression could be accounted for if the rate of layer-spreading, at a given supersaturation, varied with the index of the form bounding the edges of the multimolecular layers. That growth may proceed on some parts of a crystal surface and not on

others is shown by the lack of growth at growth shadows, as seen i topaz, quartz, and fluorite (figs. 1, 3, 6, 47, and 34).

Another point of apparent disagreement with the predictions of d location theory is the steepness of many of the vicinal forms illustrat in this paper. Frank[1] contrasts the 'unusually steep vicinal faces' (e g 3·0°) caused by twinning in fluorite 'with 20′, which is the most whi is usually observed for growth pyramids centred on some ordina point in the face of a crystal'. He says that in the steep vicinal pyram on fluorite the rate of emission of growth fronts, compared with th rate of spreading, is of the order of ten times as great as when t initiating centre is a simple dislocation or group of dislocations.

No exact measurements have yet been made on the growth forms d scribed here, but in the case of topaz one side of a vicinal hillock seems show an inclination of over 18°. There is evidence that some of t vicinal hillocks have inclinations of over 5°. All the text-figures ar photomicrographs, except figs. 22, 33, and 50. In the photomicrograph any face appears dark when its normal is inclined at approximately 5° (o more) to the optic axis of the microscope. This suggests that the face of several vicinal hillocks have an inclination of 5° (or more), while som of the moderately dark faces may have inclinations of, say, 2° to 4° Twinning was not responsible for these steep growth forms, except i the case of fluorite and possibly also in figs. 46 and 47, both of quartz

Generalizations drawn from the observations.

Regularity of layer-spacing.—A phenomenon of interest is the remark able regularity of the layer-spacing around some initiation points, as i figs. 43 and 50, which strongly suggests a rhythmic process of layer initiation. W. E. Garner[2] has suggested that layer-initiation is associate with periodic changes of the supersaturation. These may also be th cause of the regular layer-spacing.

Changes of slope on vicinal hillocks.—Some vicinal hillocks sho sudden, discontinuous changes in the slopes of their surfaces. On vicinal hillock on the 4-cm. cube of fluorite shows five such changes Other examples are seen in fluorite (figs. 29 and 33), beryl (fig. 15), an topaz (fig. 2). Since the layers show no evidence of transgressions i these cases a probable explanation seems to be a sudden change in th rate of initiation. Sir Henry Miers noted sudden changes in vicinal form during growth.[3]

[1] F. C. Frank, Discuss. Faraday Soc., 1949, no. 5, p. 187.

[2] W. E. Garner, Discuss. Faraday Soc., 1949, no. 5, p. 187.

[3] H. A. Miers, Phil. Trans. Roy. Soc. London, Ser. A, 1904, vol. 202, p. 459.

Nature of growth surfaces.—It has been shown that growth often takes ace on a general form, not necessarily of lowest index, or on special rms of high index. In the case of fluorite, deposition is taking place on *kl*} surfaces when layers spread across {100}.

Effect of flaws and particles of foreign substances on spreading layers.— n fluorite most of the flaws which reach the surface seem to have ndered the spreading layers remarkably little. In quartz the layers pear to have spread round and engulfed solid particles of an impurity ith no indication of hindrance (fig. 49). In topaz and quartz the layers ssed the particles of impurity and left growth shadows (figs. 1, 3, 6, id 47).

Habit of growth forms.—The variable habit of growth forms is well ustrated by those on {110} of topaz and on {100} and {111} of pyrite gs. 1, 9, 35–38, 39, and 41). Bunn and Emmett (loc. cit., 1949, p. 121) ve observed a change in the shape of layers when specific soluble purities were added. The variation described here is probably due to e same cause.

Striations on crystals.—It has been shown how the striations on crystals several minerals are formed by the slow spreading of the layers on ne side or two opposite sides of a vicinal hillock, while the layers travel ster on the other sides (e.g. topaz, figs. 1, 4, 8, and 9; beryl, fig. 12; uartz, figs. 46, 48, and 49; and pyrite, figs. 37 and 38). It is hard to sualize any other mechanism which would account for the striations id oscillatory combinations. The surface of the striations may be plane, ncave, or convex.

The views of Bunn and Emmett.

The present work gives general support to their views on crystal owth by deposition on the high-index surfaces at the edges of layers. hey usually found only one system of spreading layers on each face. hat the author sometimes found quite large numbers of vicinal hillocks n a face may be due to the larger crystals observed, the majority of ces having areas between 0·25 and 2 square cm. In fig. 16 (beryl) the acing of the vicinal hillocks varies from about 0·1 to 0·3 mm. Bunn id Emmett (loc. cit., 1949, p. 120) and Bunn[1] record that layers very ten start from the centres of faces. The initiation points of the layers em to have a random distribution on the crystal faces. No evidence as been found to suggest that they are preferentially situated at face-ntres. Apart from two possible exceptions (figs. 19 and 45) none of the itiation points were situated at the corners or edges of crystal faces.

[1] C. W. Bunn, Discuss. Faraday Soc., 1949, no. 5, p. 140.

The growth layers were all observed on substances of low solubili
Even in the presence of mineralizers at high temperatures and pressur
it seems unlikely that these substances would have solubilities as h
as 6 %, which was the lowest solubility of any substance on wh
Bunn and Emmett saw layers during growth.[1]

The different habits of layers recorded here are very likely to ha
been produced by impurities, as noted by Bunn and Emmett (loc. c
1949, p. 121).

These authors suggest that the absence of flat surfaces on faces a
edges of layers during growth may be due to indiscriminate deposit
(Bunn and Emmett, loc. cit., 1949, p. 128). D. R. Hale[2] quotes
rounded surfaces on the basal pinakoid of artificially grown quartz
support of this view. A very high degree of order, in structure a
growth, is the outstanding characteristic of crystals. It seems wr
to invoke indiscriminate processes if ordered processes can expl
phenomena satisfactorily. Indiscriminate deposition suggests a rand
process. Random deposition would, in time, add uniform amounts
solute all over a face, and would not tend to make it rounded, eith
locally or as a whole. It seems more satisfactory to account for curv
surfaces as closely-spaced series of molecular layers which have grow
under one of the conditions which can give rise to curved surface profile
as shown in table I.

The author finds it hard to accept Bunn's view (loc. cit., 1949, p. 13
that diffusive flow, once started, can initiate layers. An inconceivabl
complex structure of diffusive flow would have to be evolved to deliv
sufficient solute to initiate layers at points about 0·2 mm. apart but n
between them. It seems more likely that the controlling factor is
structure-sensitive process of some kind.

It also seems improbable that once growth is started its velocity bea
no relation to supersaturation.

Growth of multimolecular layers.

A qualitative hypothesis is suggested below to account for th
observed growth properties of multimolecular layers, in particular th
variable velocities of spreading and the stopping and restarting
growth. It takes into account deposition on the high-index edges
layers while also allowing a relation between supersaturation and rat
of growth. Five postulates are made:

[1] C. W. Bunn and H. Emmett, Discuss. Faraday Soc., 1949, no. 5, p. 124.
[2] D. R. Hale, Discuss. Faraday Soc., 1949, no. 5, p. 189.

1. That growth velocity is a function of supersaturation, such that an increase of supersaturation increases growth velocity.
2. That in general, at a given supersaturation and temperature, forms of higher index grow more rapidly than those of lower index.
3. Each form has a critical supersaturation below which growth will not take place on a perfect face.
4. The value of the critical supersaturation bears an inverse relation to the index of the form, forms of low index having a high value of the critical supersaturation, and vice versa.
5. Deposition is entirely, or almost entirely, confined to the high-index surfaces forming the edges of the layers.

1 and 2 above are widely accepted: and 5 seems to be supported by bservation. There is a small amount of evidence for 3, but it is very ifficult either to prove or to disprove experimentally.

Nature and functions of growth layers.—The layers on crystals may be egarded as having two morphologically distinct parts with different inctions, the high-index edge, or *growth surface*, and the comparatively irge low-index plane upper surface, or *resting surface*. The growth sur-ace has an index which is, in general, high, but may vary during growth. ir Henry Miers has recorded changes of index of vicinal forms during rowth (loc. cit., 1904, p. 459).

If the present hypothesis is correct the growth surface will have a low ut variable value of the critical supersaturation required for growth, nd the low-index resting surface will have a high value of the critical ipersaturation, growth only taking place at high, perhaps very high, upersaturations. A crystal placed in a solution of moderate supersatura-on will grow by deposition on the growth surfaces, thus extending the esting surfaces, on which no deposition is taking place.

This concept of growth surfaces and resting surfaces on crystals mphasizes the dual functions of the layers. The growth surface pro-ides a surface on which growth can take place easily while the plane esting surface keeps the crystal polyhedral, and tends to minimize the rface energy of the whole crystal. In fluorite, for example, the growth rface is {*hkl*} and the resting surface is {100}. The cube appears to be ie equilibrium form for fluorite grown from solution. Sir Henry Miers ays, 'The habit of fluor is remarkably constant; no mineral crystallises nore persistently in cubes'.[1] If the cube is indeed the equilibrium form , is the one best suited to be the resting surface, as it possesses the owest surface energy.

[1] H. A. Miers, Mineralogy. 2nd edit., 1929, p. 357.

Velocity of spreading of growth layers.—Sinuous edges betwee 'crystallographically equivalent' faces of vicinal hillocks, caused b differential growth rates, could be accounted for by a difference in t index of the growth surfaces on the two sides. The 'equivalence' wou apply to the zone in which the faces lie, but not to their indices. Th in fig. 17 all the growth surfaces would have an index {*hhl*}, but the val of *l* would vary.

Stopping and restarting of growth.—The stoppage of growth of a fa has been observed by Bunn (loc. cit., 1949, p. 132) and S. P. F. Hu phreys-Owen.[1] The latter has also seen the restarting of growth According to this hypothesis growth will cease when the growth surfa changes from one of higher index to one of lower index, if the critica supersaturation for growth of the new face is higher than the supe saturation prevailing in contact with the crystal. The restarting o growth may be due to an increase in the supersaturation above t critical value for the new face, or to a dynamic interchange of a few io or molecules between the crystal and its environment, producing minute element of face with a low enough critical supersaturation t allow growth to proceed. The latter suggestion would agree wit Humphreys-Owen's observation that the restarting of growth began a a single point on the face.

Justification of high-index surfaces.—A crystal which is in equilibriu with its exactly saturated solution will be bounded by the form o combination of forms, the equilibrium form(s), giving the lowest tota surface energy for the crystal. Equilibrium forms can only be expecte to appear at negligibly small supersaturations and are of theoretica rather than practical importance. They should not be expected, no should their non-appearance be regarded as anomalous, on crystal grown at appreciable supersaturations. In the thermodynamic sens crystallization is a spontaneous process and therefore not a reversibl reaction. Thus the maximum energy cannot be obtained from th change. Of the total energy potentially available in the reaction th major part will be liberated as heat, but the rest will be retained a surface energy, so that the total surface energy of the crystal will b above the minimum value. This implies that forms will be develope which have a higher surface energy than the equilibrium form(s).

Stimulation of growth by twinning.

In fluorite growth may be stimulated by twinning. Sir Henry Mie (loc. cit., 1929, p. 358) states, 'In these twins, at the exact point where a

[1] S. P. F. Humphreys-Owen, Discuss. Faraday Soc., 1949, no. 5, p. 144.

dge emerges, the cube-face is often raised into a very low pyramid consisting of four vicinal faces {*hk*0}'. In the same connexion Frank (loc. it., 1949, p. 187) states, 'Each face of these twin crystals shows a pronounced growth pyramid of unusually steep vicinal faces centred on the ommon line of the twin faces which meet on the composition plane'. The latter is taken to mean that the centre of the growth pyramid may occupy any position on any of the three lines common to the cube face nd the re-entrant corner. The author's observations suggest that *steep* icinal pyramids only form at the exact point of contact of the *edge* of a e-entrant corner with a cube face. A few layers may sometimes be seen o have spread from the common lines of the cube face and re-entrant orner, but no steep vicinal pyramids have been observed in such positions. The edges of the re-entrant corner seem to be particularly active n initiating layers, even when bevelled by {*hk*0}. The layers then start rom the edges common to adjacent pairs of {*hk*0} faces, and not from he edges between {*hk*0} and {100}. All three edges of one re-entrant corner nay initiate layers, as on the 4-cm. cube, two edges of its re-entrant orner being seen in figs. 27 and 28. The layers may be square, 'squares' with gently curved sides, or octagonal in plan. When only one edge seems to have initiated layers the interesting question arises as to why he other two edges were not similarly active.

The phenomenon of the stimulation of growth by the re-entrant angles of twins has been raised by I. N. Stranski[1] and F. C. Frank (loc. cit., 1949, p. 186). While it certainly applies in many cases to fluorite, it seems doubtful if it applies to all twins with re-entrant angles. The very thin crystals of cerussite, tabular on {010}, which form stellate trillings do not support this contention, and many other mineral examples could be cited in this connexion. The re-entrant angles of some twins may be self-perpetuating, while others may not, as in the cube and octahedron, respectively, twinned on the spinel law. In the latter case, if stimulation of growth occurred in the re-entrant angle, it would soon cease to exist, and so would the stimulus. The very presence of the re-entrant angle in these twins argues against its effectiveness in promoting growth.

Effect of mode of growth on the Donnay-Harker hypothesis.

This hypothesis[2] postulates that the morphological importance of a form is proportional to its reticular density. If growth takes place by two-dimensional nucleation and subsequent spread of the layers, the

[1] I. N. Stranski, Discuss. Faraday Soc., 1949, no. 5, p. 69.

[2] J. D. H. Donnay and D. Harker, Amer. Min., 1937, vol. 22, p. 446. [M.A. 7-241.]

growth-velocity of a face is entirely determined by the rate of initiation of layers and is unaffected by their rate of spreading. If the Donnay-Harker hypothesis is true this implies an inverse relationship between reticular density and rate of layer-initiation.

On the other hand, growth may take place by the spreading of multimolecular layers originating at screw dislocations. If, as suggested above, the growth-velocity of a face, at a given supersaturation, depends on the nature of the growth surface at the edge of the layer, the change of index which occurs on vicinal surfaces during growth would make the calculation of reticular density, and hence of morphological importance, impossible. In fluorite it would be useless to calculate the reticular density of {100} in order to determine the morphological importance of the cube, if growth is taking place on {*hkl*} surfaces; while in topaz a layer which has spread across {110} has grown on three different kinds of surface, {*hk*0}, {*kh*0}, and {*hkl*}, and each of these surfaces might consist of several forms in the zone concerned.

Explanation of Plates I–IX.

Plate I.

Fig. 1. Topaz, Cornwall? (110), *c*-axis parallel to length of page. Steep, dark side of vicinal hillock faces (120). Concave surface on left faces (100). ×55.

Fig. 2. Topaz, same as fig. 1. Shows fine curved lines. Concave surface on right faces (120). ×55.

Fig. 3. Topaz, Cornwall? (110), *c*-axis parallel to length of page. Steep side of vicinal hillock faces (120). Two growth shadows near apex of hillock formed by particles of impurity. ×55.

Fig. 4. Topaz, Cornwall? (110). Steep side of vicinal hillock forms striations parallel to *c*-axis. Striations have concave surfaces. ×55.

Fig. 5. Topaz, Cornwall? (110), *c*-axis parallel to length of page. Angle of 4° between edges of adjacent vicinal hillocks indicates high-index pyramidal surfaces. ×55.

Fig. 6. Topaz, Cornwall? (110). Striation, in shadow, parallel to *c*-axis. Particle of impurity at apex of vicinal hillock causes long growth shadow. ×55.

Plate II.

Fig. 7. Topaz, Thomas Range, Utah. (110), *c*-axis parallel to length of page. Steep side of vicinal hillock faces (120). ×43.

Fig. 8. Topaz, Ouro Preto, Brazil. (120). Longer striations parallel to *c*-axis. ×43.

Fig. 9. Topaz, Nigeria? (110), *c*-axis parallel to length of page. D-shaped vicinal hillock; steep side faces (120). ×33.

FIG. 10. Topaz, Ouro Preto, Brazil. (110). Arcuate layers form striations parallel to *c*-axis. ×43.

FIG. 11. Topaz, Ouro Preto, Brazil. (120). D-shaped vicinal hillock showing transition from quadrilateral to arcuate layers. Steep side faces (110). ×50.

FIG. 12. Beryl, Brazil. ($10\bar{1}0$). Longer sides of vicinal hillock form striations parallel to *c*-axis. Sinuous layers are asymmetric extension of another vicinal hillock. ×36.

PLATE III.

FIG. 13. Aquamarine, Spitzkopje, South-West Africa. ($11\bar{2}0$), *c*-axis parallel to length of page. Vicinal bosses, each with an etch pit at the centre. ×33.

FIG. 14. Aquamarine, Spitzkopje, South-West Africa. ($11\bar{2}0$), *c*-axis parallel to length of face. Vicinal boss with concave surfaces. ×33.

FIG. 15. Aquamarine, Spitzkopje, South-West Africa. ($11\bar{2}1$). Vicinal hillock showing convex curvature and abrupt change of slope. Trace of *c*-axis parallel to length of page. ×33.

FIG. 16. Aquamarine, Spitzkopje, South-West Africa. (0001). Edges of hexagonal layers parallel to intersections of $\{10\bar{1}0\}$ and {0001}. ×33.

FIG. 17. Baryte, Frizington, Cumberland. (001). In upper part of the figure layers spread approximately from left to right, prevented from spreading downwards by the ledge or step. When end of step was reached layers spread round it and returned along lower side, from right to left. ×33.

FIG. 18. Baryte, Frizington, Cumberland. (001), *b*-axis coincides with the major axis of the parallelogram-shaped layers. Layers are initiated at the ends of steps. ×33.

PLATE IV.

FIG. 19. Baryte, Frizington, Cumberland. (110). Long edges of layers parallel to *c*-axis. Layers initiated at, or very near, edge of face. ×33.

FIG. 20. Baryte, same specimen as fig. 19. (110). Long edges of layers normal to *c*-axis. Edges of layers stepped. ×33.

FIG. 21. Baryte, Silverband mine, Westmorland. (011). Circular vicinal bosses. ×36.

FIG. 22. Fluorite, Weardale, County Durham. Part of (100) face of 4-cm. cube, showing transgression of steeper, convex part of vicinal hillock over layers beneath, projection of layers along the salient edge, and depression in top left-hand corner where layers were hindered by a fracture. ×2·1.

FIG. 23. Fluorite, Weardale, County Durham. (100) face of 4-cm. cube, showing part of salient edge of vicinal hillock. Layers have travelled from right to left along the steps from the salient edge. ×55.

PLATE V.

FIG. 24. Fluorite, Weardale, County Durham. (100) face of 4-cm. cube, showing part of salient edge of vicinal hillock. The layer-edges on adjacent sides are not at right angles, as they would be if growth had taken place on an $\{hk0\}$ form. ×36.

Fig. 25. Fluorite. (100) face of 4-cm. cube, showing a part of the salient edge a which projecting layers appear. They give rise to layers which trave laterally along the steps on the faces of the vicinal hillock. ×36.

Fig. 26. Fluorite. (100) face of the 4-cm. cube, showing a part of the salient edg at which a thick layer appears to transgress across two thinner layers ×36.

Fig. 27. Fluorite. (001) face of the 4-cm. cube. Vicinal hillock initiated by re-entrant corner of twin crystal. The layers are octagonal, and repre sent an {*hkl*}, not an {*hk*0}, vicinal form. ×36.

Fig. 28. Fluorite. As fig. 27; octagonal layers initiated by another edge of the same re-entrant corner. ×36.

Fig. 29. Fluorite, County Durham. A cube face. Surface of vicinal hillock on the green fluorite, showing two abrupt changes of slope and three pr jecting tongue-like layers. ×33.

Plate VI.

Fig. 30. Fluorite, County Durham. Face of vicinal hillock on cube face of the green fluorite. Layers with zigzag edges; an aggregate of many triangular tongues. × 50.

Fig. 31. Fluorite, Weardale? View of the mauve fluorite normal to (100) which reflects the light. Triangular layers project from the (dark) (*hk*0) face. ×36.

Fig. 32. Fluorite. Another projection on same specimen as fig. 31, but viewed approximately normal to the (*hk*0) face (mottled). Upper surfaces of projections bounded by {100}, lower surfaces by {*hkl*}. ×36.

Fig. 33. Fluorite, County Durham. Cube face of the green fluorite showing steep vicinal hillock with convex surfaces, curved edges of the layer-aggregates forming the faces of the hillock and ellipses due to layers parallel to the cube face projecting from the sloping surface of the vicinal hillock. ×2·2.

Fig. 34. Fluorite, Weardale? (100). Growth shadow (broad dark band running left to right) on the mauve fluorite caused by re-entrant corner of twin crystal (black triangle on left). ×36.

Fig. 35. Pyrite. (100). Irregular square layers with edges parallel to intersections of {100} and {111}. ×110.

Plate VII.

Fig. 36. Pyrite. (100). Octagonal layers with edges parallel to intersections of {100} with {*hk*0} and {*hkl*}. ×33.

Fig. 37. Pyrite, Elba, Italy. (100). Hexagonal layers with length parallel to striations on (100). Bounding surfaces on long edges are {*hk*0}, on short edges probably {*hkl*}. ×36.

Fig. 38. Pyrite. (100). Very deeply striated cube. Shows one striation, formed of elongated vicinal hillock, similar in habit to fig. 37. ×50.

Fig. 39. Pyrite, Elba. (111). Triangular vicinal hillock probably bounded by diploidal surfaces. ×36.

1

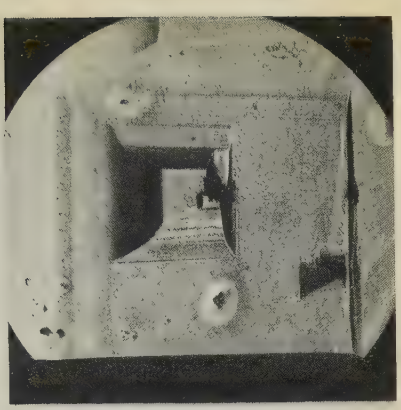

2

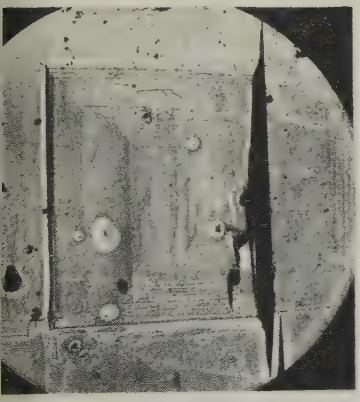

3

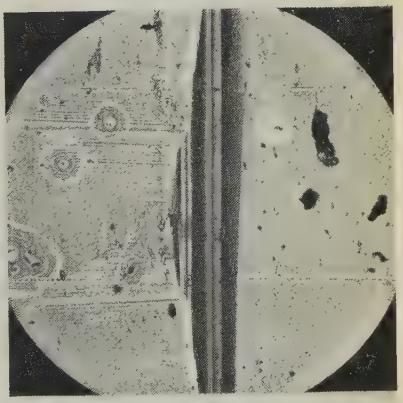

4

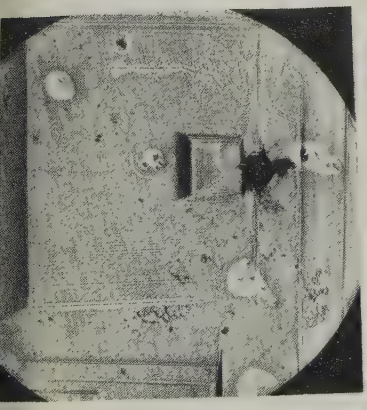

5

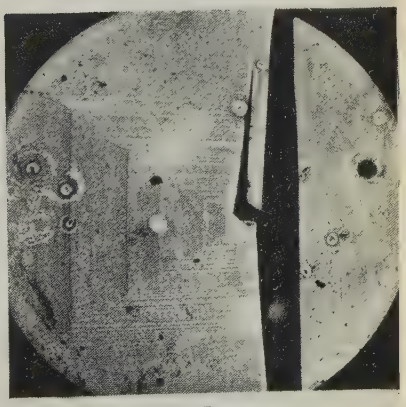

6

A. F. Seager: Surface Structure of Topaz

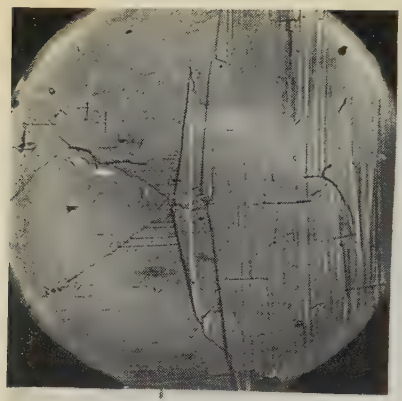

7

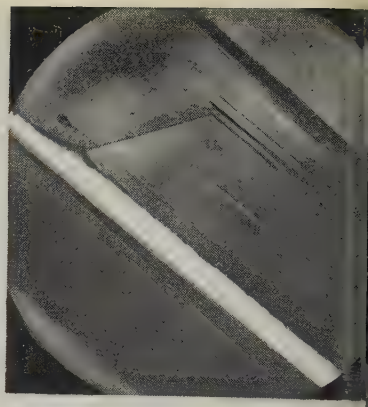

8

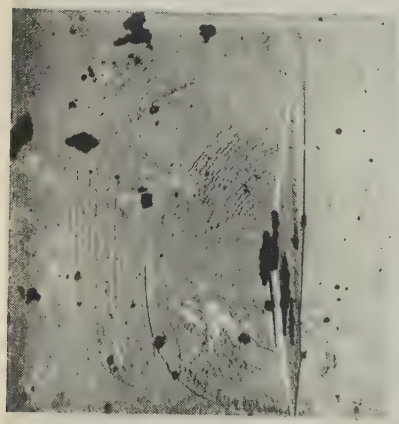

9

10

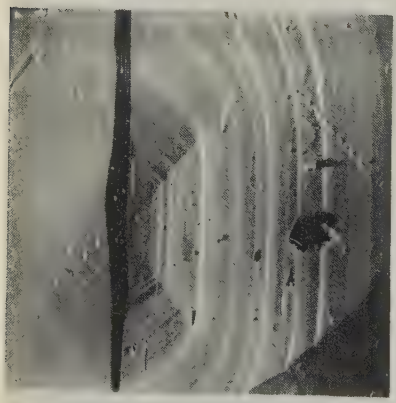

11

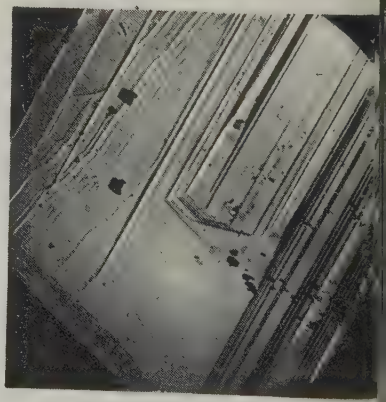

12

A. F. Seager: Surface Structure of Topaz and Beryl

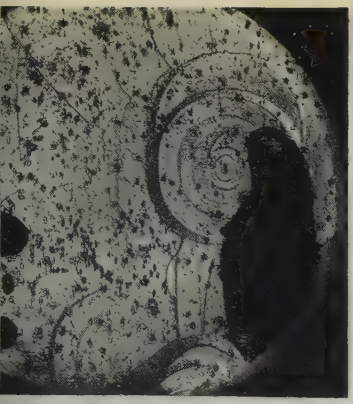

13

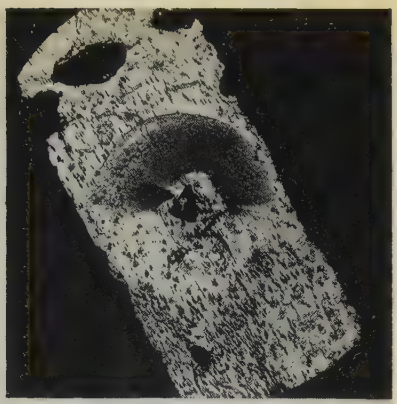

14

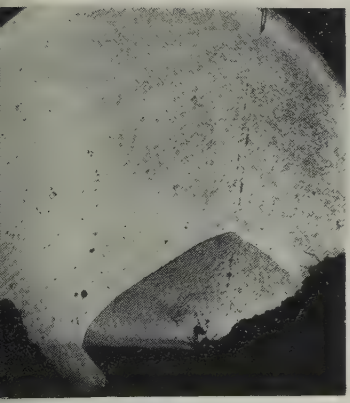

15

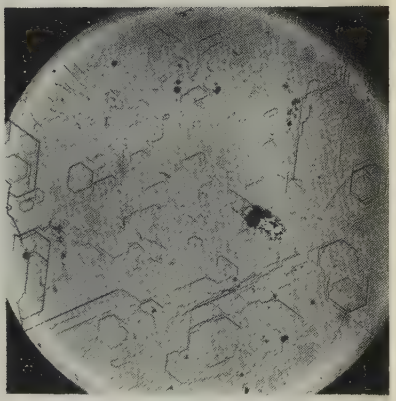

16

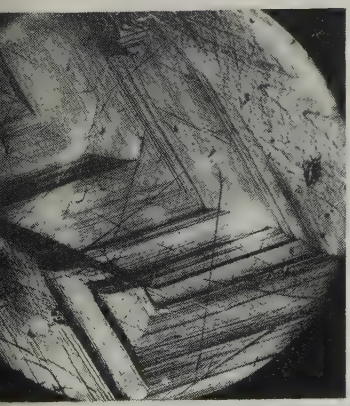

17

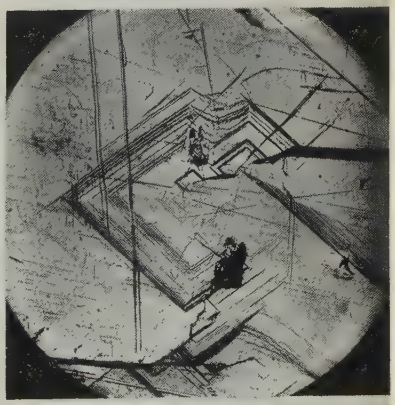

18

A. F. Seager: Surface Structure of Beryl and Baryte

19

20

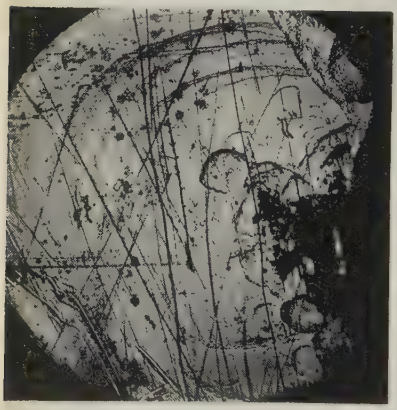

21

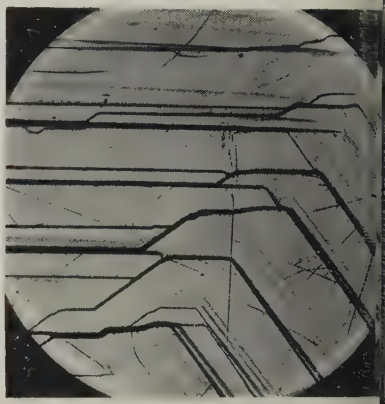

23

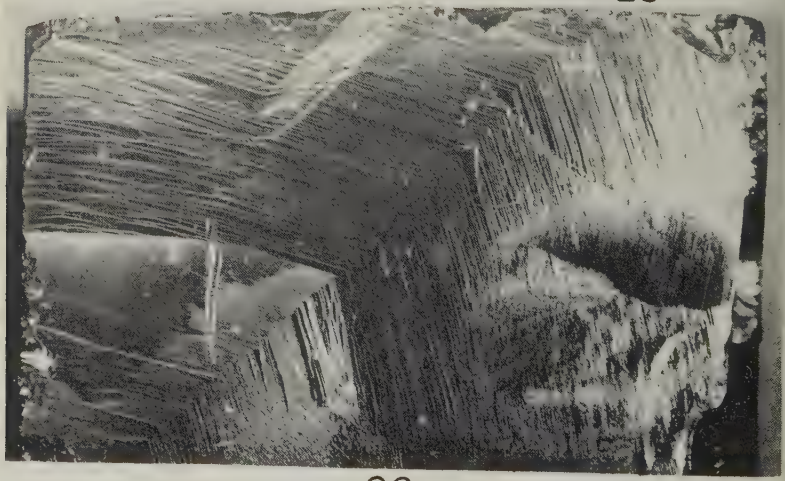

22

A. F. Seager: Surface Structure of Baryte and Fluorite

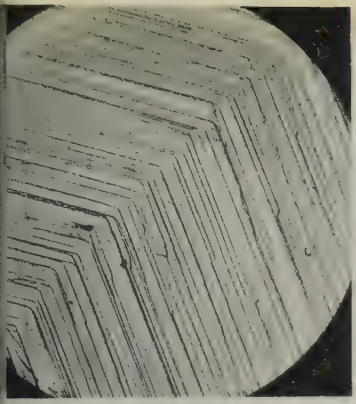

24

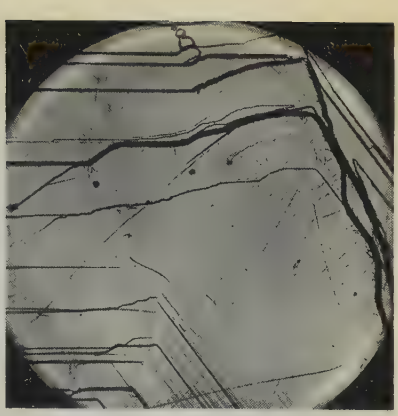

25

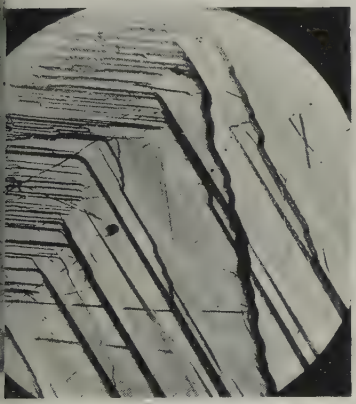

26

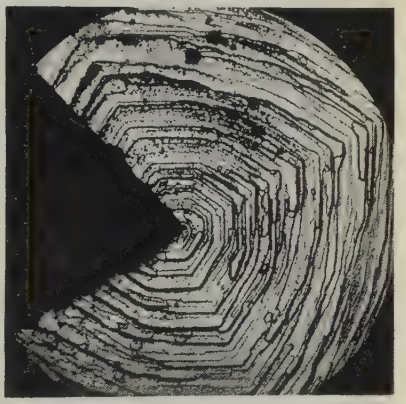

27

28

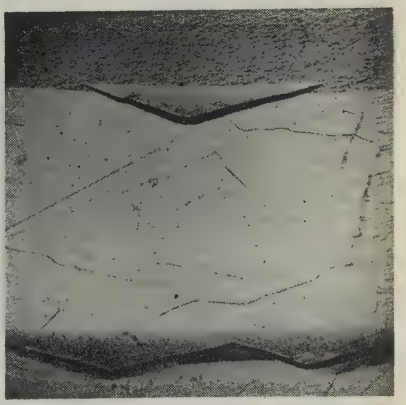

29

A. F. Seager: Surface Structure of Fluorite

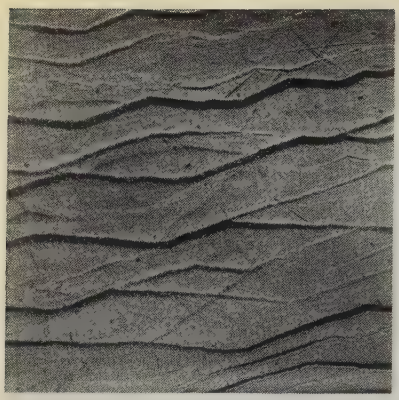

30

31

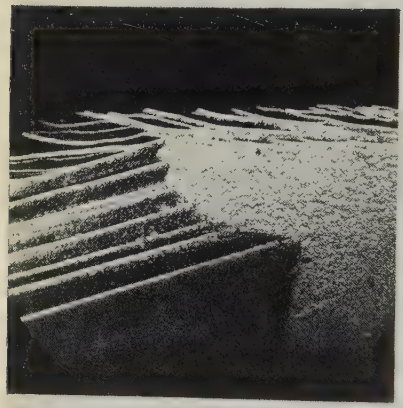

32

33

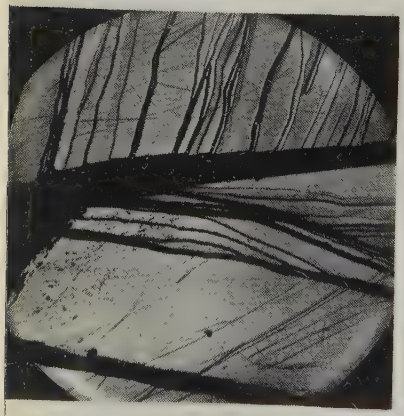

34

35

A. F. Seager: Surface Structure of Fluorite and Pyrite

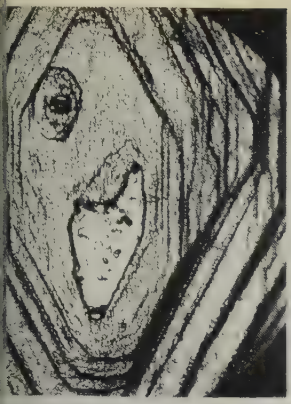

36

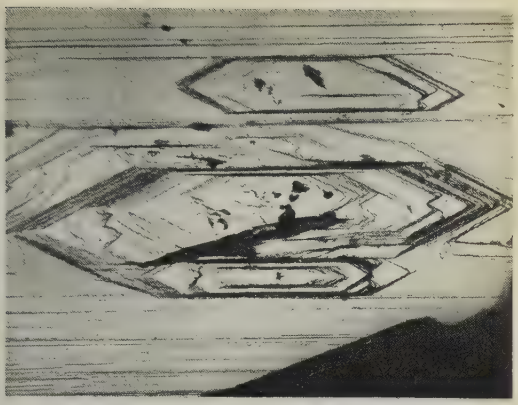

37

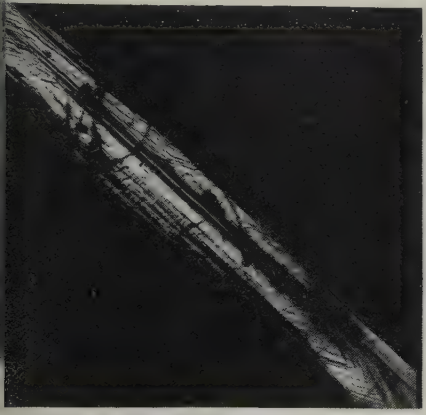

38

39

40

41

A. F. Seager: Surface Structure of Pyrite

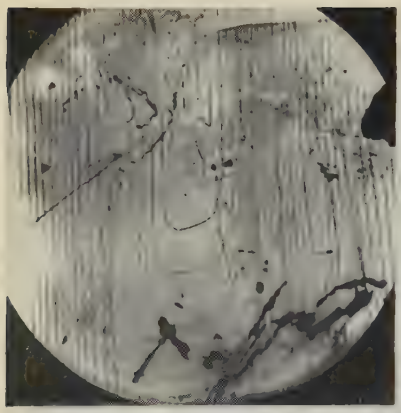

42

43

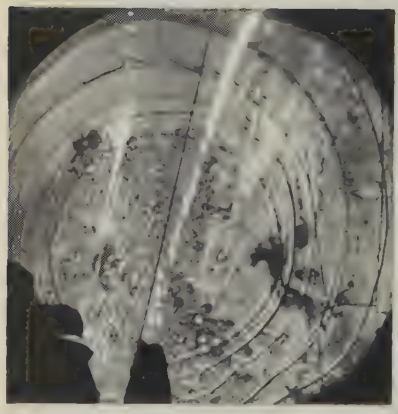

44

45

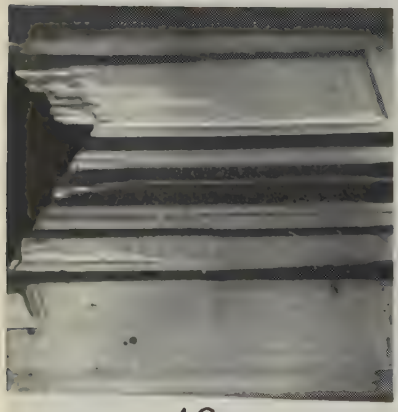

46

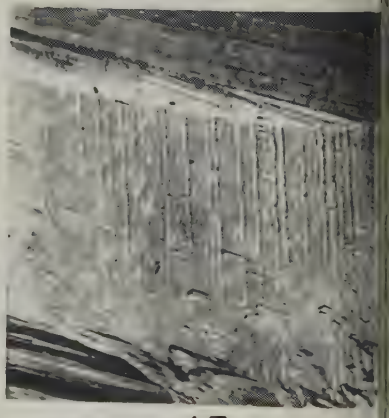

47

A. F. SEAGER: SURFACE STRUCTURE OF APATITE AND QUARTZ

48

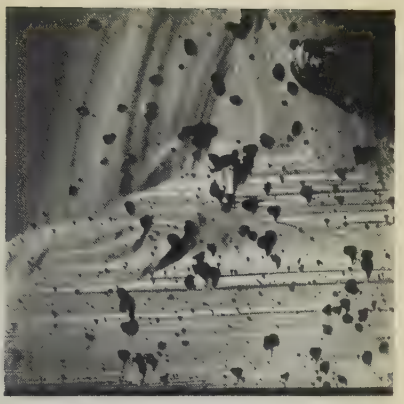

49

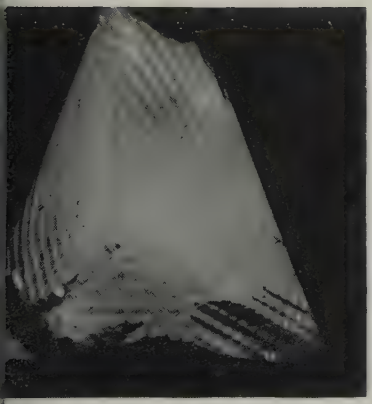

50

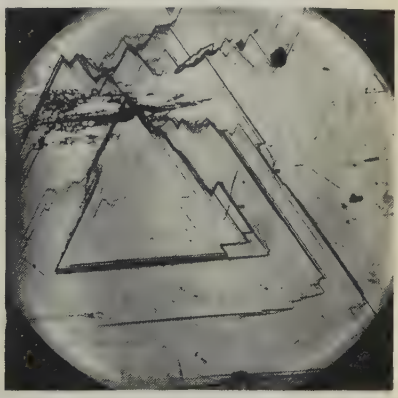

51

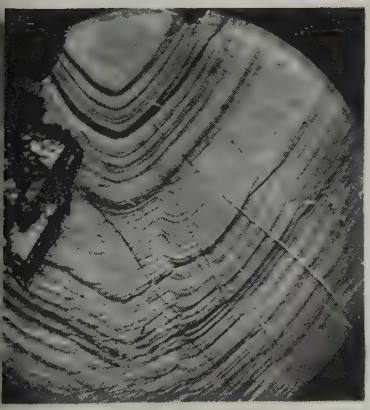

52

53

A. F. Seager: Surface Structure of Quartz, Magnetite, Celestine, and Tourmaline

FIG. 40. Same crystal as fig. 39. (111). Re-entrant angle formed in vicinal hillock by supplementary twinning. Black line is the twin boundary. ×33.

FIG. 41. Pyrite. (111). Very regular layers bounded on their edges by an {*hkl*} form. ×36.

PLATE VIII.

FIG. 42. Apatite, Durango, Mexico. (10$\bar{1}$0), *c*-axis parallel to longer layer-edges. Centre of vicinal hillock. It is intersected by several fractures. ×33.

FIG. 43. Apatite, Durango, Mexico. Another part of vicinal hillock seen in fig. 42, showing remarkably regular spacing of the layer-edges. ×33.

FIG. 44. Apatite, Durango, Mexico. Circular vicinal boss on pyramid face. ×33.

FIG. 45. Apatite, Cornwall. (1010). Longer striations parallel to *c*-axis. Vicinal hillock with sinuous salient edge, initiated at, or very near, edge of face. ×33.

FIG. 46. Smoky quartz, near Andermatt, Switzerland. (10$\bar{1}$0). The longer edges of the vicinal hillocks form the characteristic striations normal to the *c*-axis. ×33.

FIG. 47. Smoky quartz, near Andermatt, Switzerland. Same crystal as fig. 46. A similar vicinal hillock on (10$\bar{1}$0) with growth shadows caused by particles of impurity. ×33.

PLATE IX.

FIG. 48. Smoky quartz, near Andermatt, Switzerland. Vicinal hillock on rhombohedron face forms striations parallel to prism edge. ×33.

FIG. 49. Smoky quartz, near Andermatt, Switzerland. Same crystal as fig. 48, and showing particles of impurity in all stages of encirclement by the layers. ×33.

FIG. 50. Quartz, Cumberland. Remarkable regularity of layer spacing on a rhombohedron face. ×4·3.

FIG. 51. Magnetite. (111). ×33.

FIG. 52. Celestine, Yate, Gloucestershire. (011). Vicinal boss on surface of a ghost crystal re-exposed by fracture along a parting. ×33.

FIG. 53. Tourmaline, Arassuahy, Minas Geraes, Brazil. Triangular growth layers on basal plane. ×33.

Grateful acknowledgement is made of a grant from Birkbeck College for the publication of the plates in this paper.

This paper forms part of a thesis approved for the degree of Ph.D. by the University of London.

Observations on the colouring of pink and green zoned tourmaline.

By J. E. S. Bradley, B.Sc., Ph.D., and Olive Bradley, B.Sc., Ph.D.

Geology and Physics Departments, King's College, University of London.

[Read March 27, 1952.]

THIS investigation was concerned with two aspects of the colour-zoning in tourmaline: firstly, the origin of the green and pink colours; secondly, the reason for the apparent incompatibility of these two forms. Much of the previous work on the colour of tourmaline has involved the use of emission spectra.[1,2,3] This method provides information as to which elements are present; it does not, of course, indicate which of the twenty or so elements identified is responsible for the colour, although it may be possible to infer this. Absorption spectra, on the other hand, are directly concerned with colour. They have been employed quite extensively in Germany,[4,5] and more recently in Russia,[6,7] but the earlier data and instruments were often inadequate. The last decade has seen marked improvements in the technique of absorption spectroscopy, particularly in the development of photoelectric methods for the quantitative recording of spectra, and the method is likely to prove one of increasing value.

The tourmalines studied form part of the collection of the late Prof. W. T. Gordon, and are from San Diego County, California. The pink-green colour zoning is most generally parallel to the basal pedion,

[1] G. Carobbi and R. Pieruccini, Spectrographic analyses of tourmalines from the island of Elba with correlation of color and composition. Amer. Min., 1947, vol. 32, pp. 121–130. [M.A. **10**–317.]

[2] J. P. Mateos, El color en la tourmalina. Notas y Comunic. Inst. Geol. y Minero de España, 1944, no. 13, pp. 217–289. [M.A. **9**–198.]

[3] T. W. Warner, Spectrographic analysis of tourmaline with correlation of color and composition. Amer. Min., 1935, vol. 20, pp. 531–536. [M.A. **6**–266.]

[4] E. Kolbe, Über die Färbung von Mineralien durch Mangan, Chrome und Eisen. Neues Jahrb. Min., Abt. A, 1935, Beil.-Bd. 69, pp. 183–254. [M.A. **7**–135.]

[5] B. Lange and W. Eitel, Über eine Methode zur Untersuchung der Absorption.... Tschermaks Min. Petr. Mitt., 1931, vol. 41, pp. 435–452. [M.A. **5**–122.]

[6] N. M. Melankholin, On the colouring of magnesial-ferruginous mica. Trav. Lab. Crist. Acad. Sci. URSS, 1940, no. 2, pp. 61–72. [M.A. **9**–197.]

[7] S. V. Grum-Grzhimailo, On the colouring of minerals caused by chrome. Trav. Lab. Crist. Acad. Sci. URSS, 1940, no. 2, pp. 73–86. [M.A. **9**–190.]

hough it may be parallel to the prism faces. This latter zoning is s common, but is often shown by the larger crystals, characteristically th a less strongly marked colour change. Irregular patchy pink-green louring, unrelated to the crystal form, is most uncommon. Where the lour changes from a strong pink to a strong green there is usually a arp contact between the two zones. Where a pink crystal grades into een, it often does so by means of an intermediate colourless zone. ie colouring of both pink and green forms can be markedly inhomo- neous, although this is not often the case. A common feature of this lifornian tourmaline is the occurrence of long cylindrical cavities nich run parallel to the *c*-axis of the crystal.[1] These are possibly egative' crystals, since they may be striated internally in the same ay as the prism face is striated. It is this material that is used for tting 'cat's-eye' cabochons. It seems likely that the cavities are formed der conditions of rapid growth and it would be satisfactory to be able correlate the different coloured forms with different conditions of owth. However, the cavities occur equally in the pink and green rms; they may stop sharply at the boundary between the two, or they ay pass from one to the other without interruption. It appears likely at the change from pink to green or vice versa, with the boundary rallel to a crystal face, marks a change in the composition of the rent solution during growth. The existence of the cavities is controlled r the rate of formation of the crystals; a change in the rate of forma- on may or may not coincide with the change in composition.

The instrument used to measure the absorption was a Hilger medium uartz-spectrograph. This has been fitted with a photo-electric attach- ent which moves a vacuum photocell slowly across the emergent light eam. The changes in the intensity of the light are recorded by the notocell and are used to produce corresponding changes in the position a small light beam. The movements of this beam are recorded on notographic paper on a revolving drum, thus providing automatically n accurate and detailed record of the absorption. The wave-length gion studied was from 350 to 600 mμ. The tourmaline crystals were ctioned parallel to the *c*-axis, $\frac{1}{8}$–$\frac{1}{4}$ inch thick, and both sides of the slice ere polished carefully. A polaroid plate placed between the light source n over-run thin-envelope car-headlamp bulb) and the crystal section ade it possible to measure the absorption of both ordinary and extra-

[1] R. Johns and L. A. Wright, Gem and lithium-bearing pegmatites of the Pala strict, San Diego County, California. Special Rep. Division Mines, California, 51, no. 7-A, 72 pp. [M.A. **11**–487.]

ordinary rays. Both the pink and green crystals, when free fro inclusions and internal cracks, gave well-defined and reproducib curves. Crystals with a brownish tinge were unsatisfactory and co not be used for absorption measurements; it appears that the bro colour is due to finely divided included material.

The absorption curves of a number of solutions coloured by meta ions were measured by the same method for the purposes of compari

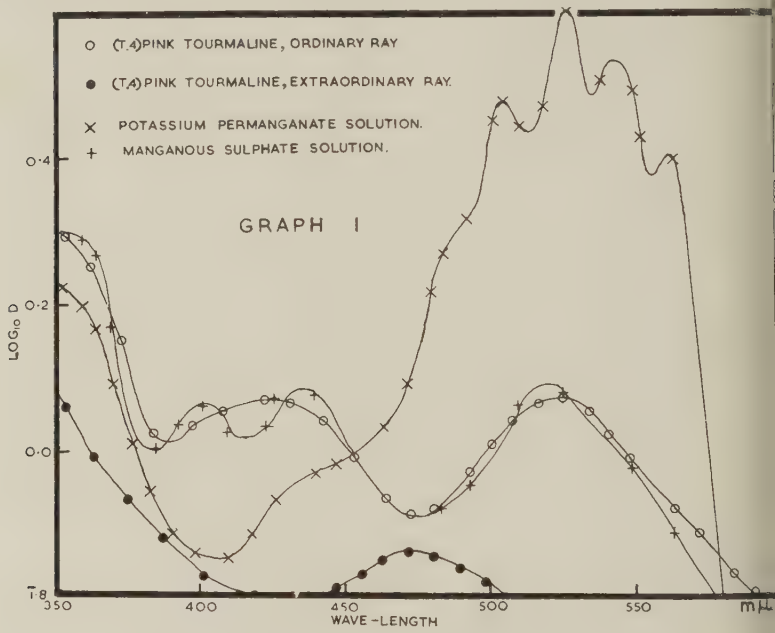

Fig. 1. Absorption curves of pink tourmaline.

Absorption curves (graphs 1–4).[1]

Graph 1.—It can be seen that the absorption of the ordinary ray pink tourmaline corresponds very closely to that given by manganou sulphate solution, although some of the fine structure is lacking. Th absorption maxima are in the yellow-green and blue-violet, so that ligh emerging from the crystal is enriched in red and blue-green. Th absorption curve of pink tourmaline has been compared to that potassium permanganate (Kolbe, 1935, loc. cit.). There is clearly n justification for such a comparison in the case of the Californian crystals

[1] D = optical density = $\log_{10}$ (incident intensity/(transmitted intensity).

A solution containing the trivalent manganese ion (manganic alum
es an absorption curve somewhat resembling that of the permanganate
MnO_4, but without the fine structure and with much less contrast
tio of maximum to minimum). It also has a subsidiary peak in the
e region so that the light transmitted is mainly red and violet. The
Mn^{+++} ion is unstable, except in the presence of excess acid, so it is
likely to be the cause of the colour of tourmaline.

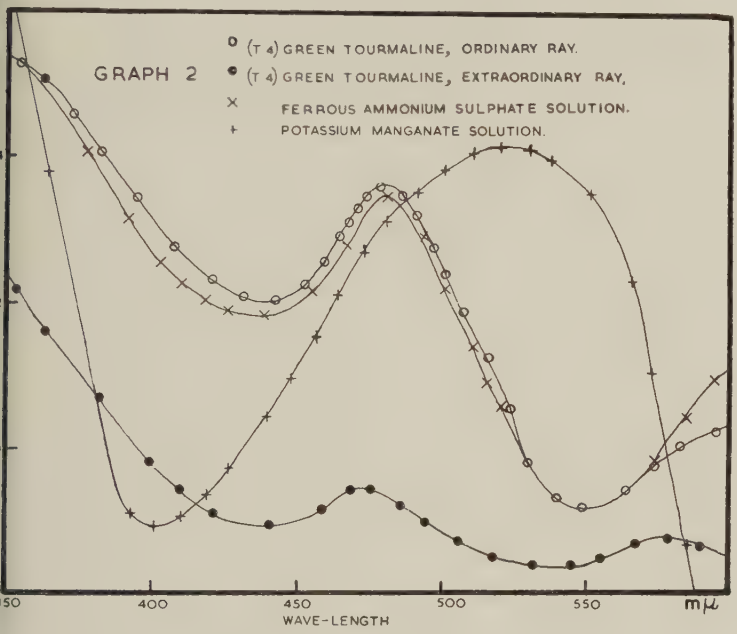

FIG. 2. Absorption curves of green tourmaline.

Graph 2.—The absorption curve of the ordinary ray of green tourmaline
very similar to that given by ferrous ammonium sulphate solution:
e maximum absorption for both is in the blue-green and red regions
d there are minima in the blue and yellow-green. This is unlike the
rve given by the rather unstable brownish-green solution of potas-
ım manganate (K_2MnO_4).

Graph 3.—In the green part of the crystal (T. 4) the absorption of the
dinary and extraordinary rays are similar in form; they differ in
tensity and in the position of the absorption maxima. There is only
small shift in the position of the latter, but it is in the sensitive
ue-green region of the spectrum and results in the clearly marked

pleochroism seen in the hand-specimen. The absorption of the extra-ordinary ray of the pink crystal, while almost negligibly small, shows the general form of the green absorption curve.

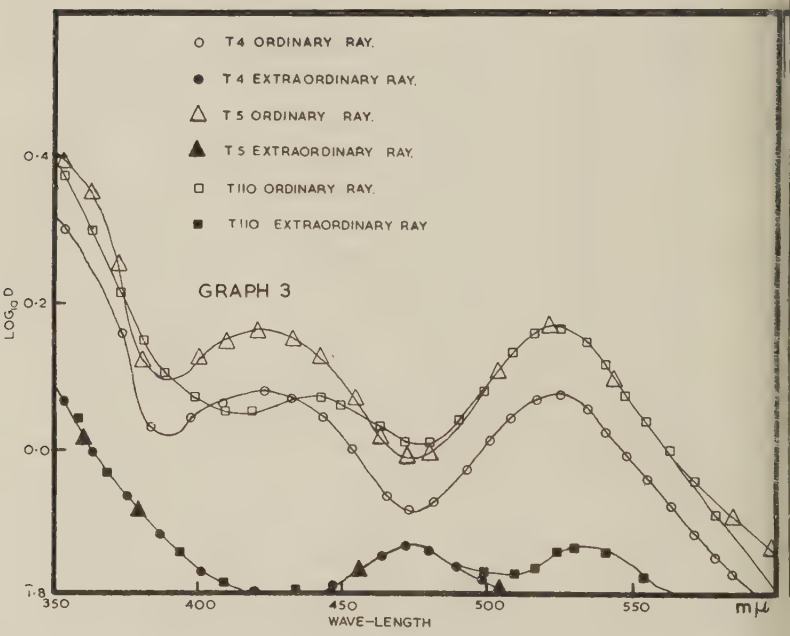

Fig. 3. Comparison of absorption curves of pink and green tourmaline.

Graph 4.—This graph compares the absorption of the pink sections of three crystals. Two of the crystals (T. 4 and T. 5) agree closely although with some difference in the depth of colour. It is considered that the general form of these curves is typical of the absorption of this group of crystals. T. 110 diverges from the normal: the pink colour is stronger than usual and is also more complex. In addition, this crystal reacts differently on heating and may be from another locality—possibly Brazil.

A comparison of the green portions of the same three crystals gives a graph similar to graph 4.

Thus from the absorption curves it may be concluded that the pink colour is due mainly to divalent manganese; the green colour to divalent iron. It is important to see how far these conclusions are endorsed by chemical analyses and by the behaviour of the mineral on heating: also

so suggest if possible why crystals are either pink or green, but never pink plus green (the brownish tinge of some large crystals is due to included solid material).

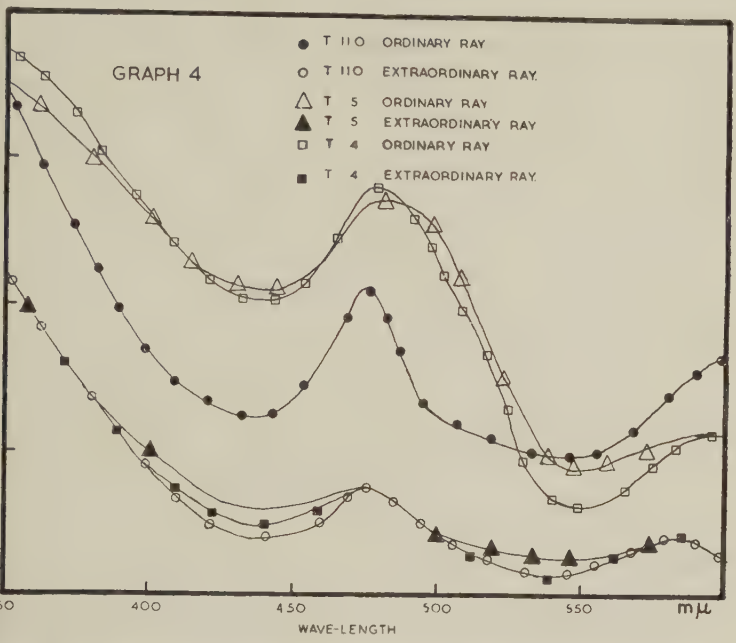

FIG. 4. Comparison of absorption curves for three crystals of pink tourmaline.

Effect of heating.

When the colour of a crystal is caused by a lattice-defect or colour-centre type of structure, the colour tends to be destroyed by quite moderate heating (300° C. or thereabouts). The tourmaline crystals are quite unaffected by heating at less than 800° C.; between 800° and 1000° C. the pink crystals are decolorized with some loss in weight and with partial destruction of the lattice.[1] This suggests that the colouring material is an essential and integral part of the lattice.

Some experiments were carried out to see whether the green and pink forms reacted differently on heating. The tourmaline crystals were heated at 900–1000° C. for 1–3 hours, i.e. until the weight was constant. The results are summarized in table I. After heating the pink crystals were white and opaque; the green crystals were also opaque, but

[1] F. Machatschki, Notiz über die Entwässerung des Turmalins. Zentralblatt Min., Abt. A, 1941, pp. 135–137. [M.A. 8–382.]

brownish—the depth of colour depending on the intensity of colour in the original. Where the green crystal was unevenly coloured, this colour-zoning was preserved in the heated specimen. In almost all the experiments the green crystals lost more weight than the pink. In one experiment, where the crystals were weighed after one, two, and three

TABLE I. Pink and green tourmaline: loss of weight on heating to 900–1000° C.

Crystal.	Time.	Loss %.	Crystal.	Time.	Loss %.
T. 4. pink	3 hrs.	3·49	T. 4. green	3 hrs.	4·19
		3·71			
T. 13. pink	3 hrs.	2·61	T. 13. green	3 hrs.	4·08
T. 110. strong pink	3 hrs.	6·29	T. 110. pale green	3 hrs.	3·11
T. 12. colourless-pink	3 hrs.	3·59			
		3·98			
		4·08			
T. 8. strong pink	1 hr.	4·27			
			T. 7. dull green-colourless	1 hr.	3·84
			T. 9. green-yellow green-colourless	1 hr.	4·49
			T. 10. pale green	3 hrs.	4·53
			T. 111. dark green, opaque	3 hrs.	4·02
Mean (excluding T. 110)		3·68	Mean (not T. 110)		4·18

hours heating, the green crystal also lost weight more quickly than its pink counterpart. T. 110 was again anomalous, since the pink part of the crystal lost twice as much weight as the green. There is no constant value for the weight loss, which must depend on something variable in the atomic structure and chemical composition. The structure is undoubtedly destroyed in part by the heating. One of the hydroxyl groups in the crystal is more loosely bound than the others, and it may be that the loss in weight is due—at least in part—to the removal of this hydroxyl group. The magnitude of the effect (3–4 %) is compatible with this hypothesis.

Lattice structure.

The atomic lattice pattern of tourmaline has only recently been determined.[1,2] There is still some disagreement on minor points of symmetry, but the essential structure is satisfactorily established. The basic unit is a ring of six silicon atoms, with the appropriate oxygen

[1] G. E. Hamburger and M. J. Buerger, The structure of tourmaline. Amer. Min., 1948, vol. 33, pp. 532–540. [M.A. **10**–541.]

[2] T. Ito and R. Sadanaga, A Fourier analysis of the structure of tourmaline. Acta Cryst., 1951, vol. 4, pp. 385–390. [M.A. **11**–429.]

oupings, and with three (BO_3) groups and three (OH) groups symetrically placed in relation to it. Each silicon ring is linked to the ighbouring ring structures by six aluminium atoms. The large central vity of the six-sided ring is the main focus of interest for this investigaon, since it is here that replacement occurs. The centre of this cavity filled with large, loosely bonded atoms, Na, Ca, and OH or F. (It is ggested that this central (OH) group may be the one that is displaced heating.) Symmetrically arranged around the central cavity are three ore sites where replacement can occur, and where iron and manganese, present, will be situated—according to the structural analyses. The rmula for the unit cell is $NaR''_3Al_6(BO_3)_3(OH)_4Si_6O_{18}$; Ca can replace a if valency conditions are satisfied. R″ can be Fe″, Mn, Mg, (Al+Li), ‴ (if valency conditions are satisfied), &c.

Chemical composition.

Table II gives the results of partial chemical analyses of one of the ystals used for the absorption measurements. At first sight, it is somehat disconcerting to observe that both the pink and green portions of 4 contain both iron and manganese. The green portion contains more rrous iron, more ferric iron, and considerably more manganese than e pink. Both crystals contain lithium, the green one rather more than e pink, although it is doubtful if the difference is significant.

TABLE II. Partial analyses of a tourmaline crystal from San Diego County, California. (Analyst, W. H. Herdsman.)

	Pink. T. 4. %	Green. T. 4. %
Fe (ferrous) ...	0·12 ...	0·58
Fe (ferric) ...	0·36 ...	0·67
Mn ...	0·24 ...	1·12
Al ...	22·75 ...	21·84
Si ...	17·56 ...	17·32
Li ...	0·82 ...	0·94

These results may be considered together with table III which is collection of analyses[1, 2, 3] of tourmaline from different localities. The ata used to compile the tables is by no means comprehensive, but

[1] T. N. Agafonova, Chemical composition and colour of tourmalines from the orshchovochnoi Mts. Compt. Rend. (Doklady) Acad. Sci. URSS, 1947, vol. 55, . 849–852. [M.A. **10**-317.]

[2] E. S. Dana, System of Mineralogy, 6th edit., 1892, p. 555.

[3] W. Kunitz, Die Mischungsreihen in der Turmalingruppe. . . . Chemie der de, 1929, vol. 4, pp. 208–251. [M.A. **4**-203.]

TABLE III. Chemical composition of pink, green, and dark green to black tourmalines.

	Colour.	Si.	Al.	Si:Al ratio.	Mn.	Fe^{++}.	Fe^{+++}.	Fe + Mn.	Li.	Mg.	F.	H_2O.
Siberia. (Agafonova, anal. 1) ...	rose	17·86	22·20	1:1·243	0·45	0·12	0·06	0·63	0·06	0·21	0·96	5·33
Siberia. (Agafonova, anal. 2) ...	rose	17·37	22·67	1:1·305	0·36	0·17		0·53	0·07	0·37	0·80	4·15
Siberia. (Agafonova, anal. 3) ...	rose	18·27	22·26	1:1·218	0·20	0·10	0·05	0·35	0·11	0·14	0·32	2·98
Rumford, Maine. (Dana, anal. 36)	rose	17·77	22·89	1:1·256	0·27	0·20	—	0·47	0·74	0·04	0·58	4·26
Brazil. (Dana, anal. 37) ...	pink	17·36	22·47	1:1·294	0·61	0·40	—	1·01	0·82	—	—	3·90
Murminsk, Urals. (Kunitz) ...	red	17·74	21·97	1:1·238	1·15	0·21		1·36	0·83	—	0·96	3·18
Rožná, Moravia. (Kunitz) ...	pale red	17·61	21·83	1:1·240	0·67	0·94	—	1·61	0·65	—	0·64	3·16
Penig, Saxony. (Kunitz) ...	red	17·44	21·75	1:1·247	1·29	0·40		1·69	0·67	0·07	0·81	3·44
Nerchinsk, Siberia. (Kunitz) ...	dark red	17·59	21·20	1:1·206	1·58	0·40	—	1·98	n.d.	n.d.	n.d.	n.d.
$NaLi_{1·5}Al_{1·5}Al_6(BO_3)_3(OH)_4Si_6O_{18}$ ...	—	17·71	21·25	1:1·200	—		—	—	1·12	—	—	—
$NaMgLiAlAl_6(BO_3)_3(OH)_4Si_6O_{18}$ ...	—	17·84	20·00	1:1·121	—	—	—	—	0·736	2·58	—	—
Siberia. (Agafonova, anal. 4) ...	green	16·62	20·46	1:1·231	3·50	0·26	0·59	4·35	0·14	0·37	0·76	3·53
Siberia. (Agafonova, anal. 5) ...	green	16·31	19·95	1:1·223	2·53	0·90	4·58	8·01	0·14	0·24	0·41	3·38
Siberia. (Agafonova, anal. 6) ...	green	16·81	20·46	1:1·217	3·97	1·56	0·15	5·68	0·06	0·35	0.64	3·86
Siberia. (Agafonova, anal. 7) ...	green	16·61	19·95	1:1·201	4·87	1·55	0·29	6·71	0·08	0·30	0·77	3·88
Siberia. (Agafonova, anal. 8) ...	green	16·96	19·76	1:1·162	3.66	1·00	0·96	5.62	0·07	0·34	0·80	4·74
Abuurn, Maine. (Dana, anal. 38)...	colour-less	17·80	20·97	1:1·178	1·07	1·07	0·22	2·36	0·64	—	0·62	4·16
Brazil. (Dana, anal. 39)	pale green	17·45	20·99	1:1·203	1·14	1·78	0·11	3·03	0·81		0·32	3·63
Auburn, Maine. (Dana, anal. 40)...	pale green	17·67	19·97	1:1·131	0·39	3·02	0·31	3·42	0 64	0·02	0·62	4·18
Brazil. (Dana, anal. 41)	olive-green	17·23	20·18	1:1·171	1·72	2·48	0·23	4·43	0·77	0·02	0·14	3·64
Nerchinsk, Siberia. (Kunitz)	brown	16·81	19·92	1:1·184	[illegible]	—	—	[illegible]	0·81	—		

TABLE III (*continued*).

	Colour.	Si.	Al.	Si:Al ratio.	Mn.	Fe^{++}.	Fe^{+++}.	Fe+Mn.	Li.	Mg.	F.	H_2O.
Chesterfield, Mass. (Kunitz) ...	green	17·92	18·20	1:1·075	8·36	5·48	—	8·84	0·48	0·08	—	3·94
South-West Africa. (Kunitz) ...	blue-green	16·85	21·07	1:1·251	0·56	3·79		4·35	0·56	0·51	1·01	2·89
$NaLiAlFe_{0·5}Mn_{0·5}Al_6(BO_3)_3(OH)_4Si_6O_{18}$		17·28	19·35	1:1·120	—		—	5·68	0·71	—	—	—
$NaMgLi_{0·5}Al_{0·5}Fe_{0·5}Mn_{0·5}Al_6(BO_3)_3(OH)_4Si_6O_{18}$		17·14	17·85	1:1·042		—	—	5·64	0·35	2·48	—	—
Siberia. (Agafonova, anal. 9) ...	black	16·10	27·46	1:1·169	0·23	9·30	1·78	10·31	0·04	0·57	0·19	3·44
Siberia. (Agafonova, anal. 10) ...	black	16·26	26·64	1:1·136	1·07	8·92	1·33	11·32	0·02	0·21	0·43	3·74
Siberia. (Agafonova, anal. 11) ...	black	15·82	26·18	1:1·154	0·71	9·51	0·79	11·01	0·03	0·76	0·41	3·47
Siberia. (Agafonova, anal. 12) ...	black	15·82	24·68	1:1·168	0·99	8·43	1·49	10·91	0·07	0·46	0·17	3·17
Siberia. (Agafonova, anal. 13) ...	black	16·12	24.32	1:1·086	0·81	9·06	2·07	9·94	0·07	0·96	0·64	2·99
Rumford, Maine. (Dana, anal. 42)	dark green	17·05	20·18	1:1·183	0·25	5·00		5·25	0·45	- -	0·16	3·52
Auburn, Maine. (Dana, anal. 43)...	dark green	16·92	19·43	1:1·148	0·56	5·49	0·11	6·16	0·50	0·10	0·71	4·05
Auburn, Maine. (Dana, anal. 45)...	black	16·92	18·07	1:1·104	0·04	11·06		11·10	-	0·06	—	3·62
Brazil. (Dana, anal. 46)	black	16·16	17·32	1:1·070	0·09	10·64	0·23	10·96	0·04	1·28	0·06	3·42
$NaLi_{0·5}Al_{0·5}FeMnAl_6(BO_3)_3(OH)_4Si_6O_{18}$		16·54	17·19	1:1·040				10·86	0·34	—	—	—
$NaMgFeMnAl_6(BO_3)_3(OH)_4Si_6O_{18}$		16·47	15·86	1:0·962	—	—	—	10·84	—	2·38	—	—

Na, Ca, K, and B percentages have been omitted. All figures are percentages except the Si:Al ratio.

neither is it at all selective. The percentage compositions of some 'ideal' crystals thought to approximate fairly closely to the pink, green, and black types have been given for reference. The boron, sodium, potassium, and calcium figures have been omitted from the tables since none of these was expected to contribute directly to the colour. The important elements giving rise to colour are those having internal electron orbits which are normally unoccupied, i.e. the transition elements, the rare-earths, and elements allied to the rare-earths. The rare-earths (both groups) give line-like absorption spectra and fluorescence: the transition elements give broad bands and never any fluorescence. The boron content of the crystals was reasonably constant and there was always considerably more sodium than calcium or potassium.

Iron and manganese are present in the pink, green, and black crystals. The pink tourmalines have from 0·2–1·5 % Mn and up to 1 % ferrous iron. Generally speaking, the ferric iron content is low, although it is important not to place too much emphasis on this, since it is difficult to distinguish accurately between the two valency states when both are present in such small quantities. The lowest manganese content quoted is equivalent to one Mn atom to each twenty unit cells. The black crystals also contain about 1 % of manganese; the green crystals have the highest Mn content up to 5 %. Both the green and black tourmalines may contain an appreciable amount of ferrous iron in addition to ferric; the total iron content of the green crystals is always in excess of the pink.

Magnesium and lithium are present throughout in small and variable amounts. The lithium content seems to depend in part on the locality, since, for example, all tourmaline analysis quoted by Agafonova (from the Borshchovochnoi Mts., Siberia) are low in lithium.

The silicon:aluminium ratio has been calculated for the recorded analysis and for the ideal composition. It is interesting to observe that the amount of aluminium is almost always higher than that given by the theoretical formulae, suggesting a limited amount of replacement of Si by Al in the basic silicon-ring structure. There is no evidence from the analyses that this proxying occurs to a greater or lesser extent in the pink or green forms, although this does not preclude the possibility of it being more random in one case than the other.

The spectroscopic data required that the pink crystals should carry divalent manganese and the green ones ferrous iron. These conditions are fulfilled by the chemical analyses, but this is by no means the complete story. It is still necessary to account for the ferrous iron in the pink crystals and the high manganese content of the green crystals. If

the one case it is the manganese that controls the colouring and in the other the ferrous iron is responsible. The simplest explanation would be one of differing valency states. Quensel and Gabrielson[1] attempted to determine whether any of the manganese present in the pink tourmaline was in a higher state of oxidation but could obtain no evidence for this. They also suggested that the iron in pink tourmaline is trivalent and that in green mainly divalent: once again the experiments designed to test this theory gave no positive results. Carobbi and Pieruccini (1947, loc. cit.) provide a useful summary of earlier theories relating to colour. From a review of the data provided by emission spectra they suggest that the green colour is due to divalent iron, the pink colour to manganese plus caesium and lithium. Any satisfactory theory of colour must explain the mutual exclusiveness of the pink and green forms. It is here suggested, tentatively, that the solution may lie in the peculiar nature of the manganese atom which only gives rise to colour under certain rather restricted conditions. These conditions are not often satisfied, but when they are—as in potassium permanganate—the colouring can be very strong indeed. (In this case it is thought to be due to the tetrahedral co-ordination of four oxygen atoms around the manganese.) Manganese sulphate crystals are a very pale pink: the colour is somewhat strengthened in solution, possibly because of the tetrahedral co-ordination of four water molecules. The pink colour of a tourmaline crystal is more intense than that of any solution of manganese sulphate. Presumably the site provided for the Mn atom in a tourmaline lattice satisfies the stringent electronic conditions required for the production of colour in manganese. Even so, the strength of the colour is much less than the theoretical maximum, which is nearly attained in MnO_4'.

The pink colour is shown by crystals with as little as 0·2 % Mn. The green colour, on the other hand, is only seen when the total iron content (ferrous plus ferric) is 1% or more. This amount of iron seems to inhibit the production of the manganese colouring, possibly because of some slight distortion of the lattice. Note the analysis of a colourless crystal (Dana, analysis 38) which contains about 1% of both Fe and Mn: the iron content is adequate to inhibit the manganese colour, but is not sufficient to produce a distinct green colour. One interesting point to remember is the absorption of the extraordinary ray of pink tourmaline (graph 3), which is like that of green tourmaline but less intense—as

[1] P. Quensel and O. Gabrielson, Minerals of the Varuträsk pegmatite. XIV. The tourmaline group. Geol. För. Förh. Stockholm, 1939, vol. 61, pp. 63–90. [M.A. 7–335.]

would be expected from the low iron content: a similar low absorption of the ordinary ray is masked by the strong pink colour. Environmental conditions appear to have much less effect on the strength of absorption in the case of iron.

Lithium is commonly believed to play some part in the production of a pink colour, but it is not possible to confirm or deny this from the results. Lithium is certainly present in all the pink crystals, but the green and black ones also contain lithium, although sometimes in lesser amount. It is perhaps worth noting that the lowest lithium recorded for the pink tourmaline—0·06–0·07 %—would provide one Li atom for ten unit cells.

In marked contrast to the pink and green forms there appears to be a complete gradation chemically between green and black tourmaline. The black crystals are characterized by a high ferric iron content, low manganese, and low lithium.

Acknowledgements.—The authors would like to express grateful appreciation to Dr. A. K. Wells, whose scientific curiosity first inspired this investigation; and to Prof. J. H. Taylor for the ready and generous provision of all research facilities. The cost of the two chemical analyses of tourmaline was met by a grant from the Central Research Fund of the University of London.

Latiumite (*sulphatic potassium-calcium-aluminium silicate*), *a new mineral from Albano, Latium, Italy.*

(With Plates X and XI.)

By C. E. Tilley, F.R.S., and N. F. M. Henry, M.A., Ph.D.

Department of Mineralogy and Petrology, University of Cambridge.

[Exhibited June 12, 1952.]

THE ejected blocks found in the 'peperino' of the Alban Hills have long attracted the attention of mineralogists on account of their variety in content of well-crystallized minerals. It may be recalled that this Roman region provides the earliest and finest examples of the white octahedral haüyne, at first referred to a separate species (berzeline), and that this mineral with leucite, yellow garnet, wollastonite, green clinopyroxene, and melilite form characteristic assemblages in the tuffs from Albano, Frascati, and other places.[1]

In an examination of a group of specimens in the mineralogical collections at Cambridge, the occurrence was noted in two ejected blocks from Albano of a mineral bearing a superficial resemblance in section to anorthite or wollastonite, but which closer study reveals to be a new species which it is now proposed to name *latiumite* from the district of its origin (Latium). The two specimens (45482, 29799, Harker Slice Collection) are clearly the product of limestone reaction, containing as they do lime-rich minerals along with species characteristic of the Roman magmatic province, namely, haüyne and leucite. One of the assemblages contains in addition prominent crystals of kaliophilite[2] (pl. XI).

The first rock (45482, pl. X) is built of hedenbergitic pyroxene, grossular-andradite, melilite (humboldtilite), leucite, haüyne, and the new mineral in some abundance; and in the second (29799) the new mineral, more sparingly developed, is associated with clinopyroxene, garnet, leucite, haüyne, and kaliophilite (pl. XI, figs. 1 and 2). Melilite

[1] A systematic account of the 'enclaves de calcaires' of the Latium district is given in A. Lacroix, Enclaves des roches volcaniques. Ann. Acad. Mâcon, 1893. Vol. 10, pp. 334–350.

[2] That this mineral is kaliophilite, not kalsilite, is demonstrated by both powder and single-crystal X-ray photographs. The anomalous properties which the mineral shows are at present under investigation by Dr. A. M. B. Douglas at Cambridge.

(humboldtilite, analysis, table III) is also present as scattered crystals. In the rock latiumite is intergrown with the chief minerals, but crystals can be isolated from cavities. These appear characteristically with an elongated tabular habit, but are modified by narrow faces along their longer edges and terminated by imperfectly developed forms. The crystals in 45482 appear white by a powdery incrustation, but in the second rock clearer glassy crystals can be obtained. The density of analysed material is 2·93, H. $5\frac{1}{2}$–6.

Weissenberg and oscillation photographs were taken, using copper radiation, of three crystals from the two specimens with the following results:

Monoclinic, a 12·12, b 5·13, c 10·80 Å., β 108°.

These values give a unit cell volume of 638 Å.^{3} and with the density determined as 2·93 the calculated molecular weight is 1125.

The powder photograph of latiumite is very rich in lines, but few of these are strong and they fade out rapidly below spacings of about 1 Å.

TABLE I. X-ray powder data for latiumite.

Int.	d in Å.	Int.	d in Å.	Int.	d in Å.	Int.	d in Å.
vw	7·2	w	2·72	vw	1·846	w	(1·340)
m	4·6	vw	2·63	vw	1·831	vw	1·319
m	4·5	vw	2·58	m	(1·812)	m	1·308
w	4·3	s	2·54	w	1·792	w	(1·289)
w	4·0	vw	2·49	vw	1·715	w	(1·274)
m	3·83	m	2·40	w	1·687	w	(1·257)
w	3·69	m	2·37	m	1·641	vw	1·241
w	3·63	m	2·33	m	1·604	vw	1·230
vw	3·53	m	2·31	m	1·563	w	(1·209)
w	3·46	w	2·25	m	1·522	vw	1·199
m	3·38	vw	(2·15)	vw	1·504	vw	1·186
m	3·28	w	(2·12)	vw	1·484	w	1·180
w	3·14	w	2·08	vw	1·473	vw	1·171
s_2	3·06	w	2·06	vw	1·463	vw	1·163
w	3·01	w	2·05	w	1·447	vw	1·151
s_3	2·96	m	1·997	w	1·435	vw	1·134
w	2·90	m	1·957	vw	1·433	vw	1·120
s_1	2·86	w	1·943	vw	1·417	vw	1·105
m	2·82	m	1·903	vw	1·408	vw	1·095
w	2·77	w	1·858	vw	1·395	vw	1·085

In table I the strongest line is marked s_1 and the two next strongest s_2 and s_3 respectively. (s = strong, m = medium, w = weak, vw = very weak; spacings corresponding to broad unresolved lines are enclosed in parentheses.)

A small, fairly clear crystal gave some measurements in the zone of

ts elongation when studied by means of the optical goniometer. Another arger crystal from a different specimen showed a tabular habit parallel o a prominent cleavage. In both crystals a few rounded terminal faces

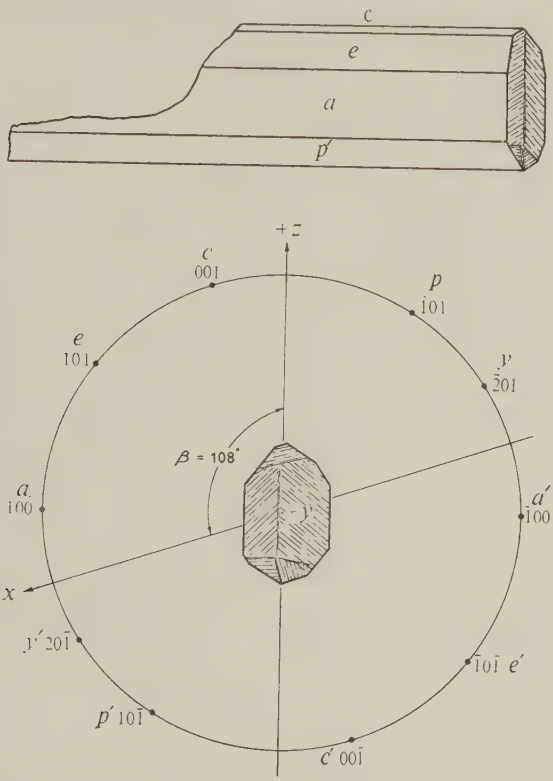

FIG. 1. Latiumite crystal elongated along b-axis (actual size $1\frac{1}{2}$ mm.). Stereographic projection on (010). Striated areas represent rounded terminal faces.

could be seen, but these did not give measurements worth recording. In fig. 1 the faces have been indexed on the X-ray unit cell. The angles fit well and the indices are simple:

$$\underset{}{a\ (100)} \underbrace{\quad e\ (101)}_{38^\circ} \underbrace{\quad c\ (001)}_{34^\circ} \underbrace{\quad p\ (\bar{1}01)}_{50^\circ} \underbrace{\quad y\ (\bar{2}01)}_{25^\circ} \underbrace{\quad a'\ (\bar{1}00)}_{33^\circ}$$

Optical examination confirms the monoclinic symmetry, the elongation corresponding to the b-axis, which is also the γ-axis of the indicatrix. The optic axial plane is thus perpendicular to (010). The tabular

face taken as (100) is a plane of perfect cleavage and is also the twi plane, twinning being simple or multiple. In sections parallel to (010) th extinction is inclined, but sections cut perpendicular to α and β sho straight extinction measured to the cleavage or long edge. Mater isolated from 45482 gave the following values of the refractive indic α 1·600, β 1·606, γ 1·614, $\gamma-\alpha$ 0·014. One characteristic feature of th mineral in both rocks is th mottled extinction, remini cent of that seen in colour clinopyroxenes. The area giving rise to the mottlin are often quite irregular i shape, and in the plane c symmetry extinction angle range 16–28° ($\alpha:c$). Dispersio is marked $r > v$. Examples c this mottled extinction ar seen in the photomicrograph (pl. X, figs. 2 and 4).

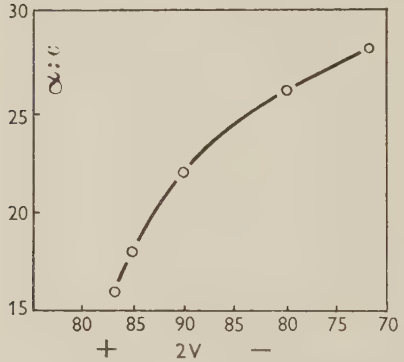

Fig. 2. Optic axial angle and extinction angle relationship in latiumite.

The mineral shows a vari able optic axial angle, sections with a lower extinction angle bein optically positive, those with higher extinction angles optically nega tive. Material in 29799 shows more consistently optically negativ crystals, and on such grains refractive indices α 1·603, β 1·609, γ 1·61 were obtained. Zoning in some crystals is sometimes more regular i that it follows the outlines of the crystal sections. A series of measure ments on the universal stage gave the following results (see fig. 2):

$\alpha:c$	...	16	18	22	26	28°
2V	...	83(+)	85(+)	90	80(−)	72°(−)

These extinction angles are measured in the obtuse angle β. The optic properties noted above clearly point to the new mineral as a solid solu tion series, but their correlation with chemical composition must awai the discovery of further material for analysis.

Microchemical tests show that latiumite is rich in calcium an aluminium. It is soluble in weak acids leaving a silica pseudomorph and it reacts for SO_3 and CO_2. In 45482 the mineral gave a reaction fo chlorine with $AgNO_3$ and HNO_3, but in grains tested from 29799 thi constituent proved absent. Single grains tested with potassium ferro and ferricyanides gave a positive reaction for ferric and ferrous iron

ne mineral fuses before the blast of the blowpipe and the resulting ass partly devitrifies at a low red-heat to a fine-grained product, niaxial negative, yielding a powder photograph closely similar to that a gehlenitic melilite. Centrifuged in heavy liquids latiumite can be

TABLE II. Chemical analysis of latiumite. (Analyst, J. H. Scoon.)

			Mol. ratios.	Oxygens.		Atoms to O = 25.			
O_2	...	28·33	472	944	5·31	5·31	10·00	5·31	7·00
$_2O_3$	...	24·67	242	726	5·45	4·69		1·69	
						0·76		3·76	
$_2O_3$	...	0·50	3	9	0·07	0·07	1·13	0·07	4·13
O	...	0·55	8	8	0·09	0·09		0·09	
nO	...	0·02	—						
gO	...	0·76	19	19	0·21	0·21		0·21	
O	...	29·41	525	525	5·91				
$_2O$	...	1·11	18	18	0·40	8·04		8·04	
$_2O$	...	7·20	77	77	1·73				
				2326					
$_2O+$	...	0·27	—						
$_2O-$	...	nil	—	106					
				2220					
O_3	...	5·42	68	—	0·76 (SO_4)	0·76	1·18	0·76	1·18
O_2	...	1·60	36	88·8	0·40 (CO_3)	0·40		0·40	
	...	0·14	2	—	0·02 (Cl_2)	0·02		0·02	
		99·98							
ess O = Cl		0·03			Mol. wt. 1121				
		99·95							

olated from the heavier garnet, clinopyroxene, and melilite and from ne lighter haüyne and leucite. Material so isolated has been analysed y Mr. J. H. Scoon. The results set down in table II are from two nalyses, one a partial analysis (i.e. less SO_3, CO_2, Cl) of pure material, nd the other a product containing a very small fraction of melilite hich itself has been subject to analysis by Mr. J. H. Scoon (table III).

A tentative interpretation of the latiumite analysis is set down in able II in the light of the molecular weight of the unit cell determined om the X-ray data. Calculated on a basis of 25 oxygen atoms, which ives a molecular weight of 1121 (X-ray data 1125), the figures of olumn 5 of table II are obtained, and on this basis the volume in cubic Å. nits per oxygen atom is approximately 22. The figures of column 5 ay be allotted alternatively as in columns 6 and 7 corresponding to

a sheet structure or one of mixed groups (?$[SiO_4][Si_2O_7]$). In view of i complexity as a solid solution, chemical analysis of additional latium material is much to be desired, and the problem of its formula may left till these further chemical data and an X-ray structural analy have been completed.

TABLE III. Chemical analyses of humboldtilite.

		1.	2.	1a. Metals in 1 to O = 7.
SiO_2	...	40·57	41·07	1·857 } 2·000
				0·143
Al_2O_3	...	10·46	10·47	0·560
				0·417
Fe_2O_3	...	0·97	3·80	0·033
FeO	...	2·62	—	0·099 } 0·991
MnO	...	0·16	—	0·005
MgO	...	6·35	6·02	0·437
CaO	...	34·42	33·92	1·689
Na_2O	...	3·49	3·25	0·308 } 2·030
K_2O	...	0·64	1·04	0·033
H_2O+	...	0·33	—	$Ca_2Al_2SiO_7$(Ge) 13
H_2O-	...	0·15	—	$Ca_2MgSi_2O_7$(Ak) 55
TiO_2	...	< 0·01	—	$CaNaAlSi_2O_7$ 32
		100·16	99·57	Sp. gr. 3·00, ω 1·637, ϵ 1·632

1. Humboldtilite in ejected block with latiumite, grossular-andradite, clin pyroxene, leucite, and haüyne, in peperino, Albano, Latium. (Analyst, J. H. Scoor

2. Humboldtilite in ejected block with yellow garnet, clinopyroxene, leucite, an haüyne, in peperino, Latium. F. Millosevich, Studi su minerali del Lazio. I melilite degli inclusi nel peperino. Atti (Rend.) R. Accad. Lincei, Roma, Cl. Sc fis. mat. nat., 1921, ser. 5, vol. 30, sem. 1, pp. 80–84. [M.A. 2–165.]

1a. Analysis 1 recalculated to 7 oxygen atoms.

EXPLANATION OF PLATES X AND XI.

Photomicrographs of slices from ejected blocks in peperino, Albano, Latium, Ital

PLATE X.

FIG. 1. A large twinned crystal of latiumite showing (100) cleavages: enclosur are green hedenbergitic pyroxene (centre), yellow grossular-andradit and humboldtilite. Ordinary light. ×22.

FIG. 2. The same section, between crossed nicols, has been rotated to show t patchy zoning in the upper half of the twin. The hedenbergit pyroxene crystal (right centre) is at extinction. ×22.

FIG. 3. Latiumite, a multiple twinned crystal, cut nearly perpendicular to t acute bisectrix (γ), enclosing grossular-andradite and bordered (lef by humboldtilite. Ordinary light. ×22.

FIG. 4. The same field between crossed nicols showing the characteristic develo ment of the mottled zone structure in the latiumite lamellae. ×22.

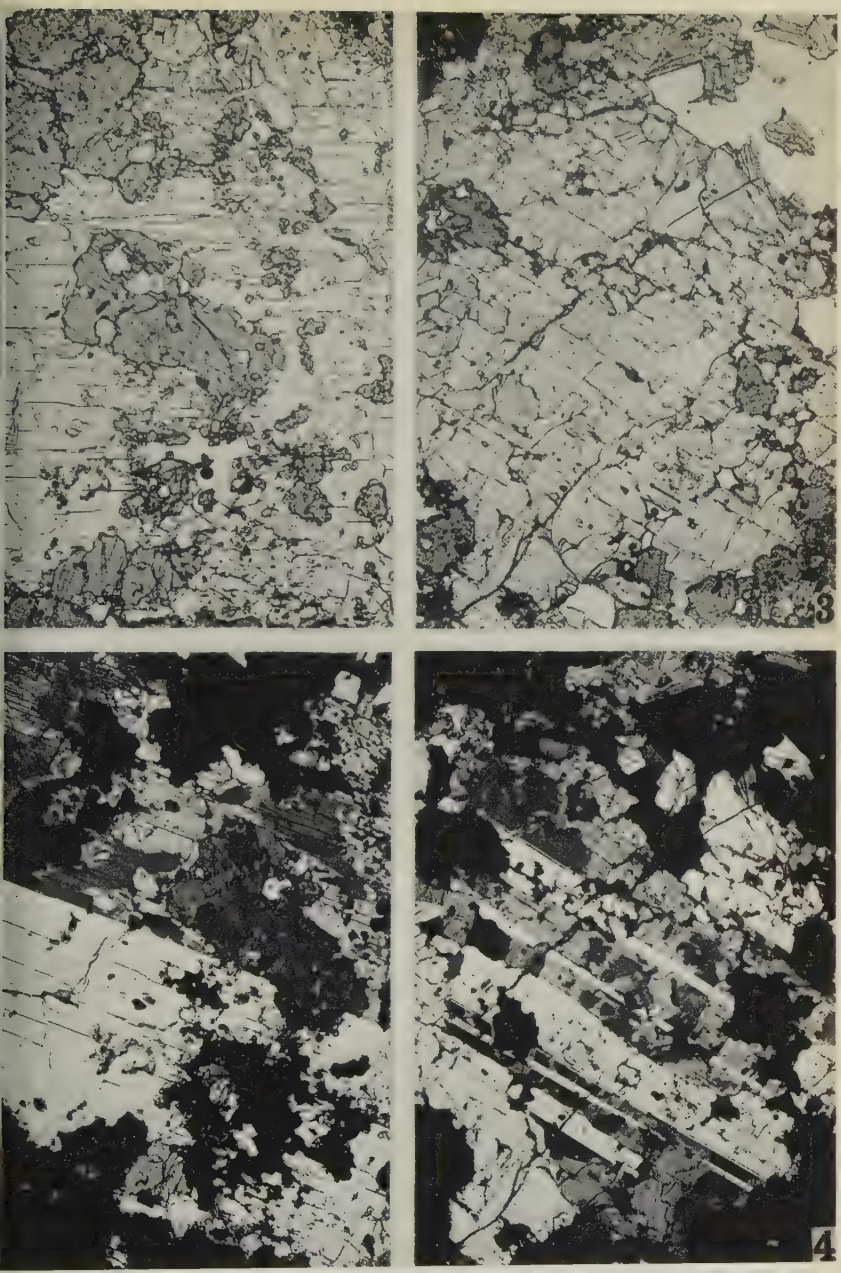

E. Tilley and N. F. M. Henry: Latiumite in Ejected Block, Latium, Italy

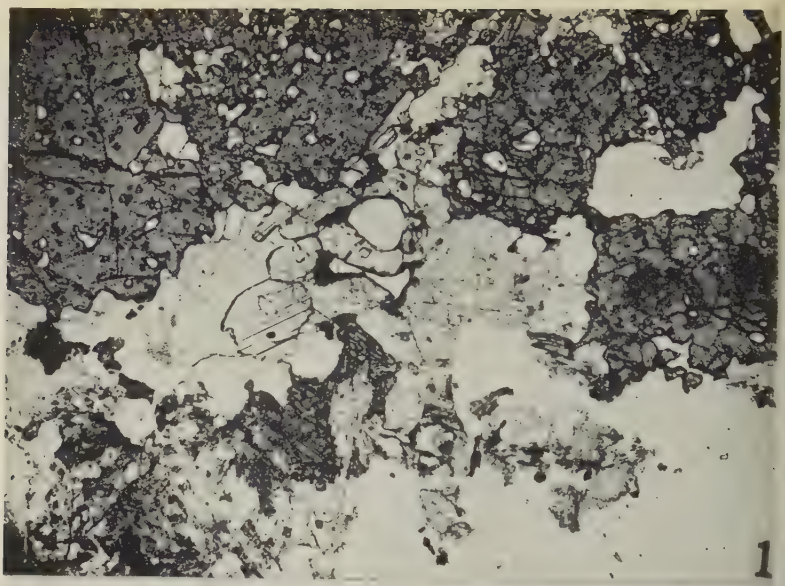

C. E. Tilley and N. F. M. Henry: Latiumite and Kaliophilite in Ejected Block, Latium, Italy

TE XI.

IG. 1. Latiumite with kaliophilite in ejected block, Albano, Latium. Above grossular-andradite with some clinopyroxene. The clear grains with high relief and good cleavage are latiumite (left centre) set in haüyne. A vertical section of kaliophilite with cross fracture is seen enclosed in clinopyroxene (below the centre and other crystals are shown to the right of centre). Ordinary light. ×20.

IG. 2. Another assemblage showing latiumite and kaliophilite. Right edge clinopyroxene and haüyne, followed on the left by clusters of humboldtilite; at the centre columnar crystals of kaliophilite with latiumite (higher relief) and darker grains of grossular-andradite. ×20.

Kalsilite in venanzite from San Venanzo, Umbria, Italy.

By F. A. Bannister,[1] M.A., Sc.D., F.Inst.P., and Th. G. Sahama[2] with chemical analyses by H. B. Wiik.[3]

[Read June 12, 1952.]

SHORTLY after the discovery of the mineral kalsilite, the pu potash analogue to nepheline, as a natural mineral occurring some volcanic lavas of SW. Uganda by Bannister and Hey,[4] Profes Arthur Holmes[5] suggested that the nepheline-looking mineral occurri in a very potash-rich lava at San Venanzo, Umbria, Italy, also might b kalsilite. His suggestion was based on the high potash:soda ratio of th bulk rock and on the optical properties of the mineral. No X-ray ev dence or chemical analysis on the supposed kalsilite has been presente so far.

During the summer of 1951 one of us (T. G. S.) was able to visit Rom where Mr. Roberto Palumbo very generously gave him two identic specimens of venanzite from San Venanzo. The constituents and th texture of this rock correspond essentially to the description of ordina venanzite reported by Holmes, and is different from the 'heteromorp of venanzite' investigated by him. Because of the fact that the spec mens available to the present authors also contained a nepheline-lookin mineral, it seemed desirable to test whether or not it really is kalsilit

The two specimens, amounting to about 1760 grams, were crushe with a jaw crusher and a small batch for bulk analysis was put aside The rest of the material was pulverized with a hammer-mill to a grai size of about 10 microns. This fine-grained material was subjected mineral separation by centrifuging it in Clerici solution. After sever centrifugings in Clerici solutions of suitable specific gravities, abo 4 grams of the supposed kalsilite and about 7 grams of leucite we obtained that were very pure. The material of the supposed kalsili contained a little colouring matter and a very few grains of leuci The leucite fraction also contained a small amount of pigments. In bo

[1] Keeper of Minerals in the British Museum.

[2] Professor of Geochemistry, University of Helsinki, Finland.

[3] Chemist, Geological Survey of Finland, Helsinki.

[4] F. A. Bannister and M. H. Hey, Min. Mag., 1942, vol. 26, p. 218.

[5] A. Holmes, Geol. Mag. Hertford, 1942, vol. 79, p. 225. [M.A. 8–318.]

ses the amounts of impurities are negligible. Refractive indices for lsilite and leucite were determined by Mr. Kai Hytönen, Institute of ology, University of Helsinki, with the following results:

Kalsilite, ω 1·543, ϵ 1·537. Leucite, n 1·511.

Chemical analyses of kalsilite, leucite, and of the bulk rock are given table I.

TABLE I. Chemical analyses of kalsilite and leucite from venanzite, and of the bulk rock. San Venanzo, Italy. (Analyst, H. B. Wiik.)

	Kalsilite.	Leucite.	Bulk rock.
SiO_2 ...	38·47	53·69	41·61
TiO_2 ...	0·00	0·15	0·85
Al_2O_3 ...	30·81	22·72	8·88
Fe_2O_3 ...	1·63	1·01	1·76
FeO ...	0·26	0·14	5·62
MnO ...	0·00	0·00	0·16
MgO ...	0·63	0·21	12·63
CaO ...	0·20	0·46	16·63
Na_2O ...	2·09	0·30	0·98
K_2O ...	25·65	20·69	7·62
P_2O_5 ...	n.d.	n.d.	1·33
H_2O+ ...	0·20	0·19	1·20
H_2O- ...	0·00	0·00	0·30
	99·94	99·56	99·57

X-ray powder photographs of both the powdered kalsilite and leucite nalysed by H. B. Wiik confirm their identification. It was also ossible to measure the unit-cell dimensions of kalsilite making use f back reflections on a cylindrical film punched so that it could be nserted into the camera with the ends meeting near $\theta = 0°$, instead of ne normal arrangement of inserting the film so that the gap in the film ccurs near $\theta = 180°$. This method, which will be described in more etail by G. F. Claringbull in his paper on dumortierite, yields cell imensions more accurate than those previously published for kalsilite nd fall nearer to those for the artificial product studied by Rigby and ichardson.[1]

The small amount of mineral available from Uganda permitted only n approximate formula, $KAlSiO_4$, to be derived (column 4, table II). is possible that the cell contents in column 3 derived from H. B. Wiik's nalysis are not only more accurate, but reveal more information about is mineral not previously available. It is clear, for instance, that there close approach to two atoms of silicon per unit cell and no evidence f replacement of silicon by aluminium. The alkali content is also nearly

[1] G. R. Rigby and H. M. Richardson, Min. Mag., 1947, vol. 28, p. 75.

two atoms and the deficit in oxygen content is unlikely to be due anything more than experimental error. The cell contents of kalsi from Italy can be written $2[(K,Na)(Al,Fe)SiO_4]$ with ratio of K/Na 0·8, and the data so far obtained for the mineral can be summarized follows:

Locality.	Refractive index.		Specific gravity.	Unit-cell data.	
	ω	ϵ		a.	c.
Uganda ...	1·542	1·537	2·59	5·17	8·67 Å
Italy ...	1·543	1·537	2·625	5·141	8·65

Kalsilite, the simplest member of the nepheline group, i.e. the with the smallest unit cell, remains as rare as kaliophilite, whe nepheline is a well-known rock mineral that so far is not known to oc in nature in any other form.

TABLE II. Chemical analyses of kalsilite.

	1.	2.		3.		4.	
SiO_2 ...	38·47	39·6	Si ...	1·99		2·13	
Al_2O_3 ...	30·81	21·3	Al ...	1·88	1·95	1·35	1·59
Fe_2O_3 ...	1·63	5·9	Fe‴ ...	0·06		0·24	
FeO ...	0·26	—	Fe″ ...	0·01		—	
MgO ...	0·63	3·7	Mg ...	0·05		0·30	
CaO ...	0·20	5·0	Ca ...	0·01		0·29	
Na_2O ...	2·09	1·6	Na ...	0·21	1·89	0·17	1·55
K_2O ...	25·65	20·1	K ...	1·68		1·38	
H_2O+ ...	0·20	—	O ...	7·91		approx. 8	
	99·94	97·2					
Sp. gr. ...	2·625	2·59					

1. Kalsilite, San Venanzo, Umbria, Italy. Analyst, H. B. Wiik; on 4 grams powder (μ 10). Specific gravity determined by K. Hytönen using a pyknomet on 1·1 gram of the powder.

2. Kalsilite, Mafuru, SW. Uganda. Analyst, M. H. Hey, Min. Mag., 1942, vol. 2 p. 219; microchemical analysis on 43 and 12 mg.

3 and 4. Contents of the unit cell calculated from analyses, unit-cell dimensio and observed specific gravities of kalsilite from Italy and Uganda, respectively.

In conclusion, we wish to thank Mr. Roberto Palumbo of Rome f his gift of specimens, Miss E. Fejer for her measurements of the X-ra photographs, and Mr. Kai Hytönen for the measurements of the physi characters.

An improved polarizing microscope. V. The ore-microscope.[1]

By A. F. Hallimond, M.A., Sc.D., and
E. Wilfred Taylor, C.B.E., F.R.S.

Messrs. Cooke, Troughton & Simms, Ltd., York.

[Read June 12, 1952.]

EXAMINATION in reflected polarized light is now widely used in metallography as well as for mineral sections. The recent introuction of graded diamond abrasives[2] has overcome most of the diffiulties in polishing that have previously hindered the widespread use this important method.

The present instrument (fig. 1) has been designed to give the best vailable control over the conditions of illumination and extinction, and provide for the complete analysis of the reflected elliptically-polarized eam. A robust stand of normal grade suitable for general research irposes and works control is provided with a stage rack, reflector unit, id the usual polarizing equipment. It may be adapted for transmitted ght by the addition of the detachable substage shown on the right of e figure.

Collimation of the plane glass reflector. —The light from a 'cover-glass' flector is not homogeneous. Rays obliquely incident on the glass surce are somewhat rotated, so that complete extinction occurs along N.-S. band in the field and similarly at the back of the objective. Fully omogeneous polarization has hitherto been obtained by the use of ecial prisms, but the restricted conditions of illumination and the jury to definition caused by occulting one-half of the objective opening ve led the present authors to abandon prism illumination in favour a modification of the plane glass illuminator. The new system will be adily understood from fig. 2. Collimating lenses have been inserted ove and below the reflector, so that the light from any point within e field iris is rendered parallel over the whole aperture during its

[1] Parts I–IV, Min. Mag., 1946, vol. 27, p. 175; 1947, vol. 28, p. 96; 1948, vol. 28, 296; 1950, vol. 29, p. 150.

[2] See H. J. Grenville-Wells, Indust. Diamond Rev., 1949, vol. 9, p. 360.

passage through the reflector, both before reflection from the object and afterwards on its return upwards to the eyepiece.

FIG. 1. Improved ore-microscope with detachable substage.

In the orthoscopic field, light coming from points on the E. or W sides is still subject to small rotations so that a dark extinction band is still visible in the field; with a × 10 eyepiece, however, the area

[1] Utilized by L. Capdecomme and J. Orcel, Rev. d'optique théor. et instr. 194 vol. 20, p. 47.

ield is sufficiently large to obviate inconvenience from this cause. When ight from the central area of the field has been isolated in the usual way by an eyepiece diaphragm, the illumination of the whole objective opening is homogeneous; with the Nakamura plate it can be shown that the xtinction is uniform within about 0·1 degree over the whole area. The xtinction obtainable is now so complete that it is necessary to give pecial attention to the question of 'parasitic' anomalies and of dye-ransmission in the polarizing filters.

The objective changer.—As is well known, few objectives are perfectly free from anomaly, and even selected lenses may vary somewhat through pressure on the mounts.[1] There remains in any case a certain anomaly arising from the rest of the optical system: selection of objectives is not, therefore, a complete remedy for this difficulty. There are also mechanical deficiencies in the majority of changers of the collar type. The objective changer used in the present instrument has therefore been completely redesigned.[2] A

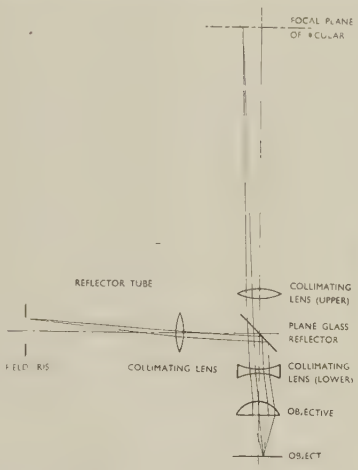

Fig. 2. Plane glass reflector with additional collimating lenses to give homogeneous aperture.

anged inner collar with a small locking head permits the objective to be rotated about the axis of the microscope. Since the anomaly is in all cases well below $1/10\,\lambda$ the objective will act as an elliptic compensator, and is so used. It should in fact have an anomaly somewhat greater than that of the rest of the system. It can then be rotated till it neutralizes the rest of the optical anomalies. A bright isotropic surface is placed in the field and the extinction is checked with the Nakamura plate. On rotating the objective, the field will darken and complete extinction may be verified by means of the conoscopic image; or the absence of ellipticity may be tested in the orthoscopic field with a Koenigsberger plate. There are usually four extinction positions for the objective, but they are in pairs, not mutually perpendicular. When

[1] B. W. Mott, H. R. Haines, and J. Woodrow, Atomic Energy Research Establishment, Report M/R856, 1952, Harwell.

[2] A. F. Hallimond, Brit. Pat. 638334/1950. Property of the National Research Development Corporation.

the object causes rotation of the plane of polarization the objecti compensation will have a slightly different value for the returning ligh but for the small angles usually met with this is negligible. For th highest accuracy in measuring it would probably be rather better to u a completely isotropic objective and allow for the small zero val representing the anomaly of the remainder of the system, but co plete extinction is better for ordinary visual work.

Dye-transmission of the polarizing filters. –If a sufficiently strong ligh is used there will always be a certain transmission of light at 'extin tion'. Part of this light is due to ellipticity in the glass mounts, and pa to transmission of the absorbed vibration by the dye. Anomaly due t the mounts is now compensated by rotation of the objective, but the remains a bluish tint in the extinction. For most purposes this negligible and may even be a useful indication that the ellipticity h been compensated. The dye-transmitted light vibrates at right angl to the transmission direction of the polarizing filter, and can be elimi ated by introducing a second filter parallel with the first on the si distant from the object. This filter need not be so intensely dyed as th principal filter; a sheet of 'sun-glass' polaroid in front of the lamp often useful, without doubling the analyser.

Adjustment of the reflector to the symmetry position.—Since the gla plate causes rotation it must be situated exactly at right angles to th principal plane of the polarizer. The most accurate setting is made b transmitted light. The extinction is first verified with the plate hor zontal; the plate is then set at its normal inclination, in which positio it resembles a birefringent object. The reflector unit must be rotate about the axis of the microscope till complete extinction is obtaine preferably indicated by the Nakamura plate. The illuminator shou be locked at this azimuth and need not be again disturbed.

Measurement of rotation and ellipticity.—In most crystal sections th path-difference between the components along the principal directio is very small. The rotation angle can therefore be measured with co siderable accuracy without compensating the ellipticity. Even th incomplete determination is of considerable interest, and rotating an lysers have been fitted for this purpose though not always with means accurate measurement. The special ocular shown in fig. 3 has graduat rotation, reading by vernier to 0·1 degree and to 0·05 by estimatio It is provided with slots that permit the use of rotary compensato for path-differences below $1/10\,\lambda$ and of quartz-wedge types for larg values.

Analysis of the reflected beam (A. F. H.).

Berek[1] has described very clearly the conditions for the use of the liptic compensator. Briefly, the section is brought to one of the 5° azimuths and the ocular is turned so as to restore 'extinction'. he elliptic compensator is then adjusted to give complete extinction, nd the extinction condition is again checked until both rotation and ompensation are giving the maximum extinction. The rotation can be

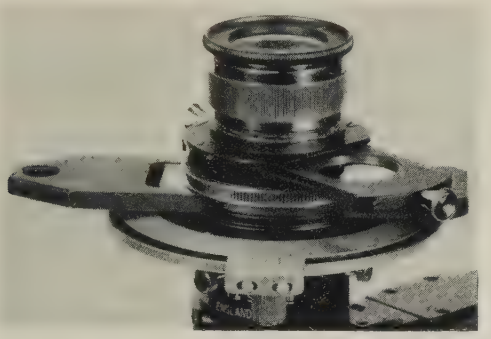

Fig. 3. Graduated rotating slotted ocular and analyser.

hecked conoscopically by the Nakamura plate and the compensation y the Koenigsberger plate. The section is then turned on the stage hrough 90° and the setting is repeated. The difference between the nalyser readings is twice the rotation angle, and the difference between he compensator readings is twice the angle θ. If Γ_0 is the constant for he compensator plate, the path-difference Γ is $\Gamma_0 \sin 2\theta$. If the com- ensator is in the ocular slots it rotates by the same angle as the ellipse nd the path-difference is simply that required to compensate the ellipse long its 45° azimuth. The compensator can also be used in the tube lots, in which case its readings must be increased or diminished by the otation angle in order to obtain the correct value.

For values larger than 1/10 λ it is necessary to use a different kind f compensator, of which the quartz-wedge may be taken as the type. f the quartz-wedge is inserted at 45° to the axis of an elliptically polarized eam (e.g. the beam from a birefringent object in the familiar procedure vith transmitted light) a black compensation band appears at the angu- ar phase-difference $\phi - 2 \tan^{-1} b/a$, where b and a are the axes of the llipse. If the wedge is not exactly at 45° azimuth the extinction of the and will be impaired.

[1] M. Berek, Fortsch. Min. Krist. Petr., 1937, vol. 22, p. 1. [M.A. 7–250.]

By means of the rotating slotted ocular the same arrangement can b- used to analyse the rotated beam in the ore-microscope. The quartz wedge must first be *accurately* set at 45° with the vibration-direction of the analyser. It is best to use a special carrier for the final adjustment since the slots are not usually exactly at 45° with the analyser. Th analyser is rotated by exactly 45° from its normal position; this brings the direction of the wedge nearly to extinction (tested with a loose filte

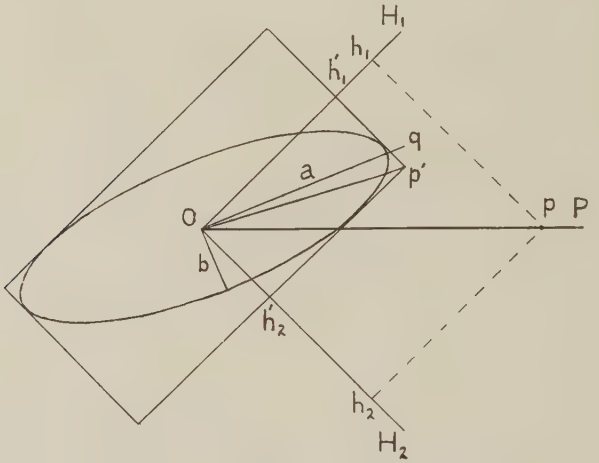

FIG. 4. Formation of elliptically polarized light by reflection from a polished surface at normal incidence.

instead of the usual analyser) and the final adjustment to extinction can be completed. When a crystal section has been brought into place at its 45° position, the ordinary analyser is brought in and the ocular is rotated, carrying the wedge round with it, until the extinction band is found and is brought to maximum extinction. The position of the band then gives the phase-difference, and the rotation angle of the analyser gives the azimuth of the reflected ellipse.

The accuracy so attainable for azimuth is not very good, but ful accuracy could no doubt be obtained if the quartz-wedge was replaced by a Soleil compensator, with Nakamura and Koenigsberger plates used conoscopically.

Calculation of the reflectivity ratio R_2/R_1 and path-difference Δ for the principal directions of the crystal section.—With the notation of fig. 4 the relations for the ellipse inscribed within the rectangle $h'_1p'h'_2$, &c., are

given by a well-known set of equations[1] of which the following two give the desired values:

1) $\cos 2 \tan^{-1} b/a \cos 2 H_1Oq \cdot \cos 2 H_1Op' = \cos 2 \tan^{-1} \sqrt{(R_2/R_1)}$ when $H_1OP = 45°$).

2) $\tan 2 \tan^{-1} b/a / \sin 2 H_1Oq = \tan \Delta$.

OP is the vibration-direction of light coming from the polarizer and OH_1 OH_2 the principal directions of the crystal section. Δ is the angular phase-difference. If Δ is in circular measure, $2\pi/\Delta = n$ where $\lambda \times 1/n$ is the path-difference.

For the present purpose graphical solution is hardly needed, but reference may be made to the method due to H. Poincaré.[2] Since the above-mentioned equations are formally analogous with the familiar 'Napierian' set of equations for solving right-angled spherical triangles, the values concerned can be set off as a right angled triangle on the stereographic projection, and solved with the Wulff net. A brief summary of some of the literature is given by C. Burri.[3]

For large values ϕ and Δ will not be the same. When the path-difference is less than $1/10\ \lambda$ the axis Oq nearly coincides with Op'.

For small values of b/a,

from (1) $\cos 2 \tan^{-1} b/a = 1$ and $H_1Oq = H_1Op' = \tan^{-1} \sqrt{(R_2/R_1)}$

from (2) if the rotation angle POp' is small, $\sin 2H_1Oq = 1$ and $2 \tan^{-1} b/a = \Delta$.

But the compensator gives $2 \tan^{-1} b/a = \Gamma$ (expressed as the phase-angle ϕ). The elliptic compensator therefore gives directly the approximate path-difference for the principal directions of the crystal, provided that the rotation angle is small. $\tan (45° - POq) = \sqrt{(R_2/R_1)}$.

Determination of the rotation (and ellipticity) due to return of the light through the inclined plane glass reflector.—With transmitted light the polarizer is removed and a polarizing filter is laid on the stage. After the extinction reading has been noted, the stage is set to positions at 2, 4, 6, &c., degrees on either side of extinction and the corresponding extinction positions of the analyser are read on the analyser scale. The analyser readings are larger than the stage readings, which give the true rotation of the light, on account of the further rotation produced by skew incidence on the inclined glass plate. Up to 20° the two series are strictly proportional, and the ratio can be ascertained, e.g. 5:4. Measurements made with the plane glass reflector must be reduced in this

[1] A. Schuster and J. W. Nicholson, Theory of optics. 3rd edit., 1924, p. 14.

[2] H. Poincaré, Théorie mathématique de la lumière, II. 1892, p. 275.

[3] C. Burri, Das Polarisationsmikroskop. Basel, 1950, p. 31. [M.A. **11** 181.]

proportion. It has been assumed throughout the preceding notes that this has been done.

In the same way, the ellipticity can be measured with the elliptic compensator. The values found were very small, a rotation of 20° giving only one degree difference in the compensator reading. Even this value is doubtfully due to the inclined plate, for the change in azimuth toward the objective might cause this small variation. With ordinary rotation angles of 5° or less this effect seems negligible. One degree on the compensator used represents about 0·0025 λ Na.

In considering the corrections required for the return of light through the glass plate the usual procedure will be to resolve into components along and at right angles to *OP* (fig. 4). Owing to the greater transmission of vibrations in the plane of incidence, the components at right angles will undergo a relative extension in the ratio that has already been determined above by observations on rotation angles up to 20°. Although the glass plate itself produces a negligible path-difference, any existing ellipse will undergo a small distortion. If the observed ellipse is plotted as in fig. 4, it should be corrected by reducing the vertical scale in this ratio. For the small ellipticities (up to 1/10 λ) and rotation angles (up to 20°) usually met with in work on ores and metals, the correction will amount simply to reducing both the ellipticity and the rotation angle by the known ratio. Example: stibnite cleavage: measured rotation 2·4°, path-difference 0·0071 λ Na. Constant for the inclined glass plate 6/5. Corrected values: rotation 2·0°, path-difference 0·0060.

Photometry is not here dealt with, but attention should be drawn to the great advantage of using the central beam given by a plane glass reflector in comparison with the restricted oblique aperture required for the Berek prism. There is also a full aperture for the conoscopic polarization figures.

Ferrous chamosite and ferric chamosite.

By G. W. Brindley, Ph.D., F.Inst.P., and
R. F. Youell, B.Sc., A.R.C.S.

Physics Department, University of Leeds.

[Read November 6, 1952.]

1. *Introduction.*

In a previous paper (Brindley, 1951) chamosites from a number of localities were examined, and their structure was shown to be of kaolin-type. Furthermore, it was shown that many of the variations in X-ray powder diagrams of chamosites can be accounted for by the existence of two kaolin-type structures, one hexagonal and one monoclinic, with simply related cell dimensions.

Previous work (Brindley and Ali, 1950; Brindley and Robinson, 1951) had shown that chlorite minerals produce a modified form on heat-treatment at about 600° C., characterized by a large increase in intensity of the 14 kX basal reflection. In general, however, kaolin-minerals did not show any such phenomenon, and accordingly, thermal examination has been used in conjunction with X-ray powder diagrams in cases where a mixture of chlorite and kaolin minerals was suspected (Brindley, Haughton, and Youell, 1951).

During the course of an investigation on the Frodingham and Northampton sedimentary ironstones, a modified structure was observed after heat-treatment of an exceptionally good chamosite specimen, and although this structure was clearly still of kaolin-type, it was largely dehydrated and oxidized. The new structure is accordingly termed *ferric chamosite* to distinguish it from the common *ferrous chamosite*. Taylor (1949) describing the preparation of rock sections from chamosite oolites and mudstones says: 'Any excessive heat treatment in this operation causes a flaky recrystallization of the chamosite and, at a higher temperature, converts it to a mass of brown and yellow-brown material. Oolides indistinguishable from those of weathered chamositic oolites and mudstones may, in this way, be produced from fresh material.' It is probable that this product was similar to the ferric chamosite described here. A detailed thermal and X-ray study of the two types of chamosite was carried out, and forms the subject of this paper.

The X-ray powder technique employed was identical with that us previously (Brindley, 1951) and need not therefore be described i detail. Methods of heat-treatment were in the main convention although the technique used for reducing the ferric chamosite will b described in a later section.

2. *X-ray data for ferrous and ferric chamosites.*

The chamosite specimen used came from location A3, Stanion La pit, Corby, Northamptonshire, and was supplied by Dr. W. Davies o

TABLE I. X-ray powder data for ferrous and ferric forms of chamosite, Stanion Lane pit, Corby, Northamptonshire.

Ferrous chamosite. *d*. (kX)		*I*.		Ferric chamosite. *d*. (kX)		*I*.
obs.	calc.	obs.	(*hkl*).	obs.	calc.	obs.
7·105	7·100	vs	001	7·05	7·048	s
4·67	4·680	m−	02*	4·535	4·540	m−
4·295	—	w−	—	—	—	—
3·927	3·899	w	021	—	—	—
3·546	3·550	vs	002	3·520	3·524	s
3·060	—	w−	—	—	—	—
2·704	2·702	m−	200	2·622	2·622	m
2·520	2·524	vs	201	2·460	2·458	ms
2·147	2·146	ms	202	2·103	2·103	m−
1·775	1·776 1·769	m	203 240	1·749 —	1·749 —	w+ —
1·560	1·560	ms	060	1·514	1·513	m
1·523	1·524	m−	061	1·483	1·479	w
1·478	1·478	m	204	1·462	1·462	w
1·429	1·427	w+	062			
1·413	1·420 1·410	vw	005 044	1·395	1·391 1·409 1·392	w
1·324	1·327	w+	401	—	—	—

* This denotes the head of a 2-dimensional diffraction band rather than a 3-dimensional reflection.

		Lattice parameters. Ferrous form.	Ferric form.	% contraction.
a	...	5·404 kX	5·244 kX	3·00
b	...	9·360	9·080	
c	...	7·100	7·048	0·75

the United Steel Cos. Ltd., Rotherham. The hand-specimen was clear green colour with no obvious sign of oxidation or weatherin Dr. Davies's petrological description is 'mixed ooliths of dark gree chamosite, and of limonite and siderite surrounded by chamosite, in matrix of siderite'. X-ray diagrams showed that it contained abo

ual quantities of chalybite and chamosite, with traces of quartz and psum. The chamosite was fine-grained, and after crushing, a simple limentation in distilled water followed by drying on a steam-bath oduced a fine fraction containing about 94 % chamosite, chalybite ming most of the remainder. It is unusual to have so pure a specimen ailable in quantity.

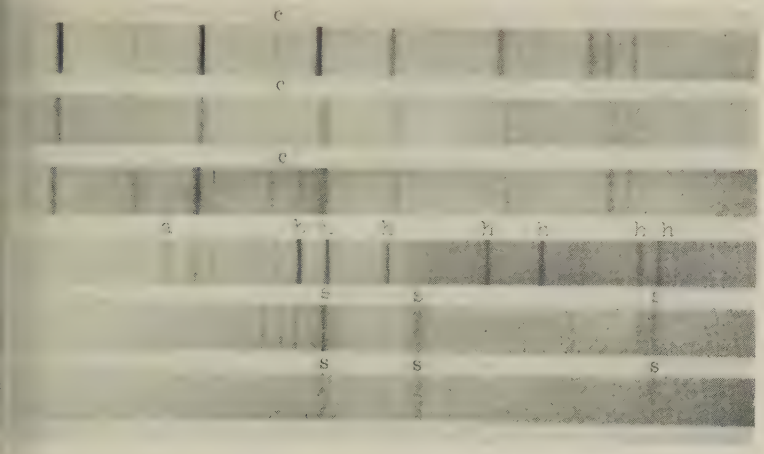

G. 1. X-ray powder diagrams. Marked lines: c = chalybite; a = anhydrous calcium sulphate; h = haematite; s = spinels.
Ferrous chamosite, Corby, Northamptonshire.
Partial conversion to ferric chamosite by heating at 300° C.
Ferric chamosite, after heating at 400° C.
Formation of haematite by heating in air at 900° C.
Formation of spinel and ferrous aluminate by heating ferrous chamosite in steam at 800° C.
Formation of ferrous aluminate by reducing ferric chamosite in H_2/H_2O mixture at 650° C.

The ferric chamosite was formed on heating the sample in air to 00° C. for two hours. Further heating at this temperature did not oduce any apparent further change. Heating at 300° C., however, oduced a mixture of the ferrous and ferric types. The colour of the ineral changed progressively from green through yellow to brown.

X-ray powder diagrams were obtained with a 20-cm. diameter semi-cusing camera, employing filtered Co-$K\alpha$ radiation. The specimens ere set 9° to the incident beam. The spacings for the two forms are own in table I, and the photographs in fig. 1, numbers 1 and 3. The rongest line of chalybite appeared on the diagrams but is omitted from

the table. The ferrous chamosite diagram is virtually identical with th ortho-hexagonal form found in the Ayrshire chamosite described previ ously (Brindley, 1951). The unit cell, a 5·40$_5$, b 9·36, c 7·10 kX, is slightl larger than that of the Ayrshire material, but small differences composition easily account for the discrepancy. The most noteworth feature is that there is no trace of the monoclinic form which was presen to extents varying from 10 to 55 % in the previous chamosites examin The specimen is clearly a nearly pure ortho-hexagonal form, with n contaminant apart from the chalybite.

A direct comparison of the ferrous and ferric diagrams shows th oxidation is accompanied by an overall displacement of the lines cor sponding to a shrinkage of the lattice. There was also a progressiv diminution in intensity of the (20l) reflections as l increased. The (20 reflection is about equally strong in the two forms, the (201) is appre ably diminished, the (202) markedly diminished in the ferric form, an so on. Another easily noticeable feature of the photographs, and on which is very useful for diagnostic purposes, is the conversion of t medium strong line at 1·560 to a medium strength line at 1·514 kX, an the virtual disappearance of the 1·523 and 1·478 lines.

The values of the spacings calculated for the ferric form assuming t to retain the ortho-hexagonal structure are also included in table I, an they agree closely with the observed values. A comparison of the para meters for the two forms shows that the a and b parameters have con tracted by 3 % and the c parameter by 0·75 %. The change in parameter arises largely from the change in the ionic radius of iron, namely, 0·83 Å for ferrous and 0·67 Å. for ferric ions. The difference in percentag contraction of the a and b parameters on the one hand and the c para meter on the other may be explained by considering the positions of th iron atoms in the kaolin-type structure of chamosite (Brindley, 1951 The iron atoms, being in the octahedral layer of the unit cell, can b regarded as influencing only a portion of the structure in the c direction about one-third, but the whole structure in the ab plane.

3. *Chemical analyses and structural formulae.*

As regards the general chemical properties of the two forms o hexagonal chamosite, the ferrous form is the less stable and therefo is the more reactive. In particular it dissolves more readily in acids an even in the absence of air it decomposes at a lower temperature than th ferric form.

The chemical analysis of the ferrous chamosite (table II, column

licated that the only appreciable impurities were chalybite and lcium sulphate. In correcting the analytical results for these im- rities, all the SO_3 with the appropriate amount of CaO was taken form $CaSO_4$. The remaining CaO and the MnO were taken with

TABLE II. Chemical analyses of ferrous and ferric chamosites.

	Ferrous chamosite.			Ferric chamosite.		
	1.	1a.	1b.	2.	2a.	2b.
$)_2$ ...	22·47	22·47	23·81	23·48	23·48	24·69
$_2O_3$ ...	21·82	21·82	23·12	22·45	22·45	23·61
$_2O_3$ ...	0·22	0·22	0·23	45·15	43·37	45·61
O ...	39·79	37·24	39·45	1·51	0·45	0·47
gO ...	2·82	2·57	2·72	2·83	2·60	2·74
O ...	0·38	—	—	0·36	—	—
nO ...	0·03	—	—	0·03	—	—
O_2 ...	trace	—	—	trace	—	—
O_5 ...	nil	—	—	nil	—	—
$)_3$ ...	0·11	—	—	0·12	—	—
... ...	trace	—	—	trace	—	—
$_2O_3$ ...	nil	—	—	nil	—	—
$_2O_3$ ...	nil	—	—	nil	—	—
$)_2$ ...	2·04	—	—	1·14	—	—
oss on ignition to constant weight ...	(7·72)	—	—	(3·72)	—	—
$_2O+$* ...	10·07	10·07	10·67	2·74	2·74	2·88
	99·75	94·39	100·00	99·81	95·09	100·00

* H_2O+ = loss on ignition less CO_2 plus (FeO) × 8/72. Loss in weight in preparing rric chamosite, 4·05 %.

1. Ferrous chamosite, Stanion Lane pit, Corby, Northamptonshire, Analyst. . F. Youell, on 1·5 grams dried at 105° C.

1a. After correction for $FeCO_3$ 4·11, $CaCO_3$ 0·54, $MgCO_3$ 0·47, $MnCO_3$ 0·05, aSO_4 0·19 %.

1b. Scaled to 100 %.

2. Ferric chamosite, prepared from the same sample of material by heating in ir at 400° C. for two hours.

2a. After correction for $FeCO_3$ 1·70, $CaCO_3$ 0·49, $MgCO_3$ 0·49, $MnCO_3$ 0·05, aSO_4 0·21, Fe_2O_3 1·78 %.

2b. Scaled to 100 %.

$'O_2$ to give carbonates. In considering the correction for the remaining $'O_2$, an analysis was made of a sample of chalybite from the Northamp- onshire field which showed that it contained iron, calcium, and mag- nesium carbonates in molecular proportions very nearly 7:1:1. This grees with published analyses by Harvey (Taylor, 1949, pp. 48 49) f chalybite specimens which included one from Stanion Lane pit. Although the amount of chalybite in our purified chamosite ore and

the resulting corrections were small, it was considered preferable to divide the remaining CO_2 in the ratio 7:1 between iron and magnesium carbonates. On taking the resulting figures with the $CaCO_3$, the molecular ratio was Fe:Mg:Ca = 7:1:1·08 which is in satisfactory agreement with the known composition of chalybite. The water content was calculated from the loss on ignition with allowance for the CO_2 and FeO contents. No correction was made for any possible dehydration of a hydrated calcium sulphate in view of the very small amount present. The corrected chamosite analysis is given in column 1a of table II, and in column 1b the corresponding ratios after scaling the total to 100 %.

The ferric chamosite was prepared from the same sample as that used for the ferrous analysis. Correction of the result was complicated by the partial decomposition of the chalybite at 400° C. An analysis of chalybite heated under identical conditions showed that $CaCO_3$ and $MgCO_3$ remained, while about 60 % of the $FeCO_3$ had decomposed to give CO and Fe_2O_3 by oxidation. Calcium sulphate, calcium carbonate, and manganese carbonate were corrected as before. From the weight loss in preparing the ferric form, the $MgCO_3$ and $FeCO_3$ contents before partial decomposition were calculated. The CO_2 remaining after allowing for calcium, magnesium, and manganese carbonates was attributed to $FeCO_3$ and the difference between original and actual $FeCO_3$ was allowed for as Fe_2O_3. The decomposed fraction amounted to 61 % of the total $FeCO_3$, in good agreement with the independent results. Column 2a gives the corrected analysis and column 2b the chamosite figures scaled to 100 %. Subsequent direct determination of water gave 10.00 % for the ferrous and 2·66 % for the ferric chamosite as compared with the values calculated from ignition weight losses of 10·07 and 2·74 % respectively.

If the previous conclusion (Brindley, 1951) is accepted that chamosite is a kaolin-type structure with a formula of the type $X_n(Si_2O_5)(OH)_4$ where X represents the 'octahedral' atoms and n varies between 2 and 3 being ideally 2 when X is wholly trivalent and 3 when X is divalent, then the formula for ferrous chamosite may be evaluated on the basis of five oxygen atoms per formula weight. The following result is obtained:

$$\underbrace{(Al_{0\cdot83}Fe^{3+}_{0\cdot01}Fe^{2+}_{1\cdot82}Mg_{0\cdot23})}_{2\cdot89\text{ atoms}}(Si_{1\cdot32}Al_{0\cdot68}O_5)(OH)_{3\cdot96}.$$

It is particularly satisfactory to find that the amount of (OH) agrees almost exactly with the ideal value of 4.

This formula may be compared with two others: A Frodingham chamosite analysed by Harvey and described by Hallimond (1939) gives:

$$\underbrace{(Al_{0\cdot43}Fe^{3+}_{0\cdot30}Fe^{2+}_{1\cdot78}Mn_{0\cdot02}Mg_{0\cdot39})}_{2\cdot92\text{ atoms}}(Si_{1\cdot40}Al_{0\cdot60}O_5)(OH)_{4\cdot00}.$$

An Ayrshire chamosite analysed by Dixon and quoted by Brindley (1951) gives:

$$\underbrace{(Al_{0\cdot76}Fe^{3+}_{0\cdot02}Fe^{2+}_{1\cdot73}Mg_{0\cdot16}Ti_{0\cdot15})}_{2\cdot82\text{ atoms}}(Si_{1\cdot24}Al_{0\cdot76}O_5)(OH)_{4\cdot00}.$$

The analysis of the Corby material in the ferrous state is therefore in agreement with these previous analyses.

The calculation of the structural formula of the ferric chamosite raises a difficult and fundamental problem. In any mineral containing structural water, as (OH), there is always a possibility of loss of water before the sample is analysed, and the tendency of actual analyses to fall short of the idealized (OH) figure is clearly due to this cause. The deviation is, however, usually a small percentage of the total water content. In the case of ferric chamosite the chemical analysis (table II) shows a marked decrease in the percentage of H_2O and without a detailed knowledge of the structure there is no justification for proceeding on the basis of five oxygen atoms in the formula and indeed this leads to an unconvincing result. The only reasonable approach is to keep the number of Si and Al atoms constant. Proceeding on this basis, we obtain for the structural formula of ferric chamosite the following expression:

$$\underbrace{(Al_{0\cdot81}Fe^{3+}_{1\cdot83}Fe^{2+}_{0\cdot02}Mg_{0\cdot22})}_{2\cdot88\text{ atoms.}}(Si_{1\cdot32}Al_{0\cdot68}O_{5\cdot00})O_{2\cdot30}(OH)_{1\cdot02}.$$

This formula retains the original number of cations in the octahedral positions, which would be expected since oxidation does not alter this figure. Furthermore, the fact that we now find only one (OH) in the formula in place of the original $(OH)_4$ also admits of a simple structural interpretation. In fig. 2 is shown diagrammatically the distribution of atoms in layers in ferrous chamosite and the probable distribution in ferric chamosite. In the first place there is the same number of cations in both tetrahedral and octahedral positions. These layers are therefore probably closely similar in the two structures. Secondly, one (OH) per formula weight is needed, together with two oxygen atoms, to complete

the middle layer of two O and one (OH) atoms. It seems reasonable to suppose that the single (OH) is used to complete the middle layer. This is probable not only on numerical grounds, but also because it occupies a central position in the layer and therefore may be less easily dehydrated than the outermost hydroxyls. (The OH groups in analogous

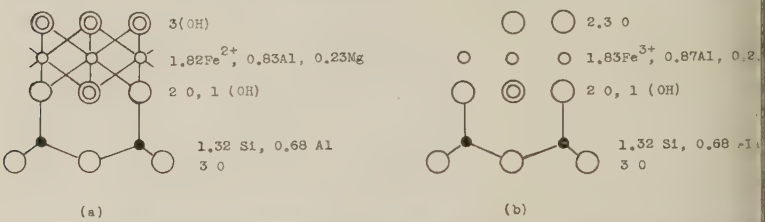

FIG. 2. Diagrammatic representation of layer structures of: (*a*) ferrous chamosite and (*b*) ferric chamosite. The positions of the 2·3 oxygen atoms in (*b*) are uncertain.

positions in the mica structure, for example, are not removed below about 800° C.) The oxygen atoms in excess of five in ferric chamosite, namely 2·30, must presumably replace the 3(OH) layer in ferrous chamosite.

The combined process involving oxidation and dehydration may be considered as follows: Each ferrous ion on oxidation gives a ferric ion and an electron. The electron reacts with a hydroxyl group to give an oxygen ion and a hydrogen atom.

$$Fe^{2+} + (OH)^{-} \longrightarrow Fe^{3+} + O^{2-} + H$$

The O^{2-} ions remain in the lattice, and the H atoms are removed as water by aerial oxidation. In the absence of oxygen for this removal of H as water, the reaction does not take place, as we have shown experimentally. This process accounts for a part only of the loss of (OH) ions from the lattice, namely, a diminution of (OH)'s equal in number to the ferrous ions.

It appears that a second reaction, involving dehydration only, occurs of the form:

$$(OH) \longrightarrow \tfrac{1}{2}H_2O + \tfrac{1}{2}O^2$$

For a lattice containing x octahedral ferrous ions the combined oxidation-dehydration process is obtained by adding together x (reaction I) and $(3-x)$ (reaction II). Taking account also of the atmospheric oxidation we obtain finally:

$$x\mathrm{Fe}^{2+} + 3(\mathrm{OH})^{-} + \frac{x}{2}\,\mathrm{O\ (atmospheric)} - x\mathrm{Fe}^{3+} + \frac{3+x}{2}\,\mathrm{O}^{2-} + \frac{3}{2}\,\mathrm{H_2O}.$$

n the present case $x = 1{\cdot}82$. We therefore expect $\frac{3+1{\cdot}82}{2}$ or 2·41 xygens replacing 3(OH). This is in good agreement with the analytical sults.

4. *Reduction of ferric to ferrous chamosite.*

If ferric chamosite differs from ferrous chamosite only by the removal H and H_2O from the lattice, then a suitable treatment based on the ermodynamic properties of the system FeO–Fe_2O_3–H_2–H_2O may bring bout the reverse process. The eat of formation of hydrous licates from oxides is low and erefore the free energies of rrous and ferric hydrous layer licates should not differ reatly from those of ferrous nd ferric iron oxides. A nixed' silicate structure anagous to the oxide Fe_3O_4 is onceivable, but no definite ntermediate products have een observed during the boratory oxidation. Since ontinuous replacement of divalent by trivalent iron in the lattice is ossible, the existence of a ferroso-ferric chamosite is largely an artificial nsideration. Intermediate states of oxidation, not corresponding to ny simple ratio ferrous/ferric have been identified in naturally occurring hamosites, and will be described in a later paper.

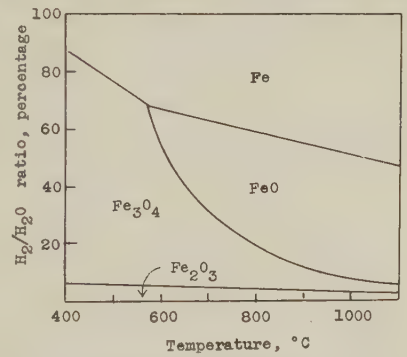

FIG. 3. Equilibrium diagram of iron–iron oxides system in relation to temperature, and H_2/H_2O ratio.

The equilibrium diagram of iron and its oxides in relation to tempera- ure and H_2/H_2O ratio has been studied by many investigators (Glass- one, 1948; Mellor 1929). The essential features of the system are nown in fig. 3.

The reaction $Fe_2O_3 + H_2 \rightleftharpoons 2FeO + H_2O$ is reversible and the ratio $= p(H_2)/p(H_2O)$ determines the relative stability of ferrous and ferric on.

By passing hydrogen several times through water in a saturator, an quilibrium mixture of hydrogen and water vapour, of known composi- on, was obtained. With suitable arrangements to prevent premature ondensation, the mixture was passed over the ferric chamosite in a ubular electric furnace. By altering the temperature of the saturator

the H_2/H_2O ratio was adjusted to be below the Fe-stable region b[illegible] above the Fe_2O_3-stable region. The reaction was rather slow, and th[illegible] temperature conditions were critical. The optimum temperature w[illegible] 460° C., at which temperature ferrous chamosite was present after s[illegible] hours, together with some lines on the X-ray diagram due to impuriti[illegible] and a heavier background, both presumably due to decomposition by side reactions. The specimen was a light greenish-brown colour, showing that although the original ferrous chamosite was not completely restored the change had proceeded to a considerable degree.

At lower temperatures little or no reaction occurred, while at higher temperatures the chamosite structure disintegrated and the product corresponded to ferrous aluminate. This indicates both reduction and lattice breakdown either concurrently or consecutively. The same spinel, as will be shown later, occurs when ferrous chamosite is heated in absence of air. The product was greenish in colour, confirming the reduction process.

5. *Thermal decomposition of chamosites.*

In order to obtain a more complete picture of the properties of ferrous and ferric chamosities, they were examined after heating at 100° C. intervals (*a*) in air or oxygen, (*b*) in a vacuum, (*c*) in steam. X-ray photographs were taken at critical temperatures to detect any line in the 14 kX region which is diagnostic of a chlorite structure (Brindley and Ali, 1950), but the bulk of the photographs were taken with the camera set to record reflections from 9 kX downwards. No chlorite structure was observed at any stage, confirming the previous finding of one of us (Brindley, 1951).

Generally any observable reaction was complete in about 2 hours at any particular temperature. The reactions proceeded rapidly during this time and photographs taken after $\frac{1}{4}$, $\frac{1}{2}$, and 1 hour showed incomplete reactions, whereas prolonged heating did not produce a substantial difference from the 2-hour heating. At low temperatures, however, 2-hour heating did not always produce complete change. For example, at 300° C., ferrous chamosite was converted to the ferric form only partially in 2 hours, but prolonged heating caused more reaction to take place.

The original chamosite, roughly purified by sedimentation, and ferric chamosite prepared from it at 400° C. were used for the experiments. The results obtained are represented diagrammatically in fig. 4.

Heating in air.—The chamosites pass from or through the ferric stage

o an amorphous state without further change of colour at 450–500° C. ittle is visible on the X-ray diagram at this stage except general back-round scattering, which is to be expected from an amorphous or largely morphous material.

Recrystallization commences at about 550° C., when some haematite nes appear, together with a small quantity of anhydrous $CaSO_4$ im-urity. The sedimentation processes were carried out in distilled water, howing that the $CaSO_4$ is a natural trace-mineral and not introduced in

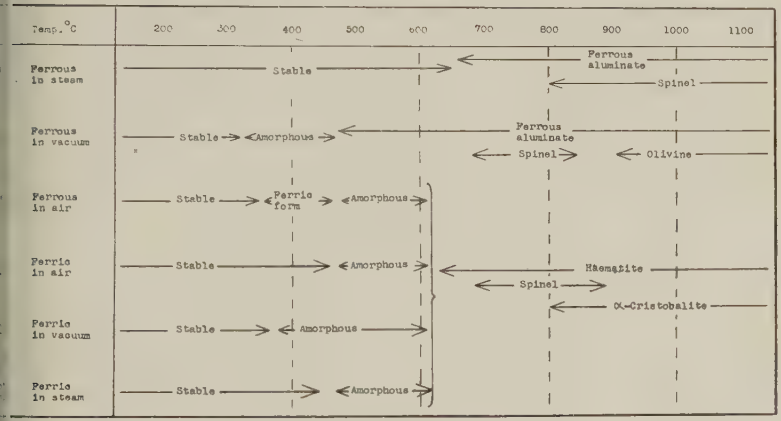

FIG. 4. Heat-treatment of chamosite.

nanipulation. The haematite (α-Fe_2O_3) improves in crystallinity up to .000° C., at which temperature it gives all the expected lines with harpness. Spinel appears at 800° C. and is present in quantity at 900° C. but no longer at 1100° C. The lines from this spinel correspond o true spinel $MgAl_2O_4$ and not to the spinel-type $FeAl_2O_4$ found in non-oxidizing conditions.

α-Cristobalite appears at 900° C. and is present in quantity at 1100° C. Weak lines visible at 1000° and 1100° C. are probably due to enstatite nd mullite.

Ferrous chamosite in steam and in a vacuum.—When heated in absence f air, the ferrous form does not oxidize to ferric chamosite. If we con-ider that the dehydration of layer silicates is, to some extent at least, eversible, then it is to be expected that in a reaction, such as

$$\text{chamosite} \longrightarrow x\text{H}_2\text{O} + \text{dehydrated form},$$

aising the partial vapour pressure of water surrounding the mineral, hould delay the change, while reducing it should accelerate dehydration. This is confirmed by experimental results. The ferrous form is stable up

to 650° C. in steam at 1 atm. pressure, but only to 350° C. in a vacuum. Recrystallization occurs in steam at 675° C., without any amorphous phase intervening, to ferrous aluminate of quite well-developed form (fig. 1, no. 5). Ordinary spinel appears transiently at 800° C., but as the various spinel forms $MgAl_2O_4$ and $FeAl_2O_4$ are capable of solid solution no pure type is likely. The occurrence of lines in the regions 1·42–1·43, 2·00–2·04, and 2·40–2·48 kX is, however, characteristic of all spinels and all materials examined after treatment at these temperatures gives lines or bands in these positions.

In a vacuum, ferrous chamosite gives an amorphous product before recrystallization, and the spinel product is less well developed than in steam. Some olivine lines appear at 900–1000° C. after vacuum treatment. The products are all dark green to black in colour.

Ferric chamosite in steam and vacuum.—Little difference is observed between the thermal transformations in air, vacuum, and steam. This is to be expected since the ferric form contains only a small amount of water. In vacuum, the amorphous form appears at a rather lower temperature than in air, but the decomposition is not appreciably retarded in steam. Haematite and minor constituents appear as in the treatment in air.

Heat-treatment of monoclinic chamosite.—An Ayrshire chamosite found by one of us (Brindley, 1951) to contain 55 % of a monoclinic form of chamosite, the remainder being ortho-hexagonal, was subjected to heat-treatment. At 400° C. a well-crystallized ferric form appeared, identical with that from the ortho-hexagonal ferrous chamosite. The line at 2·40 kX, previously shown to be a good indicator of the monoclinic form, disappeared and additional weak lines at 1·68, 1·88, and 3·28 kX appeared. Possible interpretations are: (i) the bulk of the monoclinic ferrous form passes to the ortho-hexagonal ferric form and the additional lines are impurities due to side-reactions, (ii) the monoclinic form breaks down to a poorly crystallized form yielding only a few weak lines.

6. *Significance of ferrous and ferric forms in chamosite identification.*

The principal findings of sections 1–5 are as follows: (1) Substantially pure ortho-hexagonal chamosite can be obtained free from the monoclinic form. (2) A stable oxidized, largely dehydrated form can be obtained with somewhat smaller unit-cell dimensions but an essentially similar structure. (3) This process implies a 2-stage thermal decomposition not previously observed in a kaolin-type structure. (4) The ferrous-ferric change is to a considerable extent reversible. (5) The breakdown

of ferrous chamosite depends largely on the water-vapour pressure surrounding it as well as on the temperature. (6) A variety of decomposition products can be obtained from the various forms of chamosite. (7) The absence of a chlorite-type chamosite conforms with the previous conclusion.

These findings, combined with those of the previous paper (Brindley, 1951), shed considerable light on many problems arising in connexion with chamosite. Not only can the X-ray diagrams vary with composition and the unit-cell type, but also with the state of oxidation of the mineral. Position and intensity of the lines vary between those of the ferrous and ferric forms, and this provides a further reason for the diversity of X-ray diagrams reported for chamosite. Moreover, the fact that a sample contains little structural water need not rule out the possibility of its being a kaolin-type mineral in the structural sense. This also has a bearing on identification of chamosite by differential thermal analysis. The endothermic peak depends on loss of water from the structure, and this depends in chamosite on the availability of atmospheric oxygen without which the ferric dehydrated form does not occur. Moreover, the ferric form would not be expected to give a prominent endothermic peak, since it is already largely dehydrated. The results obtainable by thermal analysis of chamosite minerals are therefore likely to vary with the design of the apparatus and the particular variety of chamosite which is being tested.

Finally, we wish to express our thanks to Mr. F. H. Saniter, Director of Research, The United Steel Cos. Ltd., and to Mr. W. C. Bell of Messrs. Stewarts & Lloyds Ltd., and to their respective firms for a grant which made this research possible. We also wish to thank Dr. W. Davies of The United Steel Cos. Ltd., and Mr. T. H. Williams of Stewarts & Lloyds for providing the specimens used in this work and for numerous discussions.

References.

Brindley (G. W.), 1951. The crystal structure of some chamosite minerals. Min. Mag., vol. 29, pp. 502–525.

—— and Ali (S. Z.), 1950. An X-ray study of thermal transformations in some magnesian chlorite minerals. Acta Cryst., vol. 3, pp. 25–30. [M.A. **11**–104.]

—— and Robinson (K.), 1951. X-ray identification and crystal structures of clay minerals. Chap. VI. Mineralogical Society (Clay Minerals Group), London. [M.A. **11**–253.]

—— Oughton (B. M.), and Youell (R. F.), 1951. The crystal structure of amesite and its thermal decomposition. Acta Cryst., vol. 4, pp. 552–557.

Glasstone (S.), 1948. Thermodynamics for chemists. New York, p. 282.

Hallimond (A. F.), 1939. With Harvey (C. O.) and Bannister (F. A.). On the relation of chamosite and daphnite to the chlorite group. Min. Mag., vol. 25, pp. 441–465.

Mellor (J.), 1929. Comprehensive treatise of inorganic and theoretical chemistry. London, vol. 13, p. 715.

Taylor (J. H.), 1949. Petrology of the Northampton sand ironstone formation. Geol. Survey Memoir, p. 29.

An X-ray method for studying orientation of micaceous minerals in shales, clays, and similar materials.

By G. W. Brindley, Ph.D., F.Inst.P.
Physics Department, University of Leeds.

[Taken as read November 6, 1952.]

1. *Introduction.*

MICACEOUS minerals, such as the micas, the chlorites, and most clay minerals, usually develop as thin lamellae parallel to the crystallographic basal plane (001). In sedimentary deposits these lamellae tend to lie parallel to the bedding plane and in slates parallel to the cleavage. Their degree of orientation is likely to vary with the conditions of formation of the material, and in the case of slates Bates (1947) has shown that it is closely related to their fissility. In relatively coarse-grained materials the degree of orientation may be studied directly by suitable microscopic techniques, but with fine-grained materials X-ray methods must be used, and even with coarser-grained materials the use of X-ray methods may have advantages, especially if a scanning technique, such as that described by Thewlis and Pollock (1950), is employed.

The orientation of micaceous minerals is most easily investigated by considering the intensities of X-rays reflected from their basal (001) planes in different directions with respect to the bedding or cleavage plane of the material. With X-ray powder cameras of conventional type in which the reflected X-rays are recorded through an aperture on a strip of film, a series of photographs for different angular settings of the material will be required. If, however, a complete Debye-Scherrer diagram is recorded, then a single photograph taken with one angular setting of the material suffices to give the required information.

Custers (1948) has analysed in detail this method for studying orientation with particular reference to rolled metal sheets. The practical problems are somewhat different with micaceous materials, since the fragility of many specimens makes the use of small blocks of material almost essential and these can be studied only by surface reflection methods. With thin sheets both surface reflection and transmission arrangements may be employed. With metals more penetrating radiations of shorter wave-length can be usefully used than are practicable

with micaceous minerals, since their low-order basal reflections are mainly used. MacEwan and Norrish (1951) have also considered the effect of orientation on the intensities of X-ray diffractions from clays, but their analysis, which has so far been published only in abstract, appears to be more general than is essential for the study of orientation alone. The present paper is restricted to the study of orientation in blocks of micaceous materials by a surface reflection method. The analysis differs somewhat from that given by Custers, but the same final expressions are obtained.

2. *General description of the method.*

If OP (fig. 1) represents the normal to a lamella surface or basal plane and ON the normal to the plane of cleavage or bedding, then the orientations of the lamellae can be expressed by the distribution function, p, of the normals OP with respect to ON. If the angle P$\hat{O}$N is denoted by ξ, then p will usually be a function only of ξ; but if necessary a second angular variable χ can be introduced, giving the variation of p around the normal ON. $p(\xi)$ can be defined as the number of normals, OP, per unit solid in angle in direction ξ, and $p(\xi, \chi)$ the number in direction (ξ, χ).

In fig. 1, the incident X-ray beam lies along the Y-axis of the rectangular co-ordinate system OX, OY, OZ. The specimen block is placed with its natural cleavage face containing the Z-axis and with surface normal ON lying in the plane XOY and making an angle α with OX. The photographic plate, SYT, lies parallel to XOZ. The arc SRT represents a portion of a Debye-Scherrer ring corresponding to a Bragg angle θ, so that R$\hat{O}$Y $= 2\theta$. Then OP, the normal to the reflection plane, bisects R$\hat{O}$Y′. As R sweeps over the arc SRT, OP generates a conical surface with a semi-vertical angle $(90-\theta)$.

Consider now a sphere of unit radius surrounding O with contours of equal $p(\xi)$ or $p(\xi,\chi)$ on its surface. If p is a function of ξ only, as we may generally assume (see, however, § 7), the contours will be circles concentric with ON. The X-ray intensity recorded at a point R, with co-ordinates (r, ψ) on the photographic plate, will depend (inter alia) on the value of p at the point P. As R moves round the Debye-Scherrer ring, P traces on the sphere a circle lying parallel to the plane XOZ, the path of which in relation to the p-contours determines what information concerning p is obtainable from a single Debye-Scherrer ring. The most complete information is obtained when P passes through N, and this requires that $\alpha = \theta$. The powder block is then set symmetrically with respect to the incident and reflected X-rays in the horizontal plane.

If we consider now a small range of directions $\Delta\theta$ for the incident radiation so that the Debye-Scherrer ring has a finite radial width, and consider also a small circumferential element $r\Delta\psi$, then the corresponding area in which P lies on the unit sphere will be $\Delta\theta\Delta\xi$ where $\Delta\xi$ is the movement of P corresponding to $\Delta\psi$. The number of planes reflecting

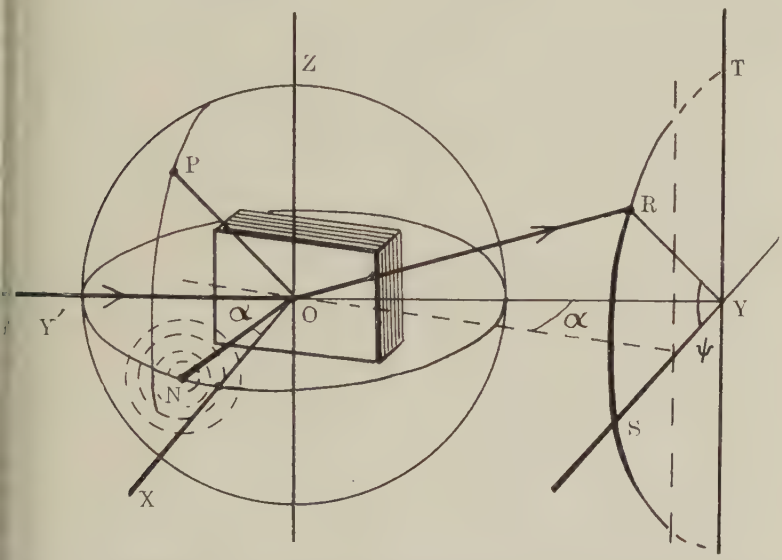

FIG. 1. To illustrate X-ray reflection from a flat block of fine-grained material. Y'O = incident beam; OR = typical reflected beam; OP = normal to reflecting plane; SRT = Debye-Scherrer arc; ON = normal to block surface; NÔP = ξ. Dashed lines surrounding N represent contours of $p(\xi)$.

into the small radial segment of the Debye-Scherrer ring will therefore be $p(\xi)\Delta\theta\Delta\xi$ and the reflected intensity will be given by

$$I(\psi)\Delta\psi \propto p(\xi)\Delta\theta\Delta\xi A(\alpha, \theta, \psi) \qquad (1)$$

where $A(\alpha, \theta, \psi)$ is the absorption factor appropriate to the conditions specified by (α, θ, ψ). To obtain $p(\xi)$ from measurements of $I(\psi)$, two calculations are required, viz. $A(\alpha, \theta, \psi)$ and the relation of $\Delta\xi$ to $\Delta\psi$.

3. *The absorption factor,* $A(\alpha, \theta, \psi)$.

X-ray absorption in flat powder blocks has been analysed and discussed by Brentano (1927, 1935) and by Brindley and Spiers (1934), and although they were then concerned primarily with rays such as OS

in the equatorial plane (fig. 1), their analysis is equally applicable to the present problem and the same expression is obtained for A, namely

$$A = \frac{1}{\mu} \frac{\sin \beta}{(\sin \alpha + \sin \beta)}$$

where α and β are the glancing angles of incidence and of emergence of the X-rays with respect to the surface of the block and μ is the linear absorption coefficient. The integration involved in obtaining A presupposes that the block is sufficiently thick to absorb fully the incident radiation.

The angle β is the complement of N$\hat{O}$R in fig. 1 and is calculated as follows:

The direction-cosines of ON and OR are respectively,

ON, $\cos \alpha, -\sin \alpha, 0$;

OR, $\sin 2\theta \cos \psi, \cos 2\theta, \sin 2\theta \sin \psi$.

Then $\cos \text{N}\hat{\text{O}}\text{R} = \sin \beta = \sin 2\theta \cos \psi \cos \alpha - \cos 2\theta \sin \alpha$

Whence $$A = \frac{1}{\mu} \left(\frac{\sin 2\theta \cos \psi \cos \alpha - \cos 2\theta \sin \alpha}{\sin 2\theta \cos \psi \cos \alpha - \cos 2\theta \sin \alpha + \sin \alpha} \right) \quad (2$$

and for the symmetrical setting of the block, when $\alpha = \theta$,

$$A = \frac{1}{2\mu} \left(\frac{1 - 2\cos^2\theta (1 - \cos \psi)}{1 - \cos^2\theta (1 - \cos \psi)} \right) \quad (2a$$

These results agree with formulae given by Custers (1948b).

4. *The relation of ξ to ψ.*

The direction cosines of OP are obtained by using the fact that OP bisects R$\hat{O}$Y′, and are $\cos \theta \cos \psi$, $-\sin \theta$, $\cos \theta \sin \psi$. This result, combined with that for ON, gives

$$\cos \text{P}\hat{\text{O}}\text{N} = \cos \xi = \cos \theta \cos \psi \cos \alpha + \sin \theta \sin \alpha \quad (3$$

and for the symmetrical setting,

$$\cos \xi = \cos \psi \cos^2\theta + \sin^2\theta \quad (3a$$

or, for small values of θ,

$$\xi \doteq \psi \text{ and } \Delta\xi \doteq \Delta\psi \quad (3b$$

Actually θ need not be very small in order that this approximation all be a good one, as the data in table I show. For ψ in the range -60° (the following section shows that this is the full angular range ailable) ξ does not differ appreciably from ψ provided θ is less than out 20° : for micaceous minerals, θ is likely to be about 10° or less, and e condition is easily satisfied.

TABLE I. Values of ξ for a range of values of ψ and θ.

θ \ ψ	0.	10.	20.	30.	40.	50.	60°.
10°	0	9·7	19·7	29·5	39·4	49·2	59·0
20	0	9·2	18·7	28·1	37·5	46·8	56·0
30	0	8·5	17·3	25·9	34·5	42·9	51·3

5. *The maximum angular range of investigation of ξ and ψ.*

The angular range of ψ, and therefore of ξ, which can be studied is nited by the shadow cast by the specimen block on the photographic ate. It is seen that

$$\cos \psi_{\max} = \tan \alpha / \tan 2\theta$$

nd for the symmetrical setting,

$$\cos \psi_{\max} = \tan \theta / \tan 2\theta = 1/2$$

$$\psi_{\max} \doteqdot 60°.$$

The range of orientations which can be studied usefully by this method somewhat less than 60° because as $\psi \to \psi_{\max.}$ so $A \to 0$. The useful nge of investigation is therefore for values of ξ up to about 50°. lternatively, by combining equations (2a) and (3a), we find

$$A = (2 - \sec \xi)/2\mu$$

that A becomes zero when $\xi = 60°$.

6. *The distribution of $I(\psi)$ in a Debye-Scherrer ring and the determination of $p(\xi)$.*

The required result is obtained by combining equations (1), (2a), and 3b) and omitting constant factors:

$$p(\xi) \propto I(\psi) \left(\frac{1 - \cos^2\theta\,(1 - \cos\psi)}{1 - 2\cos^2\theta\,(1 - \cos\psi)} \right)$$

f $p(0)$ and $I(0)$ are values corresponding to $\xi = 0$ and $\psi = 0$, then

$$\frac{p(\xi)}{p(0)} = \frac{I(\psi)}{I(0)} \left(\frac{1 - \cos^2\theta\,(1 - \cos\psi)}{1 - 2\cos^2\theta\,(1 - \cos\psi)} \right) \qquad (4)$$

By careful photometry of the Debye-Scherrer arc, $I(\psi)$ can be obtain[ed] and hence, by means of equation (4), the variation of $p(\xi)$ with ψ, i[.e.] with ξ.

7. *The case when p is a function of ξ and χ.*

It can readily be determined whether p is a function solely of ξ or [of] two variables ξ and χ by taking further X-ray photographs after tur[n]ing the specimen block through an angle χ about the surface norma[l] ON. In this way the variation of $p(\xi, \chi)$ with respect to $p(0)$ can [be] determined within the limitation that ξ cannot exceed about 60°.

8. *Some representative X-ray orientation diagrams.*

The present paper is concerned primarily with the method and it [is] not intended to discuss detailed photometric analyses of X-ray phot[o]graphs. Fig. 2 shows six representative photographs of clays and shal[es] taken with Cu-$K\alpha$ radiation and with the specimen block set at $\alpha = 12\frac{1}{2}$° in order to satisfy reasonably well the condition $\alpha = \theta$ for both the (002) basal reflection from kaolinite and the adjacent $(10\bar{1}1)$ reflection fro[m] quartz, these reflections being indicated in the photographs. Since ther[e] is no evidence for any preferential crystallographic orientation of th[e] quartz particles, one obtains directly a qualitative picture of the degre[e] of orientation of the kaolinite particles by comparing visually the inten[si]ty variations along these two arcs.

After each X-ray exposure the specimen block was removed and th[e] direct beam recorded; this is seen in the lower left-hand corner of eac[h] diagram. Each photograph is one half of the original and correspond[s] to values of ψ above the axis SY in fig. 1. The direction $\psi = 0$ lies alon[g] the lower edge of each diagram. The shadow cast by the specimen bloc[k] is clearly seen and the maximum value of ψ is about 60°.

The photographs in fig. 2 are as follows:

(*a*) A Coal Measure shale, taken from 8 feet above the Haigh Moo[r] Coal, from a borehole core at Wentbridge, Yorks. This shale spli[ts] moderately easily. X-rays were reflected from the bedding-plane surface. The majority of the kaolinite particles are seen to be within about ± 20° of this surface, as shown by the radial line in fig. 2*a* which correspond[s] to $\psi = 20$°.

(*b*) The same Coal Measure shale. X-rays were reflected from [the] ground surface at right angles to the bedding. The (002) kaolinite ar[c] is now practically invisible.

(*c*) A well-laminated Coal Measure shale taken from 25 feet below a in coal band, Robin Hood quarry, near Wakefield, Yorks. This shale

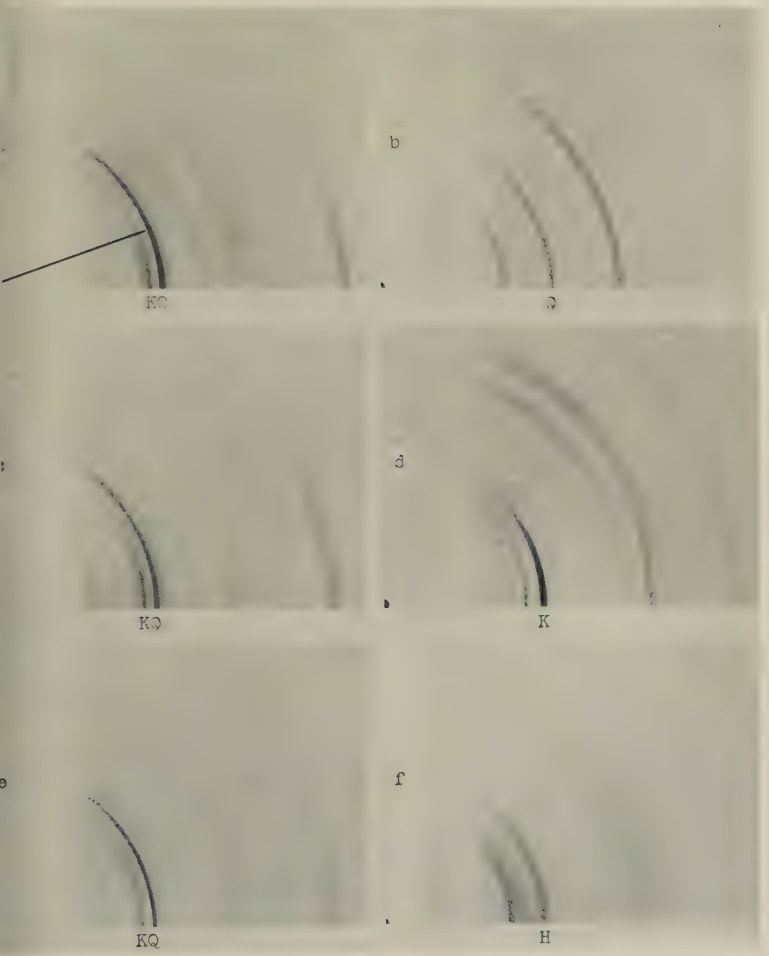

IG. 2. X-ray orientation diagrams of shales and clays. (*a*), (*b*), and (*c*), Coal leasure shales. (*d*), Cornish china-clay. (*e*), Coal Measure 'clunch'. (*f*), Utah halloysite, dehydrated at 300° C.

Q = Quartz ($10\bar{1}0$), K = Kaolinite (002), H = Halloysite (002).

plits very readily into flakes with smooth, flat surfaces. The orientation s somewhat better than in (*a*).

(*d*) A pressed block of Cornish china-clay containing no quartz. The

surface had a polished appearance. The orientation is less perfect than in (*a*) and (*c*), which is contrary to what was anticipated.

(*e*) A Coal Measure 'clunch', i.e. a shaly material, not well bedded, taken from a borehole core at Wentbridge, Yorks., 40 feet above the Flockton Thick Coal. The orientation is clearly much less perfect than in (*a*) and (*c*).

(*f*) A compressed block of Utah halloysite, dehydrated at 300°. This shows no orientation as would be expected from the known morphology of this mineral, which consists of rod- and tube-like particles rather than flakes.

I am indebted to Mr. W. Blackledge, University Photographer, for careful preparation of prints from the X-ray negatives, and to Mr. R. H. Crooke, who selected a number of shales for examination.

References.

Bates (T. F.), 1947. Investigation of the micaceous minerals in slate. Amer. Min. vol. 32, pp. 625–636. [M.A. **10**–365.]

Brentano (J. [C. M.]), 1927. Intensity measurements of X-ray reflections from fine powders. Phil. Mag., ser. 7, vol. 4, pp. 620–629.

—— (J. C. M.), 1935. The quantitative measurement of the intensity of X-ray reflections from crystalline powders. Proc. Physical Soc., vol. 47, pp. 932–947.

Brindley (G. W.) and Spiers (F. W.), 1934. A technique for the photographic determination of the intensities of X-ray reflections from powders. Proc. Physical Soc., vol. 46, pp. 841–852.

Custers (J. F. H.), 1948*a*. A new method for the determination of preferred orientations. Physica, vol. 14, pp. 453–460.

—— 1948*b*. The intensity distribution along the Debye halo of a flat specimen in connection with a new method for the determination of preferred orientations. Physica, vol. 14, pp. 461–474.

MacEwan (D. M. C.) and Norrish (K.), 1951. Second International Congress of Crystallography, Stockholm, Abstract no. A1.

Thewlis (J.) and Pollock (A. R.), 1950. X-ray scanning camera. Journ. Sci. Instruments, vol. 27, pp. 72–73.

The space-group and cell-dimensions of rankinite.

By Mrs. K. M. Moody[1]

Crystallographic Laboratory, Cavendish Laboratory, University of Cambridge

[Communicated by Dr. W. H. Taylor; taken as read November 6, 1952.]

TRICALCIUM disilicate, $Ca_3Si_2O_7$, which was first described by Shepherd and Rankin,[2] has been found in certain types of slag,[3, 4] nd recently as a natural mineral at Scawt Hill, County Antrim, to hich Tilley[4] applied the name rankinite. The present work was ndertaken after it was discovered that rankinite is formed when afwillite heated to about 1000° C.[5]

Natural rankinite crystals were extracted from sections of the Scawt ill rock, supplied by the Department of Mineralogy and Petrology, ambridge. The sample also contained melilite and spurrite. Selection f the crystals was based on observations of refractive indices and inter- erence colours, in the absence of other distinguishing features. Optical ata published by Tilley were used as standards of reference.

Oscillation, Weissenberg, and Laue photographs were taken, using u-$K\alpha$ radiation. It was confirmed that rankinite is monoclinic, and oncordant values of the cell-dimensions were obtained from three ifferent crystals. The mean values, which are accurate to within $\pm$0·05 Å., are:

$$a\ 10{\cdot}55,\ b\ 8{\cdot}88,\ c\ 7{\cdot}85,\ \beta\ 120{\cdot}1° \pm 0{\cdot}5°.$$

When reflections were indexed, it was found that $h0l$ was absent for h dd, and $0k0$ for k odd. There were no systematic hkl absences. The pace-group is therefore $P2_1/a$.

The density was determined by means of a specific gravity bottle, sing synthetic rankinite supplied by the Building Research Station. he value obtained was 2·96 g./c.c., from which it is concluded that there re four formula-units per cell. This gives a calculated density of ·00 g./c.c.

A complete structure-analysis is to be attempted.

[1] Now at Woolwich Polytechnic, London.

[2] E. S. Shepherd and G. A. Rankin, Journ. Indust. Eng. Chem., 1911, vol. 3, . 211.

[3] S. G. Gordon, Amer. Min., 1923, vol. 8, p. 110.

[4] C. E. Tilley, Min. Mag., 1942, vol. 26, p. 190.

[5] K. M. Moody, Min. Mag., 1952, vol. 29, p. 838.

Gyrolite.

(With Plate XII.)

By A. L. Mackay, M.A., Ph.D., and H. F. W. Taylor, B.Sc., Ph.D.
Birkbeck College Research Laboratory, University of London.

[Read November 6, 1952.]

THE mineral gyrolite was discovered in Skye by T. Anderson[1] in 1851. He showed it to be a hydrated calcium silicate of approximate composition $2CaO.3SiO_2.3H_2O$. Subsequently gyrolite has been found in other localities, and has been prepared hydrothermally by Flint, McMurdie, and Wells.[2] The ratio of lime to silica found by Anderson appears well established, but various values of the water content have been reported and more recent analyses approximate to $2CaO.3SiO_2.2H_2O$. X-ray powder measurements were given by McMurdie and Flint[3] but no crystallographic or other investigations of a detailed character have been reported.

A. The Present Investigation.

1. *Material.*

A sample of natural gyrolite from Bombay (B.M. 1925, 1044) was made available by the Trustees of the British Museum. The material was colourless and exhibited a pronounced basal cleavage in agreement with earlier descriptions. Relatively poor hexagonal prism cleavages were also observed. Calcite was present in contact with the gyrolite but no other minerals were found.

2. *Chemical analysis.*

The results of an analysis, carried out by Mr. F. J. McConnell (Building Research Station, Watford) are given in table I. Before this analysis the material was examined microscopically to select a sample as free from calcite as possible. Nevertheless, 0·95 % CO_2 was found; assuming this to be in the form of calcite, the ratios $CaO : SiO_2 : H_2O$ for gyrolite given by the analysis are 0·70 : 1 : 0·79. The discrepancy between these and the theoretical ratios 0·67 : 1 : 0·67 may be partly due to the presence of other

[1] T. Anderson, Phil. Mag., 1851, ser. 4, vol. 1, p. 111.

[2] E. P. Flint, H. F. McMurdie, and L. S. Wells, Journ. Res. Nat. Bur. Standards U.S.A., 1938, vol. 21, p. 617. [M.A. 7–283.]

[3] H. F. McMurdie and E. P. Flint, ibid., 1943, vol. 31, p. 225. [M.A. 9–45.]

des, particularly Al_2O_3. If it is assumed that Al replaces Si, the ratios O:(Si,Al)O_2:H_2O become 0·67:1:0·76.

TABLE I. Chemical analyses of gyrolite from Bombay.

		Mol. ratios.	A.
SiO_2	50·23	1·000	52·09
Al_2O_3	2·19	0·026	0·49
Fe_2O_3	0·20	0·015	—
MgO	⩽ 0·13	⩽ 0·004	0·29
CaO	34·04	0·700*	33·07
Na_2O+K_2O ...	⩽ 0·14	⩽ 0·002	0·52
CO_2	0·95±0·10	—	—
H_2O	11·98±0·15†	0·795	13·35
	99·86		99·86

After deduction of calcite. † Loss on ignition at 1250° C., after deduction of CO_2.
A.—W. A. K. Christie, Rec. Geol. Surv. India, 1925, vol. 56, p. 199 [M.A. 3–7]. Also SrO 0·05; sp. gr. 2·388–2·390, ω 1·549, ϵ 1·536. 2·99% water lost low 107° C. Na_2O 0·51, K_2O 0·01.

3. *Optical examination.*

Cleavage flakes gave a uniaxial negative optic axial figure. Some rstals appeared slightly biaxial, possibly due to bending of the flakes. fractive indices for white light were ω 1·545±0·01 and ϵ 1·535±0·01, reeing well with the previously published values.

4. *X-ray investigation of single crystals.*

(*a*) *Diffraction Symmetry.*—A stationary crystal photograph (pl. XII, . 1) using copper radiation filtered through nickel foil, and taken th the incident beam perpendicular to the basal cleavage, showed the ffraction symmetry of the corresponding axis to be 6. A precession otograph confirmed the absence of symmetry planes parallel to is axis. The existence of a sixfold axis in the diffraction symmetry cessarily implies that of a symmetry plane perpendicular to it. rrolite thus appears to be hexagonal, with diffraction symmetry 6/*m*. In order to provide a more sensitive test of the diffraction symmetry, cillation photographs were taken about the sixfold axis. For reasons ven in the next paragraph, certain difficulties had to be overcome before e crystal could be set accurately about this axis. The crystal was, owever, set to within ±5 minutes on each goniometer arc and 15° cillation photographs taken at exactly 120° intervals. These showed ry slight differences from each other, as regards the intensities of rresponding reflections. They, and other oscillation and Laue photo-aphs, also showed similar very slight deviations from a plane of sym-etry perpendicular to the sixfold axis. It is thus possible that the true

diffraction symmetry is lower than $6/m$. The discrepancies are, however so slight that the diffraction symmetry must in that case be to a hi[gh] degree of accuracy pseudo-$6/m$.

(*b*) *Cell size.*—In a complete rotation photograph about the *c*-axi[s] (pl. XII, fig. 5), all row-lines could be indexed on hexagonal axes havi[ng] $a = 9{\cdot}72 \pm 0{\cdot}01$ Å. From the row of $000l$ reflections in a Weissenbe[rg] photograph a value of $22{\cdot}13 \pm 0{\cdot}05$ Å. was found for the spacing in t[he] *c*-direction. The layer-lines in rotation photographs about the *c*-a[xis] show that the true repeat distance is six times this, namely, $132{\cdot}8 \pm$ 0·3 Å. Owing to the very long *c*-axis and the relatively short *a*-axis th[e] layer-lines are difficult to pick out, but row-lines are evident even if th[ere] is considerable mis-setting. A special X-ray method of setting, de[-] scribed elsewhere (Mackay),[1] based on the row-lines, had to be develop[ed].

(*c*) *Production of characteristic reflections in a stationary crystal pho[to-] graph.*—The stationary crystal photograph along the *c*-axis (pl. XII fig. 1), using Cu-K radiation filtered through Ni foil, exhibits a regul[ar] hexagonal array of spots. The use of unfiltered, as distinct from filtered copper radiation did not affect the relative intensities, but introduce[d] additional reflections due to the $K\beta$ component. Symmetrical oscillatio[n] through 15° about the mean position (pl. XII, fig. 2) affected the in[-] tensities, but not the positions of the spots. The latter are therefor[e] due to the characteristic, and not the white, radiation, and for thi[s] reason the result has not been described as a Laue photograph.

It was at first thought that the effect was caused by imperfections i[n] the crystal, giving rise to a reciprocal lattice consisting of h, k rod[s]. The row-lines in *c*-rotation photographs of good crystals (pl. XII, fig. 5) consisted, however, of quite distinct spots. The reciprocal lattice point[s] are, nevertheless, so closely packed along the h, k lines that characteristi[c] reflections always occur in stationary crystal photographs along th[e] *c*-axis. This is probably due mainly to finite divergence of the beam together with slight bending of the specimen.

(*d*) *Extinctions and space-group.*—As has been mentioned above, th[e] $000l$ reflections are only present when $l = 6n$. Other complicated regu[-] larities are visible but are not relevant to the space-group determinatio[n].

The diffraction symbol for gyrolite is thus found to be $6/m$—C[—] which is characteristic for the enantiomorphous pair of space-group[s] $C6_1$ and $C6_5$. These groups are non-centrosymmetrical and every atom occurs in multiples of six. The $hki0$ zone is centrosymmetrical but n[o] others.

[1] A. L. Mackay, Acta Cryst., 1952, vol. 5, p. 691.

(*e*) *The contents of the unit cell.*—The space-group symmetry demands that the number of molecules in the unit cell be divisible by six. The

TABLE II. Powder data for natural gyrolite.

Spacing (Å.).	Intensity.	Principal reflections contributing.	Calculated spacing (Å.) where applicable.	
22	vs	0006 only	0006	22·13
11·0	s	000.12 only	000.12	11·07
8·4—7·4	m, d } band	$10\bar{1}l$	$10\bar{1}0$	8·42
7·4—5·4	w, d }			
4·75	w	$11\bar{2}l$	$11\bar{2}0$	4·86
4·20	s	$20\bar{2}l$	$20\bar{2}0$	4·21
3·72—3·45	w, d } band	$20\bar{2}l$		
3·65	ms }	000.36	000.36	3·69
3·21—3·02	m, d } band	$21\bar{3}l$	$21\bar{3}0$	3·18
3·12	vs }	000.42	000.42	3·16
2·80—2·61	m, d } band	$21\bar{3}l$		
2·80	ms }			
2·42	w	$22\bar{4}l$ / $20\bar{2}l$	$22\bar{4}0$	2·43
2·31—2·03	vw, d }			
2·31	w } band	$21\bar{3}l$ / $31\bar{4}l$	$31\bar{4}0$	2·33
2·17	w }			
2·06	w }			
1·90	w	$32\bar{5}l$	$32\bar{5}0$	1·93
1·82—1·73	vw, d } band	$41\bar{5}l$	$41\bar{5}0$	1·83
1·82	s }			
1·57	mw	$42\bar{6}l$	$42\bar{6}0$	1·59
1·52—1·50	vw, d } band	$42\bar{6}l$ / $51\bar{6}l$	$51\bar{6}0$	1·51
1·50	w }			
1·41—1·37	vw, d } band	$51\bar{6}l$ / $43\bar{7}l$	$43\bar{7}0$	1·38
1·37	w }			
1·34	mw	$52\bar{7}l$	$52\bar{7}0$	1·35
1·28	vw	$61\bar{7}l$	$61\bar{7}0$	1·28
1·195	mw	$53\bar{8}l$ and $70\bar{7}l$	$53\bar{8}0$ and $70\bar{7}0$	1·203
1·168—1·154	w, d; band	$53\bar{8}l$ and $70\bar{7}l$		
1·060	w	$63\bar{9}l$	6390	1·061
1·040	w	$63\bar{9}l$		
0·965 approx.	vvw, d; band	$63\bar{9}l$ (?)		
0·934 approx.	vvw, d; band	?		
0·908	w	$8.2.\overline{10}.l$	$8.2.\overline{10}.0$	0·918
0·882	w	$6.5.\overline{11}.l$ and $9.1.\overline{10}.l$	$6.5.\overline{11}.0$ and $9.1.\overline{10}.0$	0·882
0·868 approx.	vvw, d	$7.4.\overline{11}.l$	$7.4.\overline{11}.0$	0·873

s = strong, m = moderate, w = weak, v = very, d = diffuse.

most likely number of molecules of composition $2CaO.3SiO_2.2H_2O$ is 48, which gives a calculated density of 2·40. Observed values, reported in

the literature, vary between 2·342 and 2·446. Alteration in the postu-lated number of molecules to 42 or 54 gives calculated densities of 2·1 and 2·70 respectively. The assumption of 48 molecules of composition $2CaO.3SiO_2.3H_2O$ would make the density 2·53. In each case the result is well outside the observed limits. The X-ray results therefore support the view that the unit cell contains 48 molecules of formula $2CaO.3SiO_2.2H_2O$. This gives a volume per O atom of 22·7 Å^3.

5. *X-ray powder photographs.*

The X-ray powder data (table II) for the natural mineral were obtained using copper $K\alpha$ radiation, with cameras of 6 cm. and 19 cm. diameter. The laboratory preparation (p. 87) gave results indistinguishable from the natural mineral.

The indexing was carried out by direct comparison of 6 cm. powder photographs with single-crystal photographs. Except for a few strong $000l$ reflections, the powder photographs consist entirely of hk bands. An attempt has been made in the table to indicate the apparent limits of each band and also any pronounced maxima within them. The limits were estimated visually and are therefore to a small extent arbitrary, but it appears unlikely that any uncertainties could arise on this account in regard to identification of the mineral.

The data are in fair agreement with those of McMurdie and Flint (1943, loc. cit.), whose data are, however, incomplete at both high and low angle ends, and no mention is made of the widely varying breadths of the lines. They also include, as the strongest spacing, one of 3·36 Å. This cannot have been due to gyrolite.

6. *Dehydration.*

(*a*) *The dehydration curve.*—A dehydration curve is shown in text-fig. 1. At temperatures up to 520° C., isobaric conditions were maintained, the partial pressure of water-vapour being 6 mm. The apparatus used has been described elsewhere.[1] For the determination of the next three points the material was transferred to a platinum crucible, which was heated in an electric furnace without control of the humidity. The final point was obtained by ignition with a large Méker burner, and the temperature quoted (1250°) is only approximate.

The result shows clearly that the water is lost in two stages. The first is complete at about 450°, and entails a loss of 9·0±0·2 %. The second begins at about 500° and is complete by 850°. After correction for the

[1] H. F. W. Taylor, Journ. Chem. Soc. London, 1953, p. 163.

$_2O_2$ present (0·95±0·1 %), the loss in the second step amounts to 0±0·3 % of the initial weight.

The loss at 100°, 4·15 %, is in fair agreement with that found by nderson, for his original sample, of 4·42 %. The total water loss, at 50°, of 11·98 ±0·15 %, is higher than that (10·95 %) required by the

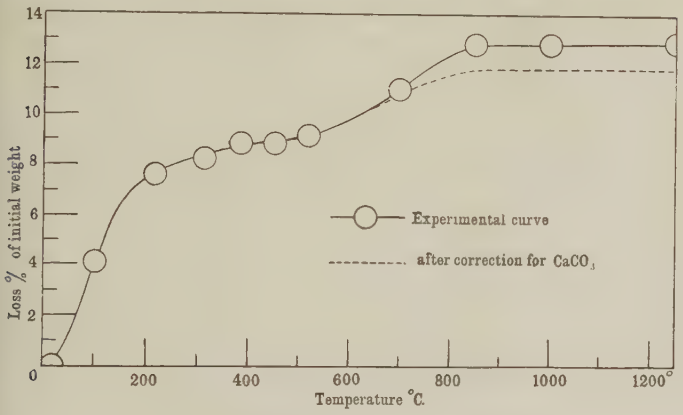

Fig. 1. Dehydration curve of natural gyrolite.

ormula $2CaO.3SiO_2.2H_2O$, but much lower than that (15·6 %) corre-ponding to $2CaO.3SiO_2.3H_2O$. The first formula would thus appear the nore probable, especially in view of the X-ray results described in the revious section. The possibility that gyrolite has some intermediate omposition, such as $4CaO.6SiO_2.5H_2O$, cannot be altogether excluded, lthough the density calculated for this formula (2·47) is outside the ange of observed values.

(*b*) *X-ray single-crystal investigation of heated material.*—Cleavage akes of natural gyrolite were heated to various temperatures, X-ray ingle-crystal photographs being taken before and after the treatment. n this way the nature of the products formed at various points on the ehydration curve was established, and the orientation relative to that f the original gyrolite crystal determined in each case.

(i) Heating to 450°, i.e. to the end of the first step in the dehydration urve.—A rotation photograph about the *c*-axis showed the positions f the row-lines to be unchanged. Within each individual row-line, owever, a marked simplification was observed, almost all the spots lying n the 22·13 Å. layer-lines. Stationary crystal photographs with the ncident beam parallel to the *c*-axis showed no appreciable change in he positions of the spots, but the intensities suggested a reduction in the

symmetry to trigonal. A zero-layer Weissenberg photograph about an a-axis showed no significant changes in the spacing or intensities of the $000l$ reflections, but certain 'extra' reflections appeared in this row in non-integral positions.

While the full significance of these effects has yet to be determined, it is clear that heating gyrolite to 450° produces certain alterations in the structure, but leaves it basically unchanged. The layers of thickness 22·13 Å. appear to be stacked in a less complicated way, in the direction of the c-axis, than in the unheated material.

A crystal, which had been heated to 450°, was exposed to water-vapour in a vacuum desiccator for four days at room-temperature. This treatment caused no further change in the X-ray pattern. Hence, if rehydration takes place at all under these conditions, it does not fully reverse the structural changes occurring on dehydration.

(ii) Heating to 550 750°, i.e. to points on the second step in the dehydration curve.—At 550° the product gave X-ray patterns very similar to those obtained at 450°. Certain additional minor changes were observed, but the structure evidently remained basically that of gyrolite. At 700° and 750° the gyrolite reflections could still be observed, but many more additional spots were also present. The most prominent of these could be attributed to the formation of α-wollastonite: this is discussed in the next paragraph. Some of the spots, however, could not easily be accounted for by the presence of gyrolite or of α- or β-wollastonite, and it is possible that some intermediate phase may be formed over a small range of temperature.

(iii) Heating to 1000°, i.e. to the end of the second step in the dehydration curve.—The photograph obtained by oscillation, through 15°, symmetrically about a position with the cleavage plane perpendicular to the incident beam, is shown in pl. XII, fig. 4. Together with oscillation photographs about the original c-axis, this showed that the gyrolite had been converted into almost a single crystal of α-wollastonite. This compound is pseudo-hexagonal, with a 6·85, c 19·65 Å. (Heller, unpublished work). The product was oriented with its c-axis coinciding with that of the original gyrolite, and its $\{11\bar{2}0\}$ directions coinciding with the $\{21\bar{3}0\}$ directions of the gyrolite. This is shown most clearly by the series of photographs in pl. XII. Figs. 1 and 2, given by the unheated material, are of gyrolite. Fig. 3, given by a crystal heated to 700°, shows just inside the ring of strong $\{21\bar{3}0\}$ reflections of the gyrolite, a ring of $\{11\bar{2}0\}$ reflections of the α-wollastonite. The two sets of spots are scarcely resolved in the reproduction. Gyrolite and α-wollastonite are

nus present together in this product. In pl. XII, fig. 4, given by the rystal heated to 1000°, the gyrolite spots have disappeared and the attern of α-wollastonite can be seen. The α-wollastonite crystal btained by the heating of gyrolite is imperfect. The *c*-oscillation hotograph showed that the directions of the *c*-axes of the crystallites f *a*-wollastonite deviated by up to 10 degrees in all directions from he normal to the cleavage plane of the flake.

7. *Synthesis.*

The laboratory preparation of gyrolite by Flint, McMurdie, and Wells (1938, loc. cit.) was confirmed in the present investigation. Calcium ydroxide and moist silica gel (20 % SiO_2), in the approximate molar proportions 2:3, were treated with water in a closed bomb at 150° for 6 days. The experimental technique has been described elsewhere.[1] Optical investigation of the product showed it to consist of sub-microscopic particles of mean refractive index 1·54. X-ray powder photographs showed excellent agreement with those of natural gyrolite (table II) over the whole range of spacings from 22 Å. to less than 1 Å.

B. Discussion.

1. *The existence of layers.*

The marked basal cleavage strongly suggests that gyrolite resembles the micas and clay minerals in having a layer structure. This is supported by the character of the 000*l* reflections, which are always thin, sharp arcs of closely defined spacing. This is true even in the case of very poor crystals; when these are mounted with the *c*-axis perpendicular to the X-ray beam, the *hkil* reflections are very weak and indefinite, but the 000*l*'s are still sharp and of approximately their usual intensities. Whatever type of disorder may occur does not, therefore, affect the spacings in the direction of the *c*-axis. This would be accounted for by a layer structure, in which the chemically discrete layers could readily be displaced parallel to each other.

2. *Composition of the layers.*

The observed space-group, $C6_1$, indicates that the unit of pattern is a layer 22·13 Å. thick, and containing one-sixth of the cell contents. The layer thus contains 8 molecules of approximate composition

$$2CaO.3SiO_2.2H_2O.$$

The fact that a product, giving a powder photograph identical with that

[1] L. Heller and H. F. W. Taylor, Journ. Chem. Soc. London, 1951, p. 2397.

of natural gyrolite, can be made artificially from pure materials, shows that the alumina and other minor constituents in the natural minera are not essential to the structure.

3. *Nature of the layers.*

The results of the dehydration experiments show that three-quarter of the water is lost in the first stage of the dehydration, and that thi does not cause any fundamental change in the structure. Loss of th remaining water, on the other hand, brings about transformation to different compound. This suggests that three-quarters of the water is present as molecules, and one-quarter probably as hydroxyl groups, which would be in accordance with the formula $Ca_4(Si_6O_{15})(OH)_2,3H_2O$. assigned by Betekhtin,[1] but he does not state on what grounds his view was based. It is, of course, not certain that some or all of the hydroxyl is not attached to silicon. However, the lamellar nature of the material suggests that the anion probably has the empirical formula Si_2O_5, giving rise to infinite sheets of linked SiO_4 tetrahedra, rather than a more basic composition which would produce a chain or ring type anion.

Sheets of $(Si_2O_5)_n$ composition, which are known to occur in silicate minerals, are of at least two kinds, which may be described as the mica type and the apophyllite type respectively. The hexagonal symmetry of gyrolite leads to a comparison with the first of these.[2] The unit cell of the mica-type sheet is hexagonal, with a 5·2 Å., and contains a single Si_2O_5 group. For comparison with gyrolite it is possible to select a larger hexagonal cell, with a 9·0 Å. and containing three Si_2O_5 groups. Assuming tentatively that sheets of this kind are present in gyrolite (which has a 9·72 Å.), each 22·13 Å. layer would contain four such sheets. This appears not unreasonable, by comparison, for example, with talc and antigorite, which contain four sheets in thicknesses of 18·8 Å. and 28·6 Å. respectively (Brindley).[3] The observed volume per oxygen atom for gyrolite, of 22·7 Å.^{3}, suggests a fairly open structure, which is also in agreement with this hypothesis.

The assumption of $(Si_2O_5)n$ sheets of the mica type nevertheless raises serious difficulties. The a-axis of such a sheet can be stretched from

[1] A. G. Betekhtin, Mineralogia, Moscow, 1950, p. 877. [M.A. **12**–1.]

[2] The space-group shows that the layers do not necessarily possess any symmetry, but the fact that they are stacked on top of each other with successive angular displacements of 60° suggests that their essential framework at least approximates to hexagonal symmetry.

[3] G. W. Brindley (editor), X-ray identification and structures of clay minerals, Min. Soc., London, 1951, pp. 72, 311, &c. [M.A. **11**–253.]

0 to 9·72 Å. only if the bond angles of the SiO_4 tetrahedra are seriously distorted, or alternatively by stretching the Si O bonds to over 1·7 Å. A similar problem arises in the case of cronstedtite, where this axis has a value of 9·49 Å., but this was accounted for by Hendricks[1] on the assumption that silicon was replaced by the larger Fe^{3+} ion. It is difficult to imagine that the Ca^{++} ion could replace silicon in this way. The structure of the gyrolite layers thus remains to be determined.

4. *Patterson projection.*

The long series of 000*l* reflections (28 observed) invited an attempt to obtain information on the structure of the layers by carrying out a one-dimensional Patterson projection along the *c*-axis. The resulting synthesis showed strong interlayer vectors of lengths 1·5, 3·0, and 7·0 Å. This is little more than could be seen directly from the intensities, and no useful deductions could be drawn from it.

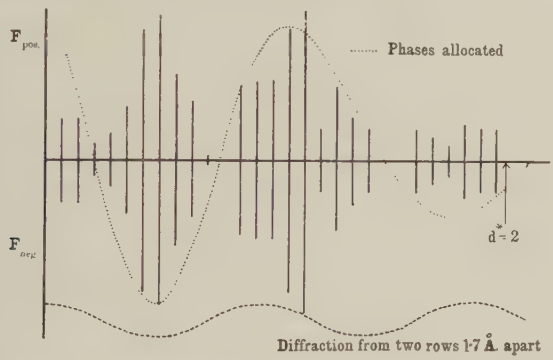

FIG. 2. Fourier synthesis, 000*l* reflections of natural gyrolite. F_{000l} plotted on an arbitrary scale both positively and negatively for allocation of signs.

5. *Fourier synthesis.*

Inspection of the row of 000*l* reflections (fig. 2) shows that the variations in intensity occur smoothly from one reflection to another. This at once suggests, in spite of the absence of a centre of symmetry, a speculative attempt to allocate phases for a one-dimensional Fourier synthesis following the method of W. L. Bragg.[2]

On the whole, in layer minerals, interatomic distances projected on to a line perpendicular to the layers are of the order of 1·7 Å. The transform of this spacing is drawn out below the observed amplitudes to give

[1] S. B. Hendricks, Amer. Min., 1939, vol. 24, p. 529. [M.A. 7–496.]

[2] W. L. Bragg, Guthrie Lecture. Proc. Physical Soc., Sect. B, 1952, vol. 65, p. 833.

a guide as to how quickly the latter can change sign. When a synthesis with the indicated signs was carried out, the result was unpromising, giving only a small peak at the origin with large peaks 1·5 Å. to each side of it. Other density deviations from the general level were small.

Patterson and Fourier syntheses may be useful in deciding between various hypotheses as to the nature of the layers, but are not really helpful in setting up a tentative structure in the present case. The hypothesis adopted for allocating the signs is only valid if the 22·13 Å. layers are centrosymmetrical in the projection, and there is no convincing reason to suppose that this is so.

6. *Conversion to α-wollastonite.*[1]

The formation of α-wollastonite on complete dehydration is of interest, since this compound is unstable relative to the β-form at temperatures below 1125° (Muan and Osborn).[2] Evidence of its formation from gyrolite was, however, obtained in the present investigation at temperatures as low as 700°. The explanation must lie in the fact that, on account of the close structural relationship between the two compounds, the energy of activation for the change from gyrolite to α-wollastonite is much less than that from α- to β-wollastonite. The latter transition, however slow, must nevertheless take place eventually, on sufficiently prolonged heating at any temperature below 1125°. Inspection of the photograph reproduced in pl. XII, fig. 4, shows the presence of certain pairs of spots, which are unlikely to be due to α-wollastonite, and it appeared possible that these were due to β-wollastonite.

This was confirmed when a crystal of gyrolite was annealed at 1050° for four days. X-ray photographs showed complete conversion to β-wollastonite. Like the transition from gyrolite to α-wollastonite, this further transition from the α- to the β-form occurs in an ordered way, apparently six crystals of β-wollastonite being produced from the original crystal of gyrolite. The orientation of these relative to that of the original gyrolite crystal was not fully determined, but the pairs of reflections visible in pl. XII, fig. 4, were identified as the strong reflections (320, *d* 2·97 Å.)[3] of the β-wollastonite crystals.

[1] Throughout this paper, α-wollastonite denotes pseudo-hexagonal pseudowollastonite α-$CaSiO_3$; β-wollastonite may indicate either triclinic wollastonite or the very similar monoclinic parawollastonite, or an intimate intergrowth of the two.

[2] A. Muan and E. F. Osborn, preprint of paper read at the American Iron and Steel Institute, May 1951.

[3] Indices on M. Barnick's unit cell for the monoclinic form; Naturwiss., 1935, vol. 23, p. 770; Strukturber., 1936, vol. 4, p. 207. [M.A. 6–332.]

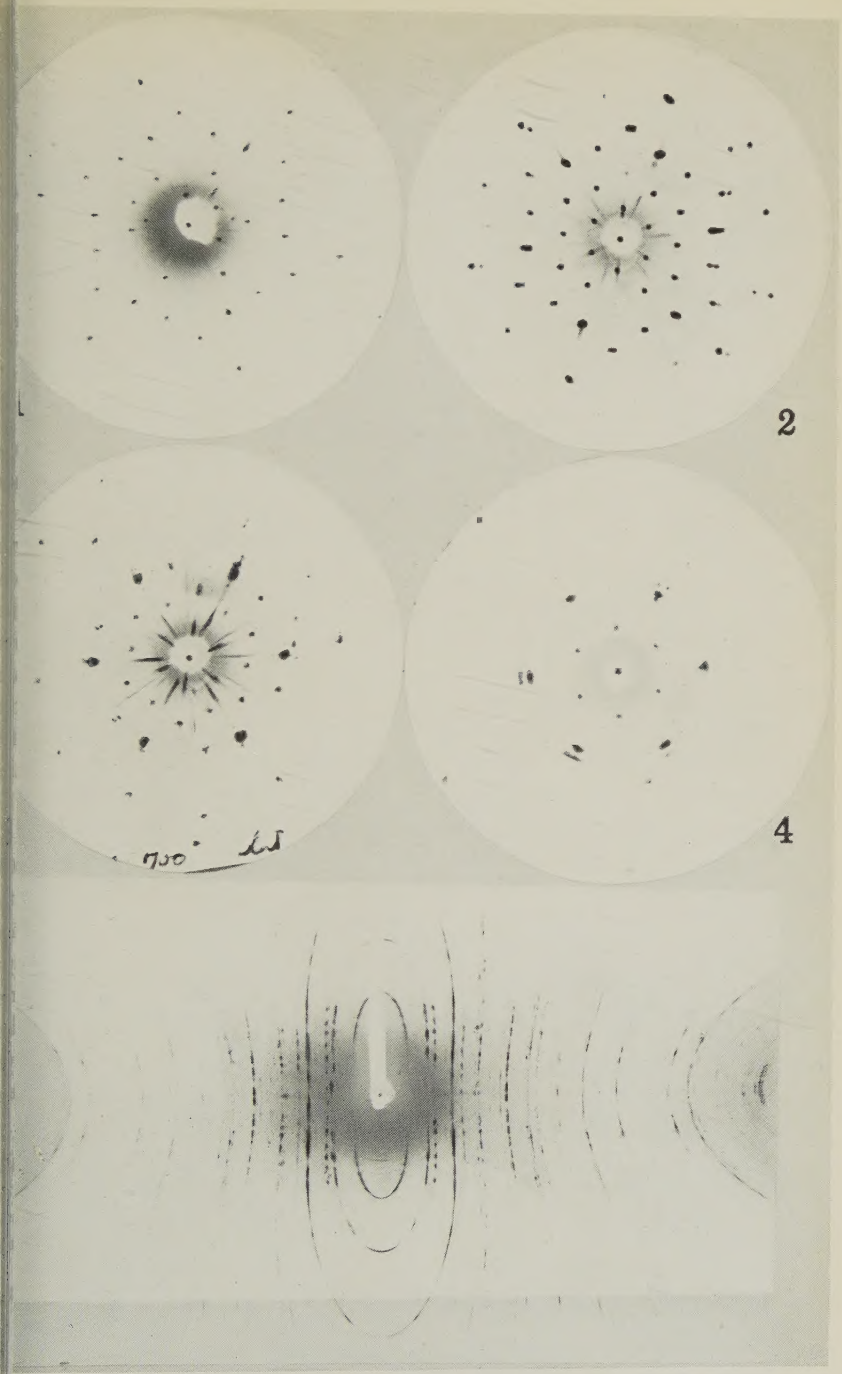

L. Mackay and H. F. W. Taylor: X-ray Photographs of Gyrolite

The structural similarity between gyrolite and α-wollastonite is evidently very close, being shown:

(*a*) by the relationship in symmetry, or pseudo-symmetry;

(*b*) by the similarity in *c*-axial lengths; and especially,

(*c*) by the relationship between the $\{21\bar{3}0\}$ planes in gyrolite and the $\{11\bar{2}0\}$ planes in α-wollastonite. The reflections corresponding to these planes are strong in each case, the spacings are similar (3·18 and 3·42 Å. respectively), and when α-wollastonite is formed by the dehydration of gyrolite, the orientations of its $\{11\bar{2}0\}$ planes are identical with those of the $\{21\bar{3}0\}$ planes of the gyrolite.

The co-existence of gyrolite and α-wollastonite in the crystal heated to 700° shows in a particularly convincing way that a very high degree of order is maintained throughout the process of dehydration. There is also evidence of the formation of any intermediate, amorphous stage. It may, however, be noted that gyrolite is richer in silica than is α-wollastonite. The absence of any evidence of crystalline silica in the X-ray photographs of the dehydrated material suggests that the excess of silica must be expelled from the structure in an amorphous condition.

Acknowledgements.—We thank Professor J. D. Bernal, F.R.S., Dr. W. W. Jeffery, and Mr. R. W. Nurse (Building Research Station, Watford, Herts.) for their interest and advice; the Trustees of the British Museum for the sample of natural gyrolite; Dr. L. Heller, for assistance in the experimental work; and Mr. F. J. McConnell (Building Research Station) for the chemical analysis. The work was carried out as part of an extra-mural contract for the Building Research Board, and we thank the Director of Building Research for permission to publish this paper.

Explanation of Plate XII.

X-ray photographs of gyrolite from Bombay.

Fig. 1. X-ray stationary crystal photograph. Incident beam parallel to the sixfold axis. Filtered copper radiation.

Fig. 2. As fig. 1, but crystal oscillated through 15° symmetrically about the stationary position.

Fig. 3. X-ray stationary crystal photograph. After heating to 700°. Incident beam parallel to the original sixfold axis. Filtered copper radiation.

Fig. 4. X-ray oscillation photograph. As for fig. 2, but after heating the crystal to 1000°.

Fig. 5. X-ray rotation photograph about *c*-axis. Filtered copper radiation.